Application of the non-uniform Fourier transform to non-uniformly sampled Fourier transform spectrometry

By:

Muqian Wen

Prepared under supervision by:

Dr. John Houlihan

Thesis submitted for award of Master by Research degree

Submitted to South East Technological University (Waterford), Ireland

Declaration

The author declares that this thesis is entirely this author's own work and has not been submitted to other institutions for degree or other similar qualification purposes.

Signed: Muqian Wen

April 2023

Acknowledgements

I did all the actual works of this study (devising and carrying out experiments, developing software codes and writing the thesis, etc) all by myself alone. However, supervisor Dr. John Houlihan's supervision has helped to significantly improve this work, especially to the published paper that this thesis is based upon. For example, he asked me the question of what the maximum frequency limit of NUFFT is which led me to discover the under-sampling feature of NUFFT. I think this is perhaps the most noteworthy discovery by this study because while NUFFT has shown advantages in many aspects, this is totally unique property to NUFFT that the interpolation method totally lacks. In another example he suggested me to use log scale graph to study spectral noise levels. This suggestion helps to make this study much more thorough and convincing. And there are other examples that his supervision has helped. I think this doesn't happen for no reason and only happened because he didn't have ego in supervision and treated me with respect and as equal. This is something I am very grateful for. His help in editing the paper has also helped a lot. I learned a lot from this paper writing experience. It is the first paper that I am the corresponding author although I have published paper (as first author) before. I think it does not happen very often that supervisors make actual contributions to the student's research.

The experience of this study was unusual. The supervisor was changed after the first year and this study was initially a PhD. The original supervisor insisted me to do research that I think is certainly wrong but I have resisted to the end until change of supervisor. For clarification I was never ruled with any wrongdoing in any formal or informal way and I'm sure if this is still a PhD it will also be successful. Being research student is very hard because unlike a job which works for contract guaranteed salaries we work for non-guaranteed degree reward at end of study which means that we will be more willing to tolerate adversity from supervisors and this combined with the power advantages by supervisors make exploitation very convenient to happen such that we need to feel lucky if the supervisor have clean research ethics and respect student even though these should be basic requirements. I want to thank the current supervisor for turning this research into success and for having empathy in supervision. I want to thank anyone who has wittingly or unwittingly helped me through hardships in these two years. I want to thank all those friendly fellow students, school staffs, housing co-tenants and some other strangers.

Table of Contents

Abstract

Application of the non-uniform Fourier transform to non-uniformly sampled Fourier transform spectrometry

by

Muqian Wen

Resampling by interpolation is the traditional method to process interferograms from non-uniformly sampled Fourier transform spectrometers. The non-uniform fast Fourier transform (NUFFT) is an alternative approach that has been mostly overlooked. With the aid of experiments, these two methods are thoroughly compared in this thesis. It is found that the NUFFT is comparable to interpolation in spectral shape and spectral noise levels and is better in spectral amplitude and computer performance. A significant advantage is also found in the case of under-sampling and noise performance due to the unique non-periodic nature of non-uniform sampling. In addition, a novel implementation of NUFFT is presented and analysed. An unconventional super-high-resolution Michelson interferometer is devised and built for the experiments in this research.

Keywords: ***NUFFT, Fourier transform spectrometer, Michelson interferometer, non-uniform sampling, non-uniform Fourier transform***

Introduction

A Fourier Transform Spectrometer (FTS) is an instrument that measures the intensity of light as a function of frequency, by using the Fourier Transform mathematical method. It is used in a variety of scientific fields, such as astronomy, chemistry, and physics, to study the composition and properties of matter. The Fourier transform spectrometer works by passing light through an interferometer, which splits the light into two beams that are then recombined. The interference pattern produced by the recombination is then transformed using the Fourier Transform to give a spectrum that shows the relative intensities of different frequencies of light. The resulting spectrum can then be analysed to determine the composition and properties of the sample being studied.

Fourier transform spectrometer is one of the three main types of optical spectrometry techniques with the other two being Fabry–Pérot spectrometer and grating spectrometer. Different types of optical spectrometers operate on vastly different principles. This gives them very different unique advantages and disadvantages, making them preferable in different situations for each type of spectrometer techniques. Fourier transform spectrometer has important applications in a diverse range of science fields ranging from fancy fundamental science in astronomy to pragmatic applicational science in chemistry. It is especially dominant in infrared spectroscopy where it is almost synonymous with infrared spectrometer.

One of the unique features of Fourier transform spectrometer is that it needs to go through relatively complicated data processing steps to obtain the spectral result. So, the data processing method is just as important as the hardware design. This thesis will study data processing method in Fourier transform spectrometer. Particularly, it will study a new data processing method based on the nonuniform Fourier transform equation. Nonuniform Fourier transform is a relatively newer signal processing technique which has been successfully applied in many fields and found to have many desirable properties. But it has not been experimentally studied in Fourier transform spectrometers. We will study the various properties of this new method and compare it with the traditional interpolation method by using a combination of theoretical analysis and experimental demonstration. In

addition, to support this study we devised and implemented a novel super high-resolution Fourier transform spectrometer which is a very notable innovation and achievement itself. The research result has been published in the journal Optics Communications.

This thesis will include seven chapters. Chapter 1 will introduce the historical background and relevant current research landscape in Fourier transform spectrometers. Chapter 2 will give the necessary basic theories of Fourier transform spectrometer such as the theory of light, Fourier transform equation, and principles of various optical elements etc. Chapter 3 will develop techniques to build a Fourier transform spectrometer such as the mirror alignment methods. Chapter 4 will develop the basic data processing methods to obtain the spectrum profile from a nonuniformly sampled interferogram result acquired from Fourier transform spectrometer. Chapter 5 will devise and build a novel ultra-high resolution nonuniform sampling Fourier transform spectrometer with a scanning length close to 5 metres and use it to measure the spectrum profile of some test light sources including a multimode laser and a broadband super luminescent light emitting diode. Chapter 6 will use this high-resolution spectrometer to study the properties of a new data processing method which is based on nonuniform fast Fourier transform and compare its advantages and disadvantages with the traditional interpolation method. Chapter 7 will discuss the properties of the various experiment hardware components used for this study and their implications to the experiment results.

Among these chapters, chapter 6 and 5 are the most important and they are the main innovations of this study. They together are published in the journal Optics Communications. Chapter 3 and 4 develop techniques to implement a nonuniform sampling Fourier transform spectrometer and although these cannot be considered as new inventions and therefore not publishable, yet they are not copies from other researchers but independent unique inventions by this study and should be useful for other researchers also implementing Fourier transform spectrometers. Chapter 7 is about properties of the particular equipment used in this study and analysing their influence on the experiment results. They are also likely not publishable results but they are important for making this study complete because it is important to know the properties of the equipment in order to properly understand the experiment results.

Chapter 1. Review of optical Fourier transform spectroscopy

1.1. History

In 1887 Albert A. Michelson and Edward W. Morley attempted to use a Michelson interferometer to detect the existence of luminiferous aether thought to be the carrier of light waves. This was the famous Michelson–Morley experiment which eventually paved the way for Einstein's famous theory of special relativity. This Michelson interferometer would be the key to the Fourier transform spectrometer technology. The interference pattern formed by the Michelson interferometer encodes the spectrum information of the light source and can be potentially used to determine the spectrum of the light source by using the mathematical technique of Fourier transform. This would be the principle of Fourier transform spectroscopy.

Michelson knew about this potential. But calculating Fourier transform requires a digital computer. It would be impossible to perform Fourier transform calculation by hand. So, Michelson invented a device that can simulate different combination of harmonic waves and generate the resulting wave pattern. This pattern is then used to compare with the inference pattern produced by the Michelson interferometer and the spectrum of the light source can then be determined through trial and error. Michelson used this method to determine the double emission lines of yellow sodium radiation as well as other materials. In fact, the Michelson interferometer was not invented to detect aether but to find a perfectly monochromatic emission source [1,2]. Michelson's solution is very genius but also has limited applicability. A proper Fourier transform spectrometer needs a computer to perform Fourier transform calculation and a photodetector to record the interference signal thus it cannot be realised until relatively modern times. The first Fourier transform spectrometer in modern sense was achieved in 1957 by Fellgett [2] and the first commercial Fourier transform infrared spectrometer arrived in 1969 [3].

The technology of optical Fourier Transform Spectroscopy finds its most success in the infrared region of light. Hence this term is also often associated with infrared spectrometry. Although Fourier Transform Spectrometer is a relatively old technology and its principle is arguably quite simple, the continuous subsequent emergence of newer technologies such as lasers, optical fibres, semiconductors, modern computers, etc continues to provide

improvements to this technology just as the way that the first digital computers and photodetectors enabled the realisation of this technology in the beginning. In 2021 a review paper titled 'Miniaturization of optical spectrometers' was published in the Science journal in which Fourier transform spectrometer is also covered [4]. The fact that such a paper about Fourier transform spectrometer appears in the top journal of science speaks to the volume how much this technology is still under active development.

Fourier transform spectrometer is a tool to analyse the frequency spectrum of a light source. This information can in turn help determine the molecular composition of a sample material etcetera. The subject of Fourier transform spectroscopy is a huge field after over half a century of development. It would be impossible to cover all aspects of the development of this field. Thus, this chapter will focus on covering related aspects of the topic in the literature that are most relevant to the research of this study and thesis.

1.2. Application

Fourier Transform Spectroscopy has found applications in a wide range of scientific and engineering fields including astronomy, chemistry, remote sensing, medical diagnosis, geological sciences, etc. Fourier transform spectroscopy is the most preferred type of technique among all the optical spectroscopy techniques in the infrared region. The majority of Fourier transform spectrometers operate in the infrared region. Hence Fourier transform spectroscopy and infrared spectroscopy are often associated with each other. But this does not mean that Fourier transform spectrometer can only be used for infrared region, Fourier transform spectrometers operating at ultraviolet region up to as short as 32nm wavelength has been reported in recent years [5,6].

Fourier transform spectrometer is very important in astronomy[7] and remote sensing [8] where it is used to study the composition, temperature, and other physical properties of celestial objects such as stars, planets, and galaxies, etc and to study the composition of the atmosphere or the Earth's surface for environmental monitoring, atmospheric science, and geology, etc. An example of use in remote sensing is greenhouse gas monitoring as in the case of the GOSAT-2 satellite which uses a Fourier transform spectrometer [9] and another example is industrial smokestack effluent monitoring [10]. The application in physics is most notable because it would represent the state of the art of this technology. For example, The

Herschel space telescope has a Fourier transform spectroscope onboard called SPIRE.[11] and the Canada–France–Hawaii Telescope observatory which is located atop the summit of Mauna Kea volcano mountain on the island of Hawaii has an optical imaging Fourier transform spectrometer called SITELLE in its instruments [12].

But the most classic use of Fourier transform spectrometer is analysing the composition of a sample material. It can be used to determine the chemical structure of complex molecules, detect presence of certain molecules in a sample, etc. It is this application that gives Fourier transform spectrometer the ubiquitous status. It has important uses in many fields in both commercial sectors and science research. For example, the U.S. Food and Drug Administration requires the pharmaceutical companies to submit IR spectra as part of their application as evidence of the putative chemical structure [3]. In polymer laboratories infrared spectrometer is the primary instrument for determination of molecular structure [3]. It is in medical diagnostics to study the composition of tissues and fluids in the human body for diagnosis of diseases such as cancer, diabetes, and Alzheimer's disease [13]. It is used to identify fossils in archaeology [14].

Thanks to this application in chemical analysis, Fourier transform spectrometer has been ubiquitous in the commercial landscape in a wide range of sectors for years and not just confining itself to science labs.

1.3. Design and comparison with alternative techniques

The most basic form of Fourier transform spectrometer is just a Michelson interferometer with a movable mirror. Figure 1 shows an illustration of such design in which the detector records the resulting interference signal generated by the movement of the moving mirror and the recorded interferogram is then processed by using the mathematical technique of Fourier transform to finally obtain the spectrum of the light source. So, the principle of Fourier transform spectrometer is quite simple. Yet it requires very sophisticated equipment such as a photodetector and a digital computer to perform Fourier transform.

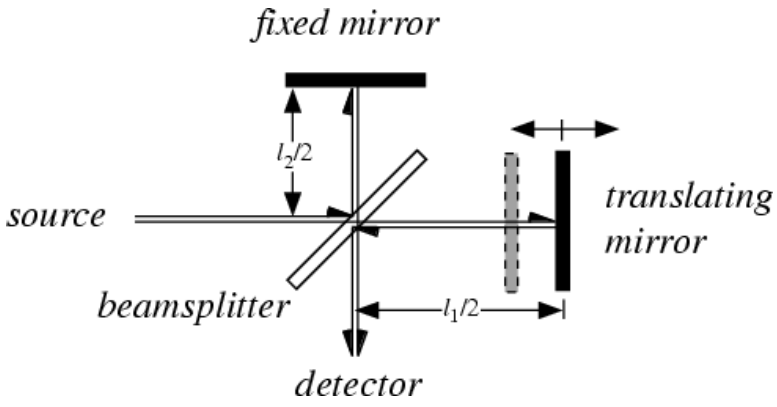

Figure 1 Schematics of the classic Michelson interferometer type of Fourier transform spectrometer. [15]

Fourier transform spectrometer is not the only optical spectroscopic technique, however. Figure 2 shows a diagram from the book *Fourier Transform Spectrometry* by Davis, S.P., 2001 illustrating the major alternative techniques to Fourier transform spectroscopy.

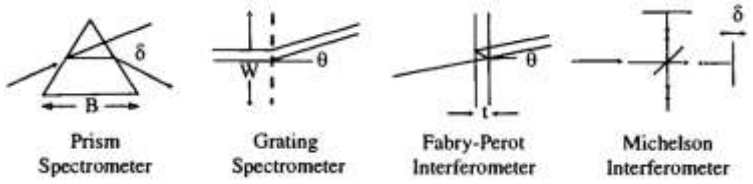

Figure 2 Block diagram of major optical spectrometer types. Source: [16]

The first type is to use a dispersive prism. This is probably the oldest type of spectrometric technique. It utilises the property that when a beam of light travels into another medium the direction of propagation can change and this change is frequency dependant for many materials. Hence, when a beam of light goes through this wedge shape prism, different frequency components will be bent at different angle and therefore will be separated. The drawback with this method is that the spectral resolution is typically low.

The second type is diffraction grating. A grating is a periodic comb-like structure. It works similarly to prism but is based on a totally different principle. It is based on the phenomenon of interference and diffraction. When a light beam shines onto a grating, different frequency components will refract at different angles. This is due to the Huygens–Fresnel principle. Every line of a grating is a source of light and the phase of these lines are correlated. As a result, light propagating at some angles will be constructively interfered to have maximum intensity while some angles will be destructively interfered, and these angles are frequency dependent. Hence the gratings can be used to separate different frequencies of a light. Grating usually have resolution better than prism as it is usually easier to create high

resolution grating patterns than to find high resolution material for prisms. They together are also categorised as dispersive spectrometers.

The third type is Fabry–Pérot interferometer. It also uses moving mirrors like Fourier transform spectrometer. But it is based on a totally different principle called optical resonance. It consists of two parallel partially transmissive mirrors which forms an optical resonator (optical cavity) whose resonance frequency depends on the distance between the two mirrors. When a beam of light passes through it, the light will bounce back and forth many times between the mirrors and only the resonant frequencies can eventually pass through it. Changing the distance between the mirrors will change the resonance frequency and that is how the spectrometer works. The shortcoming of Fabry–Pérot interferometer is that its resonance is not a single frequency but a comb of frequencies which would limit its usefulness for broadband light sources. More specifically, the spectral range of Fabry–Pérot interferometer is proportional to spectral resolution. Therefore, Fabry–Pérot interferometer cannot be used for light sources with broad spectral range without sacrificing the spectral resolution.

The above are the established optical spectrometer types that have seen countless applications. Other novel types may also exist. For example, over the past decade a new spectrometer paradigm has emerged which relies on computational techniques to approximate or “reconstruct” incident light spectra from pre-calibrated information encoded within a set of detectors [4]. In simple words, it is a computer aided brute force method that uses trial and error tactics by comparing the experimental result with predicted results from known spectral profiles to work out the spectral profile of the light source. It is reminiscent of the original method employed by Michelson to work out the double emission lines of yellow sodium radiation [1,2].

All of the traditional alternative spectrometry techniques work by separating different frequencies in one way or another. This makes the principle of Fourier transform spectrometer quite unique. One attractive feature of Fourier transform spectrometer is that there is no technical limit to how far the mirror can move which limits the maximum possible resolution and so it is relatively easier to achieve higher spectral resolution compared to other methods. Another much cited advantage by Fourier transform spectrometer is called the multiplex advantage or Fellgett's advantage. It means that when the detector noise is

independent of the light, Fourier transform spectrometer can achieve the same signal-to-noise ratio with much fewer number of measurements than dispersive spectrometer. This is because Fourier transform spectrometer measures all frequency components at once while dispersive spectrometer measures each frequency component one by one. In Fellgett's times when photodetectors were less advanced, this was a big deal. In addition, Fourier transform spectrometer also has the advantage of being able to utilise more amount of light and being able to measure the wavelength very accurately by using a monochromatic reference source with known frequency.

Finally, there are also many variants of Fourier transform spectrometers. Some of them can be very different from the classic moving mirror Michelson interferometer designs. Different components can enable different designs. For example, there are optical fibre-based designs that use mechanical stretching of optical fibres to generate optical path difference changes, there are designs that use rotation to generate optical path difference changes, there are variants that use wedge prism to generate optical path difference changes, and there are variants that use multipixel photodetectors to record the whole interferogram at once to eliminate the need for moving parts, etc [17,18,19,20]. All these variants work by generating and recording interference wave signal by one way or another and then Fourier transform the interferogram to obtain spectrum profile. Hence, they all share the name Fourier transform spectrometer and share similar data processing procedures even though they can look very differently. Different variants will have different advantages and disadvantages. In general, although there have been many novel designs, the classic moving mirror Michelson interferometer and its variants is still one of the most common designs and is the representative design of Fourier transform spectrometer.

In conclusion, there are many types of optical spectrometers and many variants of spectrometer designs. The Fourier transform spectrometer typically based on a movable mirror Michelson interferometer is one of the most important types of optical spectrometers both for now and for the foreseeable future.

1.4. Conclusion

This chapter reviews the historic development of Fourier transform spectrometer and the current landscape in their usage and comparison with alternative optical spectroscopy

techniques. It shows that Fourier transform spectrometer is a very important optical spectroscopic technology with a wide range of applications both for now and for the foreseeable future.

Chapter 2. Prerequisite Theories

This chapter will introduce the basic theories and knowledges necessary for implementing and studying Fourier transform spectrometers.

2.1. Fundamentals of light

This research mainly deals with the visible spectrum of electromagnetic waves -- light. The behaviours of electromagnetic waves are governed by a set of four equations called Maxwell equations. Maxwell equations were the culmination of centuries of research into electromagnetism [21,22]. From Maxwell equations all electromagnetic phenomena can be explained except in the realm of relativity theory and quantum mechanics. However, this project will not be needing either quantum mechanics or theory of relativity. This project will be about application of the optical interference phenomenon.

The four Maxwell equations, written in differential forms, are:

$$Gauss's\ law: \quad \nabla \cdot \vec{E} = \frac{\rho}{\epsilon} \qquad (1)$$

$$Gauss's\ law\ for\ magnetism: \quad \nabla \cdot \vec{B} = 0 \qquad (2)$$

$$Faraday's\ law\ of\ induction: \quad \nabla \times \vec{E} = -\frac{\partial \vec{B}}{\partial t} \qquad (3)$$

$$Ampère's\ circuital\ law: \quad \nabla \times \vec{B} = \mu\left(\vec{J} + \epsilon\frac{\partial \vec{E}}{\partial t}\right) \qquad (4)$$

Where $\vec{E}$ is electric field, $\vec{B}$ is magnetic field, ρ is electric charge density, $\vec{J}$ is electric current density, t is time, ϵ is a constant called electric permittivity, μ is another constant called permeability. When in the special case of vacuum the preceding two constants are customarily denoted as ϵ_0 and μ_0, respectively.

From Maxwell equations the electromagnetic wave equations can be derived. Historically it is the prediction and calculation of electromagnetic wave speed by Maxwell that revealed the nature of light [21,22]. The derived electromagnetic wave equations are:

$$\nabla^2 \vec{E} = \epsilon\mu \frac{\partial^2 \vec{E}}{\partial t^2} \qquad (5)$$

$$\nabla^2 \vec{B} = \epsilon\mu \frac{\partial^2 \vec{B}}{\partial t^2} \qquad (6)$$

These are in the form of wave equation that has been familial to people long before Maxwell's time [21,22].

The simplest solution to the electromagnetic wave equations is the plane wave. It is a sinusoidal transverse wave where both the electric field and magnetic field are perpendicular to the propagation direction and oscillates alone the propagation line. The magnetic component is perpendicular to its electric counterpart, and they are in phase with each other. The strength of magnetic field equals that of electric field divided by the propagation speed. Because of this simple relationship the magnetic part of an electromagnetic wave is often ignored in many cases. Light usually interacts with matter through electric field.

From mathematics we know that any form of electromagnetic waves can be considered as combinations of plane waves by using Fourier transformation. Hence the problem of electromagnetic waves is solved.

The propagation speed of electromagnetic waves is:

$$v = \frac{1}{\sqrt{\epsilon\mu}} \qquad (7)$$

2.2. Coherence

An ideal monochromatic point source is perfectly coherent, meaning that the phases of the light field at any point of space and any time are totally corelated. However, in real life light sources are far from perfect. This makes the concept of coherence very important.

There are generally two classifications of coherence, temporal coherence and spatial coherence. These two distinctions of coherence are not fundamentally different. They are created just for convenience. If a light source switches its phase randomly every time after a certain interval. This would result in an imperfect sinusoidal wave that reshuffles its phase randomly after a certain length. This is called **temporal coherence**. Temporal means related

to time. On the other hand, if the phases of light field at two points in space are corelated to each other, it is called **spatial coherence**.

Laser is a kind of light source with very good temporal and spatial coherence. Thus, lasers are usually the preferred tool for interference experiments.

2.3. Interference, Interferometry and Interferometers

2.3.1. Interference

When two or more corelated point sources illuminate a wall, a ripple like pattern can be observed. Such phenomenon is called optical interference. This property is due to the light being wave in nature. The principle of interference can be illustrated by a simple equation. Supposed that two coherent monochromic beams of light with the same polarization direction and amplitude but different in phase meet each other at one point. The resulting combined electric filed will be:

$$E\cos\omega t + E\cos(\omega t + a) = 2E\cos\frac{a}{2}\cos\left(\omega t + \frac{1}{2}a\right) \qquad (8)$$

Where E represents the magnitude of electric field and a is the phase difference between the two light waves. ω means the frequency of wave and t means the time.

We can see from the above equation that the resulting combined electric field is still a sinusoidal wave with the same frequency. But the strength of the field will depend on the phase difference. This phase dependant intensity is the reason why we observe ripple like patterns in interference phenomena.

A historically very important interference experiment is Young's double slit experiment [21,22]. In such an experiment a near monochromatic point source is first shined onto two slits of a wall where the two illuminated slits then serve as two corelated light sources and shine onto another wall behind to produce fringe patterns there. This experiment was first conducted to demonstrate the wave nature of light in 1801 and later when quantum mechanics arrives used to demonstrate the wave–particle duality nature of light [21,22].

2.3.2. Interferometry

Interferometry is a measurement method using the phenomenon of interference of waves (usually light, radio or sound waves). It is used to measure displacement changes, the

characteristics of the waves, or the materials that the waves interact with, etc. Interferometer is the piece of device behind interferometry. Optical interferometry has many important applications in science and technology. Optical interferometry has been a valuable measurement technique since its existence.

2.3.3. Michelson interferometer

Michelson interferometer is a historically very important kind of interferometer invented by Albert Michelson in 1881 [21,22]. It played a vital role in the development of special theory of relativity. Since then, other types of optical interferometers have been developed. However, Michelson interferometer remains a very important type of interferometer today.

The Michelson interferometer uses a beam splitter such as a half-silvered mirror to split a beam of light into two usually mutually perpendicular beams. These two beams are then reflected back by two mirrors and the two reflected beams will eventually converge onto a detector and form fringe patterns. Movement of one of the reflecting mirrors will result in periodic change of fringe patterns. This property can then be used to measure the wavelength of the wave. But in order to do so the mirror must be perpendicular to the beam. Michelson originally built such device to measure the wavelength change caused by the supposed aether but instead proved aether does not exit. The two split beams need not to be exactly perpendicular to each other depending on the specific experiment requirements. Michelson did not use lasers because lasers have not yet been invented and thus the very short coherence length of the source light must be considered. The paths of lights in Michelson interferometer look like a cross. The principle of Michelson interferometer is illustrated in the following figure.

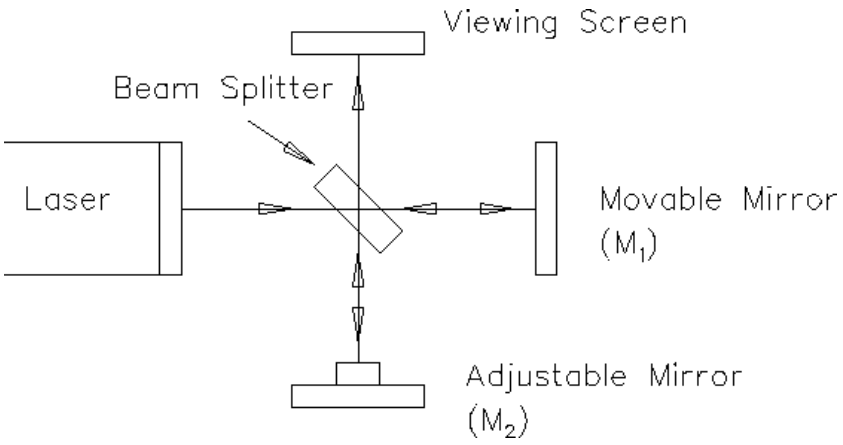

Figure 3 Illustration of a Michelson interferometer. Image from: [23]

2.3.4. Twyman-Green interferometer

There are many variants of Michelson interferometers. Twyman-Green interferometer is a variant that replaces the extended source with a point source in conjunction with a collimating lens. This is equivalent to using laser beam as light sources. The primary purpose of Twyman-Green interferometer is to detect imperfections in optical components.

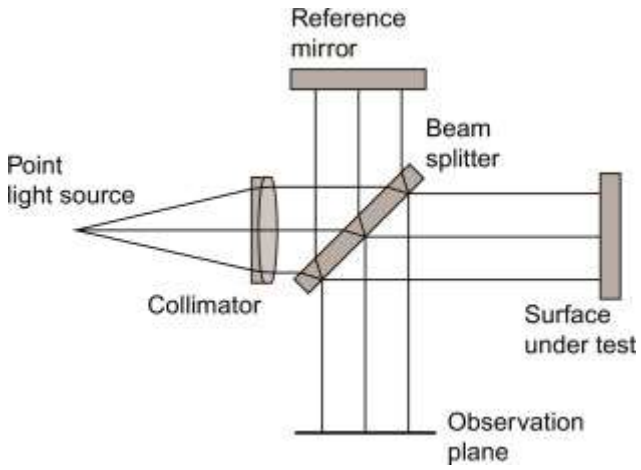

Figure 4 An illustration of Twyman-Green interferometer. Image source: [24]

2.3.5. Mach-Zehnder interferometer

Mach-Zehnder interferometer is another variant that the reflecting mirrors reflect lights at an angle such that the light paths form a square as shown in the following figure. It has application in aerodynamic research.

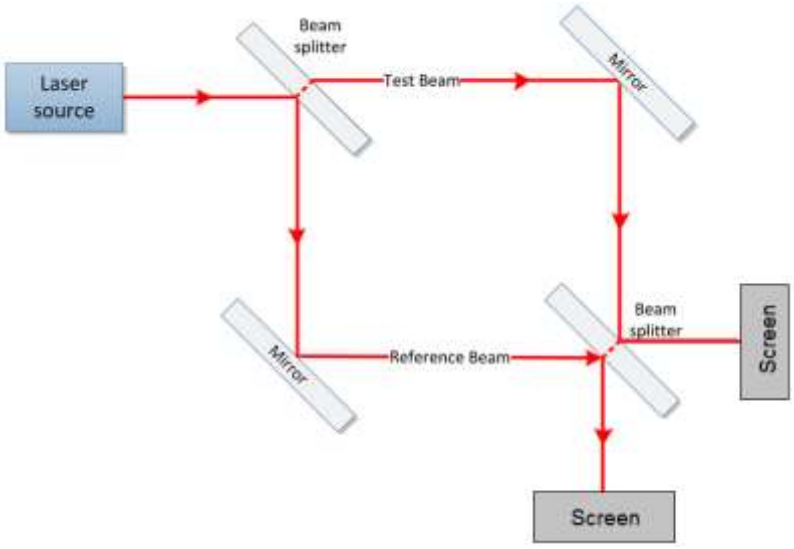

Figure 5 An illustration of Mach-Zehnder interferometer. Image source: [25]

2.3.6. Sagnac interferometer

Sagnac interferometer is a type more complex in principle. The setup also looks like a square. But this time the light travels in a closed loop. The two splitted beams will travel in the same loop but in opposite directions, clockwise and counterclockwise. When the interferometer sits still, no interference pattern can be observed. However, when the whole interferometer rotates, interference pattern would be observed. Thus, this type of interferometer can be used as gyroscope. The phenomenon of Sagnac interferometer is best understood in the context of special relativity. Although classical treatment can also obtain the interference formula correctly [21,22].

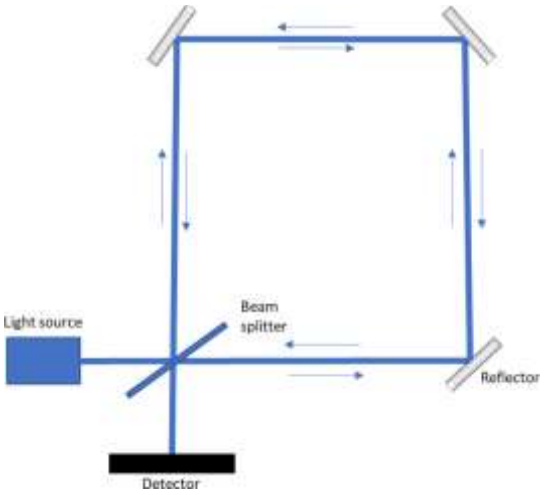

Figure 6 Sagnac Interferometer. Image source: [26]

2.3.7. Fabry-Perot interferometer

Fabry-Perot interferometer is a multiple-beam interferometer that uses two transparent parallel plates to produce interference pattern. It is a very versatile interferometer with myriad uses such as in precision wavelength measurement, determining refractive indices of gases, hyperfine spectral line analysis, etc.

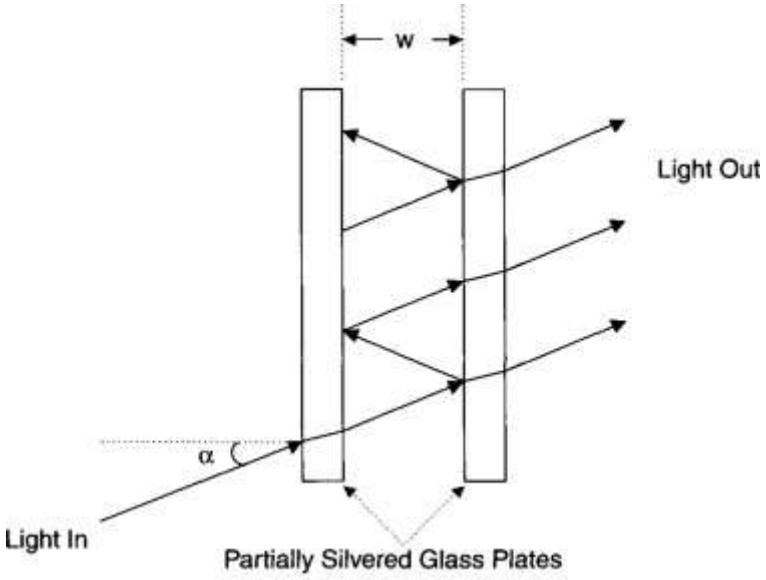

Figure 7 Illustration of Fabry-Perot interferometer. [27]

2.4. Fourier series and Fourier transformation

The interference pattern produced by the interferometers can be used to obtain the spectrum information with the mathematical theory of Fourier transform. This is the principle behind Fourier transform spectrometers.

2.4.1. Fourier series

Fourier series is the expansion of a periodic function into an infinite sum of sines and cosines. For a periodic function *f(t)* with period interval *[0, T]*, the Fourier series of it is:

$$f(t) = c_0 + \sum_{n=1}^{\infty} a_n \cos\frac{2n\pi t}{T} + \sum_{n=1}^{\infty} b_n \sin\frac{2n\pi t}{T} \qquad (9)$$

where,

$$c_0 = \frac{1}{T}\int_0^T f(t)dt \qquad (10)$$

$$a_n = \frac{2}{T}\int_0^T f(t)\cos\frac{2n\pi t}{T}dt \qquad (11)$$

$$b_n = \frac{2}{T}\int_0^T f(t)\sin\frac{2n\pi t}{T}dt \qquad (12)$$

The Fourier series can also be expressed alternatively in terms of the well-known Euler's formula, which states that $e^{ix} = \cos x + i \sin x$. This is called the complex Fourier series and would be more useful later:

$$f(t) = \sum_{n=-\infty}^{\infty} c_n e^{i\frac{2n\pi t}{T}} \qquad (13)$$

where,

$$c_n = \frac{1}{T}\int_0^T f(t) e^{-i\frac{2n\pi t}{T}} dt \qquad (14)$$

2.4.2. Fourier Transform

But for non-periodic functions the above Fourier series will not be usable. That is where Fourier transform comes in. Fourier transform is generalization of Fourier series to non-periodic functions by letting the period length in the complex Fourier series equation go towards infinity. When T goes towards infinity, $\frac{n}{T}$ becomes virtually continuous. Thus, we can let $\frac{n}{T}$ be v, $\frac{1}{T}$ be dv, c_n be $F(v)dv$, and we will arrive at the elegantly symmetrical Fourier transform and inverse Fourier transform equations:

$$f(t) = \int_{-\infty}^{\infty} F(v) e^{2\pi i v t} dv \qquad (15)$$

$$F(v) = \int_{-\infty}^{\infty} f(t) e^{-2\pi i v t} dt \qquad (16)$$

2.4.3. Nyquist sampling theorem

In practice it is usually impossible to record a wave signal continuously. They are often obtained by sampling at equal intervals. The **Nyquist sampling theorem** states that if we can sample waveform at a frequency at least twice that of the highest frequency contained in the waveform, then the full frequency spectrum of the waveform can still be obtained and the whole waveform can thus also be reconstructed. This can be more intuitively understood with the following derivation. Suppose that the frequency spectrum $F(v)$ of a wave function $f(t)$ is zero outside of the interval [-B/2, B/2], then according to the Fourier transform equation (15) we would have:

$$\frac{1}{B}f\left(\frac{n}{B}\right) = \frac{1}{B}\int_{-B/2}^{B/2} F(v)e^{2\pi i v\frac{n}{B}}dv \qquad (17)$$

Where $n = 1, 2 \ldots \infty$. But the above equation is also exactly the Fourier series equation for the periodic version of frequency spectrum function $F(v)$ with periodic interval [-B/2, B/2] and with coefficients $c_n = \frac{1}{B}f\left(\frac{n}{B}\right)$. Thus, the value of $f(t)$ sampled at $\frac{n}{B}$ points can fully reconstruct the wave spectrum.

Note however that this is the periodic version of frequency function and thus the shape of the frequency spectrum is not uniquely determined as the integration interval can be placed anywhere. But we can take advantage of the fact that the frequency spectrum must be symmetric if the wave function is real to determine the period position of the frequency spectrum.

This completes the proof.

2.4.4. Discrete Fourier transform

Suppose that the frequency spectrum is not only bandwidth limited but also discrete that it is essentially a modulated Dirac comb function. Then the sampled data will also become periodic. Thus, both data and frequency are therefore finite (or periodic) and discrete. This is called **discrete Fourier transform**. And equation (17) turns into a summation:

$$f\left(\frac{n}{B}\right) = \sum_{k=1}^{N} F\left(\frac{B}{N}k\right)e^{2\pi i\frac{kn}{N}} \qquad n = 1,2 \ldots N \qquad (18)$$

And the inverse discrete Fourier transform of it is not difficult to derive (or verify) through a process analogous to that for the continuous Fourier series:

$$F\left(\frac{B}{N}k\right) = \frac{1}{N}\sum_{n=1}^{N} f\left(\frac{n}{B}\right)e^{-2\pi i\frac{kn}{N}} \qquad k = -\frac{N}{2}, \ldots, \frac{N}{2} \qquad (19)$$

The **discrete Fourier transform** is the actual transform we would use for Fourier analysis in real life applications. Direct computation of discrete Fourier transform would be too costly because the computation time scales with the square of number of sample points. The specific method to carry out discrete Fourier transform (DFT) calculations is **fast Fourier transform** (FFT) and these two terms have become largely synonymous with each other.

Usually, the frequency distribution is continuous, so using discrete Fourier transform would only be an approximation to the actual continuous Fourier transform. The errors introduced by this approximation can be more clearly grasped with the following equation which rewrites equation (17) by dividing its integration into $N = 2K + 1$ segments, where *N, K* are positive integers,

$$f\left(\frac{n}{B}\right) = \int_{-\frac{B}{2N}}^{\frac{B}{2N}} e^{2i\pi v\frac{n}{B}} \left[\sum_{k=-K}^{K} F\left(v + \frac{B}{N}k\right) e^{2i\pi\frac{kn}{N}}\right] dv \qquad (20)$$

From the above rewritten Fourier transform equation we can see that errors can be reduced by increasing both the sampling rate and the sample size.

2.4.5. Nonuniform discrete Fourier transform

The definition of discrete Fourier transform requires the samples to be taken at exactly the same intervals. But in real life situations the samples obtained may be irregularly spaced. Non-uniform Fourier transform (NUDFT) is created to deal with such scenarios. Non-uniform discrete Fourier transform is the non-uniform variant of the regular discrete Fourier transform (DFT). It is defined by the following equation:

$$F(v_k) = \sum_{n=1}^{N} f(x_n) e^{-i2\pi v_k x_n} \qquad k = 1,2 \ldots M \qquad (21)$$

where v_k represents frequency at the k-th spectral point, x_n represents the position of the *n*-th sampling point, $f(x_n)$ represents the signal strength at the sampling position x_n, and $F(v_k)$ represents the spectral strength at the frequency v_k.

In fact, the discrete Fourier transform can be considered a special case of non-uniform Fourier transform when all positions and frequencies are distributed uniformly. When all points are distributed uniformly the equation of nonuniform Fourier transform becomes the same as the equation of discrete Fourier transform. Non-uniform discrete Fourier transform is inherently not exact. There is no continuous counterpart to it so the word discrete is often omitted from the name of non-uniform discrete Fourier transform. The frequency spectrum obtain from it will inherently not be the same as original. Nonuniform discrete Fourier transform can be categorised into three types. The first type has uniform sampling points but has nonuniform frequency points. The second type has nonuniform sampling points but

uniform frequency points. The third type has both nonuniform sampling points and frequency points. From mathematical point of view these three types are all the same. But from the computational point of view, it is very important to distinguish the three types because each type allows for different kind of optimisation techniques which are very important for practical purpose. Software libraries usually offer separate function interface for different types. In this research we are only concerned with the case where samples are unevenly distributed.

As with the case of the discrete Fourier transform, practical computation requires a fast algorithm. The fast algorithm is called non-uniform fast Fourier transform (NUFFT).

2.4.6. Resampling by Interpolation

Besides the non-uniform Fourier transform, there is another more straightforward way to deal with unevenly spaced data which is resampling by interpolation. It simply uses the mathematical technique of interpolation to convert the data into uniform ones so that the regular discrete Fourier transform can be used. This method has the practical advantage of having no additional software requirements compared to the alternative non-uniform discrete Fourier transform method because developing a fast non-uniform Fourier transform algorithm is not an easy task.

Many interpolation methods can be used. The simplest interpolation method would be linear interpolation. But in most cases, this is not the best choice. Cubic spline is one of the most common and popular alternatives to linear interpolation. Generally, the algorithm of most interpolation except linear interpolation methods are quite complex and it is beyond the scope of this study to investigate the technical details of them.

2.4.7. Analytic signal

The complex Fourier transform of any real valued waves is Hermitian symmetric, which means that the positive frequency component coefficients are always the complex conjugate of their negative counterparts. This suggests that the negative parts the frequency spectrum are redundant and can be removed without loss of information.

If we remove the negative part of the frequency spectrum from the original waveform function, we will obtain a complex valued function which is called the analytic signal. Specifically, the analytic function is defined as:

$$z(t) = f(t) + i\mathcal{H}[f(t)] = f(t) + \frac{i}{\pi}\int_{-\infty}^{\infty}\frac{f(u)}{t-u}du \qquad (22)$$

Where the symbol $\mathcal{H}$ represents Hilbert transform. It is essentially a convolution with function $\frac{1}{\pi t}$. It has the property of multiplying the positive frequency spectrum by i and the negative spectrum part by $-i$ while the zero-frequency component is zeroed out. Hence the resulting analytic signal function has no negative and zero frequencies.

2.5. Common optical elements

2.5.1. Plane mirrors

Plane mirror is the most basic type of optical components and is used by people every day. Its function is to reflect the light. It will change the direction of the light such that the component of propagation direction that is perpendicular to the mirror plane will be reversed while the component that is parallel to the mirror plane will be unchanged. A mirror is usually made by a thin film of metal with very flat and smooth surface.

2.5.2. Beam splitters and half-silvered mirrors

Half-silvered mirrors are plane mirrors that reflect light only partially and will let the remaining light transmit through it. The result is that a light beam will be split into two mutually coherent ones. It is the key component for Michelson interferometers. Beam splitters have the same function as half-silvered mirrors. But it uses different principle. It is based on the principle that light will be partially reflected when it goes from one type of transparent medium to another type of transparent medium. Beam splitters and half-silvered mirrors are usually designed to split light equally. But other variants also exist. For example, there are beam splitters that will split the light according to polarization directions.

2.5.3. Cube corner retroreflectors and right-angle prisms

Cube corner retroreflectors three pieces of plane mirrors placed perpendicular to each other. The function of it is to reflect the light such that the reflected light will be parallel to the incident light beam but not coinciding with it. It is a very useful component for Fourier transform spectrometer designs. Cube corner retroreflectors can also be made from cube corner prisms that will reflect the light using the total internal reflection principle. Figure 8 shows the principle of the retroreflector.

Figure 8 An illustration of the principle of a retroreflector.

Right-angle prisms and right angle rooftop mirrors are two dimensional version of cube corner retroreflectors. They are used in Martin-Puplett type of Fourier transform spectrometers.

2.6. Conclusion

This chapter introduces the necessary mathematical and theoretical backgrounds to Fourier transform spectrometer technology including Fourier transform theory, theory of light, and principle of various relevant optical components, etc. These theoretical knowledges are necessary for building and studying a Fourier transform spectrometer.

Chapter 3. Building the First Fourier Transform Spectrometer

In this chapter, we will try to build the first Fourier transform spectrometer in the lab for this project. We will build a classic nonuniform sampling Fourier transform spectrometer of the Michelson interferometer type with a scanning length of 2.5 centimetre. We will use this interferometer to obtain the interferogram of a 632.8 nm monochromatic helium neon laser and use this interferogram to help us develop the corresponding data processing technique and software programs for the nonuniform sampling Fourier transform spectrometer. We develop methods to align the mirrors properly in ways that is necessary for Fourier transform spectrometers. The experience gained in building this test Fourier transform spectrometer will allow us to build more advanced Fourier transform spectrometers later in subsequent chapters.

3.1. Introduction

In order to study the technology of Fourier transform spectrometer, we need to design and build a Fourier transform spectrometer first. Before going into the detail of the experiment, it is necessary to review the design of Fourier transform spectrometer a bit. The first thing to come to people's mind when it comes to building a Fourier transform spectrometer is how to move the scanning mirror at constant speed because the definition of discrete Fourier transform requires that the sampling points are to be spaced at equal distance. The first Fourier transform spectrometers were designed to operate just like that with constant mirror moving speed and sampled uniformly. But this is far easier said than done because the wavelength of a light is very short. Any slight deviation in the mirror moving speed can greatly degrade the quality of the resulting spectral profile. One of the reasons that the first Fourier transform spectrometer operates in the far infrared region is that longer wavelength has better tolerance to the errors in the mirror moving speed. Far infrared light's wavelength is between one to three orders of magnitude longer than that of the visible light.

Several solutions had been come up to address the difficulty in maintaining a constant mirror moving speed. One of the solutions is to use a pendulum to move the mirror. The classical Fourier transform spectrometer uses linear motion to change the position of the mirror. But the friction at different position can be different which would cause unpredictable variations

in the mirror moving speed. By contrast, a pendulum uses rotational motion which will have a more constant friction. Though the theoretical moving speed of a pendulum is not be exactly constant. But it will be at least more predictable compared to the classical method. In our lab there is an old long broken PerkinElmer Spectrum 1000 FT-IR Fourier transform spectrometer and it uses a pendulum to move the mirror of the Michelson interferometer inside it. But the drawback with pendulum is that it is much more difficult to achieve longer scanning length than simple linear motion Fourier transform spectrometer. Thus, rotational motion cannot replace the traditional method completely. Another solution is to use a movable wedged prism to generate optical path difference change [19]. This although is also an imperfect solution will have better tolerance to moving speed variations.

In the initial days of Fourier transform spectrometer laser technology was not yet available. Later, the availability of monochromatic laser source such as the common helium neon laser provides more possible solution by enabling detection of the mirror moving speed in real time very precisely. One such solution is to use an active feedback control loop and the real time moving speed information to maintain the speed precisely. This is only possible with the availability of monochromatic lasers. Usually, the 632.8 nm frequency stabilised helium neon laser is the laser of choice. In such a method, a monochromatic laser is used to generate a control signal whose real time frequency depends on the mirror moving speed. This control signal is then fed into a control circuit which will adjust the motor speed accordingly. An example of such design is given in the reference whose implements was a fibre-based Fourier Transform Spectrometer [20]. And there is another variant to the above method. Instead of actively adjusting the moving speed, this method would use the real time mirror moving speed information to adjust the sampling rate dynamically so that the net effect is that the sample points are spaced evenly in the optical path difference space. An example is given here [5]. This method is easier to implement than the brute force method of trying to maintain a constant mirror moving speed.

Finally, a very clever method was realised around 1990s [28]. It was realised that the monochromatic laser can not only be used to detect mirror speed in real time but can also be used to record the sample position directly. And it is not necessary to sample uniformly if we can know the position of the sample points. We only need to ensure that the average sampling rate is above the Nyquist rate. A uniform sample set can be obtained by resampling

from the nonuniform raw data using the mathematical technique of interpolation. The key principle behind this method is that the interferogram of an ideal monochromatic laser is just a simple cosine wave. And the position or distance travelled can be easily determined from this cosine wave signal. This method is also referred to as Brault's algorithm [16]. An example of this solution is given here [6,11].

This is a very important innovation because it can drastically reduce the hardware requirement of the Fourier transform spectrometer and to provide more flexibility in the design of Fourier transform spectrometers. It can lower the cost of Fourier transform spectrometer and enable it to operate in more environments. It is so useful that another company even tried to patent it even though this method has been published in the literature. Compared to previous methods, nonuniform sampling has the advantage that it does not require special-built hardware. Readily available off shelf standard components can be sufficient while previous methods would require specially built circuits or very expensive vibration isolation equipment. It is less sensitive to environment vibration and thus can operate in more situations. Nowadays, although the most advanced instruments may still choose uniform sampling methods, more implementations would use nonuniform sampling and interpolation method.

Although this lab does not have the capacity to build unform sampling Fourier transform spectrometers, it is very worthwhile to study the property of nonuniform sampling Fourier transform spectrometers and the data processing techniques of it because as has shown previously nonuniform sampling Fourier transform spectrometer has established itself as a very important subcategory of Fourier transform spectrometers.

3.2. Design

Figure 9 shows a picture of the first test Fourier transform spectrometer we built for this chapter. It is just a simple Michelson interferometer with one movable mirror. The movement of the mirror will generate an interference signal at the receiving end of a photodetector.

The movable mirror is mounted on a linear translation stage driven by an electric motor. The linear translation stage has a maximum range of 25 millimetre and would move at a roughly constant speed of about 0.2 millimetre per second. This moving speed is not adjustable. The electric motor has a built-in position sensor and is connected to a computer which has a

dedicated software controller interface for it. The controller interface can monitor the motor position error in real time. Since the purpose of this Fourier transform spectrometer is only for testing, the light source used here is just a monochromatic helium neon laser Melles Griot 05-LHR-991 with a wavelength of 632.8 nm. The photodetector used here is a single pixel photodetector Thorlabs PDA100A-EC Switchable Gain Detector with an operation range of 340 nm-1100 nm. This photodetector has several gain level settings ranging from 10 dB to 70 dB. It will output an analog signal. A data acquisition device which is a National Instrument USB-6341 X series Multifunction I/O Device is used to convert / sample the analog signal output by the photodetector into discrete digital signal and be sent to the computer. It has a maximum sampling rate of 500KHz. The software interface to this USB data acquisition device is National Instrument LabVIEW 2011. Additionally, we have an optional light intensity regulator which is not shown in the picture to avoid adding unnecessary confusion that can dim the light by several different levels.

The data acquisition device will sample the signal at a fixed rate in time domain while the mirror does not move exactly with constant speed. Hence, this is a nonuniform sampling Fourier transform spectrometer.

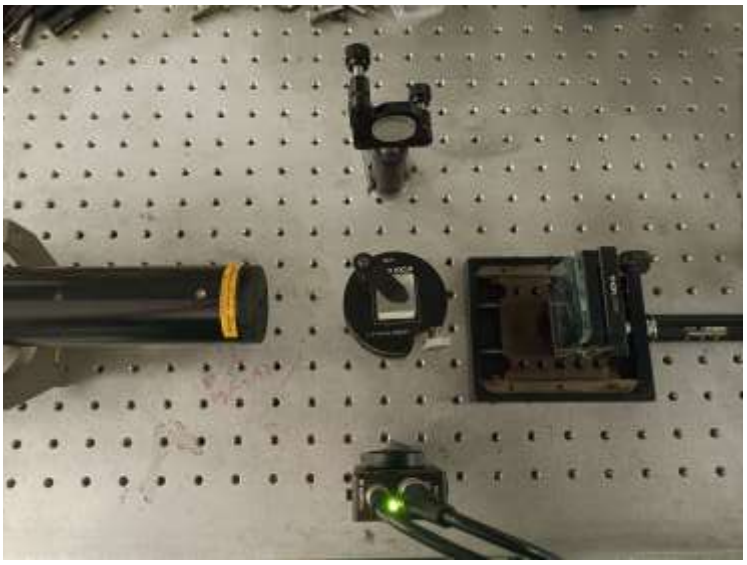

Figure 9 Photograph of the Michelson interferometer type Fourier transform spectrometer used in this experiment.

3.3. Alignment

The design of this Fourier transform spectrometer is certainly basic. The main challenge lies in developing appropriate methods to align the mirrors properly. This is not as simple as it seems. It requires a good understanding of the various principles of light. If one just makes

alignments blindly without proper understanding of the principles of Michelson interferometer and Fourier transform spectrometer, chances are that he/she will never stumble upon the correct alignment because there are simply too many combinations. If the mirror is not aligned properly, the interference signal will have a much weaker amplitude meaning that most of the input light would be wasted. This will greatly reduce the efficiency, resolution, and signal to noise ration of the spectrometer. Thus, it is essential to develop proper mirror alignment techniques if we were to build a Fourier transform spectrometer for practical purpose.

The key is to ensure that the mirror surface is perfectly perpendicular to the incoming light beam so that the reflected beam will travel back along the same path as the incoming beam. Otherwise, the reflected beam will change positions when the linear translation stage moves. This is the key difference between the classical static Michelson interferometer and Fourier transform spectrometer. Michelson interferometer does not require the mirrors to be perpendicular to the light beam and it has much higher tolerance for misalignments since the mirrors are stationary. Hence, it is much easier to align than Fourier transform spectrometer. For Fourier transform spectrometer, even a minor misalignment can turn into huge misalignment when the mirror moves from one end to the other end. Hence, even though the Michelson interferometer and Fourier transform spectrometer looks to be the same, their alignment methods are completely different.

The first step is to adjust the beams approximately. The beams will form very faintly visible traces in the air and on the surfaces of the beam splitter due to refraction, imperfections in beam splitter and tiny particles in air. This phenomenon can be used to align the beams approximately so that both beams hit the same spot in the photodetector roughly. The next step is to adjust precisely. This is done by starting up the motor to move the mirror and observe if the corresponding beam will change positions in the photodetector. If there is no visibly discernible change in positions, it means that the movable mirror has been aligned perfectly. If not, the orientation of the mirror is adjusted. It is also necessary to determine which direction to change the mirror. One direction will worsen the misalignment while the other will reduce the misalignment. Figure 10 shows an illustration of the effects of misalignment which is used to help determine which direction and how much to fine tune the mirror. This process is repeated until desired accuracy is reached. Finally, the stationary

mirror is adjusted by using the beam from the movable mirror as a reference. The adjustment procedure usually takes a very long time because the electric motor in this case can only move very slowly and there is no possibility to move the linear translation stage manually.

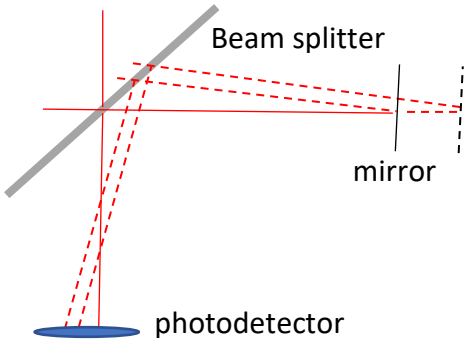

Figure 10 Illustration of the effect of mirror misalignment.

3.4. Data acquisition

LabVIEW 2011 is the software interface to acquire and store sample data into a file for later use. It is actually a programming environment. It is used by engineers to develop automated research, validation, and production test systems. It is a graphical programming environment. The programming works by adding different pre-existing built-in coding blocks together and connecting them in appropriate ways. Each coding block has some parameters that can be changed by the user. For this experiment, a basic example of the graphical code looks like the following:

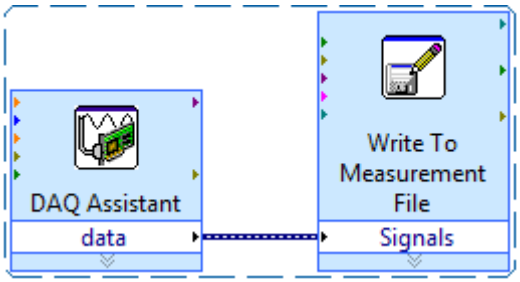

Figure 11 An example of the graphical code to record experiment data

It consists of two building blocks. The first block named ''DAQ Assistant'' will acquire data from the data acquisition device and the second block called ''Write To Measurement File'' will output the acquired data to a file. The tiny arrows on these blocks indicate data flow direction. We can change things such as sampling rate and file format through the parameters of these blocks. Overtime we will develop more complicated codes to address different needs. But the basic principle remains the same as the above example.

LabVIEW can actually do much more than basic data acquiring. But for some reasons it never worked as well as we wanted. So, we would only use it for acquiring data and use Python to do data processing.

3.5. Data processing

Obtaining the interference signal data is only half the story of Fourier transform spectrometer. The raw interferogram data must be processed into spectrum profile through Fourier transform in order for it to be useful. In this section, we will develop the software codes to read the acquired data and perform Fourier transform on it.

First, we need to decide which programming language to use. Python is currently one of the most, if not the most popular programming language in science community. There are many useful software libraries for science such as NumPy, SciPy, Matplotlib, etc in Python. The advantage of Python is that it is completely free and open source as opposed to most of its popular alternatives which are not free and expensive. Thus, we pick Python to be the programming language to develop our data processing code. We will find out later that there are many advantages by choosing python.

After settling on Python, the first step is to develop codes to read data from the data file to do calculations on it. The LabVIEW program will store the data into two types of file formats. The first type is LVM format, and the second type is TDMS format. The LVM format is essentially just a text file, and it is piece of cake to find solutions to read data from it. However, the second TDMS format is a proprietary format by National Instrument and many programming platforms lack readily available solution to read data from such file. But we found that there is a third-party Python library called npTDMS that can just do that. This is where the advantage of Python manifests itself. Due to the popularity of Python in science, we can confidently say that if there is no available solution to read TDMS file in Python, no other programming languages will have it either. It turns out later that when the sampling rate is relatively high, such as the second example given in the previous section, we will have to use the TDMS format in LabVIEW. Had we picked a different programming platform in the beginning, we may later find out that we need to switch to Python and rewrite every line of code again which would be such a huge waste of time.

NumPy is the de facto standard library for data science in Python and the backbone to many other higher-level libraries such as SciPy and Matplotlib. SciPy is a standard library that provides functions for science such as Fourier transform and interpolation. The algorithm of fast Fourier transform is a hugely complex mathematical problem. It is beyond our capability to develop ourselves. Thus, it is essential for us to rely on third party solutions. After calculation we need to plot the calculated result into graphs. Matplotlib is the standard library to draw math graphs.

The general data processing steps is then the following. First read data from file using npTDMS. Then use the SciPy's fft function to perform Fourier transform calculation. Finally use Matplotlib to plot the result into graphs.

3.6. Results

Figure 12 shows the resulting nonuniformly sampled interferogram of the 632.8nm helium neon laser and a zoom in segment of it. It can be seen from the zoom in figure that the sampling rate is very low. The sampling rate of the data acquisition device is set to 2 KHz in time while the average moving speed of the mirror is about 0.2 millimetre per second. This translates to an average sampling interval of about 200 nm in optical path difference domain which is just above the Nyquist rate. It can also be seen that the amplitude envelop of the interferogram is largely stable throughout the scan and that the minimum intensity is close to zero while the maximum is close to twice the mean value of the interferogram. The amplitude envelop increases slightly over time and there are also several smaller local variations.

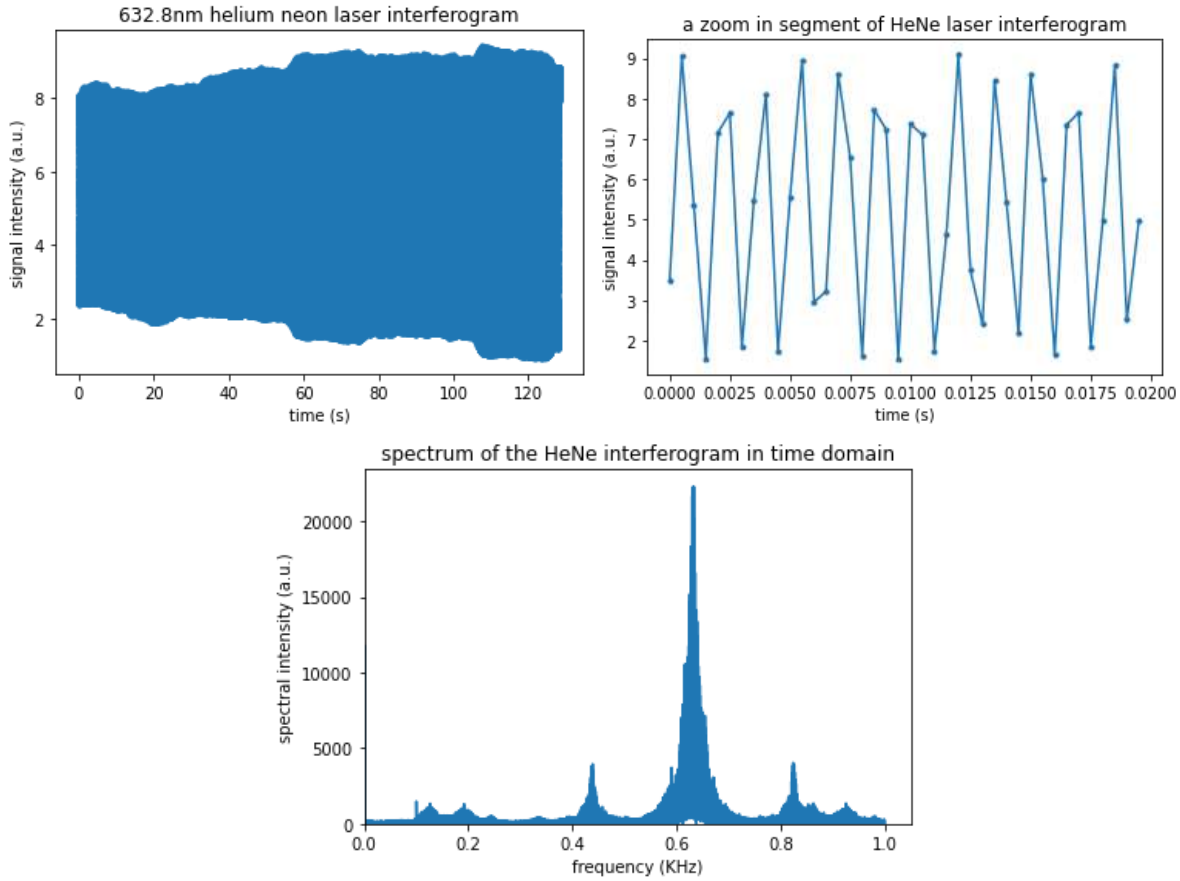

Figure 12 An example of the obtained 632nm helium neon laser interferogram(top left) and a zoom in segment of it(top right) as well as the Fourier tranform of this nonuniformly sampled inerferogram(bottom). The sampling rate is set to 2 KHz while the linear translation stage speed is fixed at 0.2mm/s.

Next, we dismantle the interferometer and rebuild it again to repeat the measurement. This time we set the sampling rate to five times higher to 10 KHz. The result is shown in Figure 13. It can be seen that the signal is clearly a sinusoidal wave. But the signal frequency is not constant because the mirror moving speed is not constant. This profile exhibits similar characteristics as the previous example.

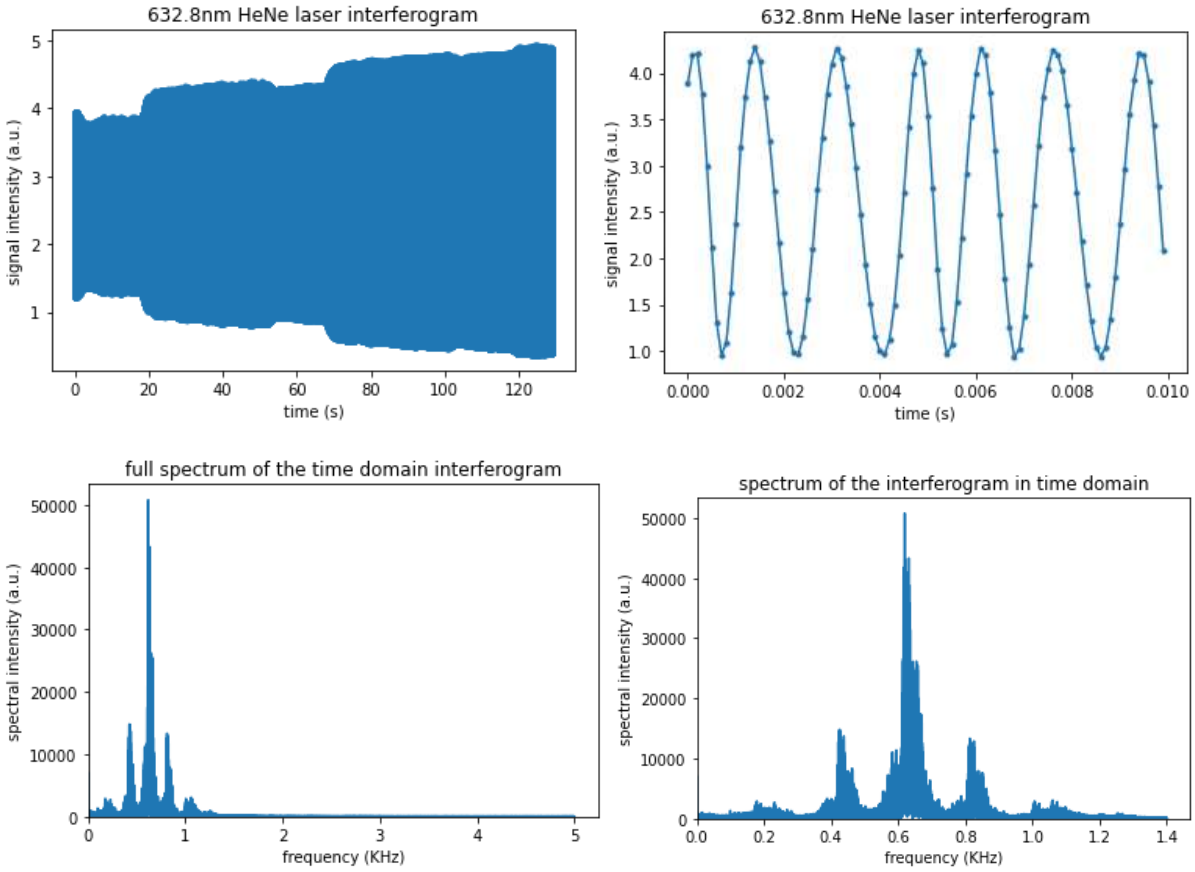

Figure 13 Another more densely sampled example of the helium neon laser interferogram(top left) and a zoom in segment of it(top right) as well as the Fourier tranform of this nonuniformly sampled inerferogram(bottom left) and the nonzero part of it(bottom right). The sampling rate is set to 10 KHz while the linear translation stage speed is fixed at 0.2mm/s.

3.7. Discussion

It can be seen from the interferogram figure that the lowest point of the interferogram is close to zero while the maximum value is close to twice that of the mean value of the interferogram. This is indication that the mirrors of this interferometer have been aligned very well. According to the theory, the minimum value should have been zero in the ideal scenario because the two beams will completely cancel each other out. But the lowest point of the interferogram in above experiment results never reaches zero.

This does not necessary mean that there remain some misalignments with the mirrors. There can be other reasons for that. One of the potential reasons is that the movable mirror did not cross the point where the optical path difference between the two beams is zero. This is because we did not pay attention to making the lengths of the two arms of the interferometer equal at some point of the scan when building this spectrometer since we are using laser source only for this experiment and with laser sources there is no need to cross the zero

optical path difference point to generate a strong interference signal. The size of a beam of a laser or any optical sources will increase as it travels due to diffraction. As a result, When the optical path lengths of the two arms are different, the diameters of their spot on the photodetector will be different. Hence, the minimum value of the interference wave cannot reach zero when the optical path difference is not zero. It should be mentioned here that the reception area of the photoreceptor is larger than the size of the laser beam in this experiment.

The amplitude of the interference wave in the experiment result is also not constant. It tends to increase linearly over time overall. Again, apart from possible mirror misalignments, this can also be explained by different lengths of the two arms of the interferometer. In addition, there are also many smaller irregular local variations in the signal amplitude. There are two possible reasons for this eccentric fluctuation, one is that the output intensity of the helium neon laser is not constant. This is the general characteristic of the laser product used in this experiment. It takes a long time to reach a more stable state, which we usually do not bother to wait for. And it may never reach a state where the amplitude does not fluctuate even if we wait indefinitely. The second possible reason is the vibrations of the mirrors or the linear translation stage during their movement. The electric motor of this experiment is very noisy and will certainly generate a lot of vibrations. This can cause temporal misalignments during the scanning process.

Finally, this chapter also calculates the Fourier transform of the interferogram in time domain. It shows that the direct time domain Fourier transform of a nonuniformly sampled interferogram is not directly useful because the spectrum will be heavily broadened and distorted. Thus, some more processing is required.

3.8. Conclusion

This chapter has successfully developed techniques to build a classic Michelson interferometer type of nonuniform sampling Fourier transform spectrometer with a moderate resolution. The techniques developed in this chapter will be useful for subsequent studies.

Chapter 4. Developing the method to determine sampling position and obtain spectrum profile

The data processing technique for nonuniform sampling Fourier transform spectrometer is an order of magnitude more complicated than the conventional uniform sampling Fourier transform spectrometers. But it has the advantage of simplifying hardware designs. The most important part which cannot be bypassed in nonuniform sampling Fourier transform spectrometer is to determine the sampling point positions of the obtained interferogram. Afterwards methods will exist to process the nonuniformly sampled interferogram into spectrum of the light source. This chapter will develop such a sample position determination scheme suitable for this research.

4.1. Introduction

One of the uniqueness of Fourier transform spectrometer over other optical spectroscopy techniques is that the hardware is only half of the story. The directly obtained raw interference data is usually useless without proper transformation. The data processing methods and the design of the instrument are equally important. An appropriate data processing technique can greatly simplify the design of the instrument while the design of instrument determines the corresponding data processing methods. By comparison, other optical spectroscopy techniques usually obtain the spectrum profile directly and there is minimal need to do data processing.

In the previous chapter, we have calculated the time domain Fourier transform of the nonuniformly sampled interferogram data. It shows that direct Fourier transform of the nonuniformly sampled data is mostly useless for analysing the spectral content of the light source because the spectral lines will be heavily broadened. It can be seen from the figures in the previous chapter that the spectral profile of the helium neon laser has been broadened by at least 50 percent. And this broadening is very irregular. The spectral amplitude varies between zero and the maximum possible value randomly and widely within the broadening range. Thus, a proper data processing technique is required to obtain proper spectral profile of the helium neon laser source with nonuniform sampling Fourier transform spectrometer.

Of course, such methods have been found and reported before in the literature [28,29,30]. The principle is that the interferogram from an ideal monochromatic source is just a simple

cosine wave. And the position of each sampling point in optical path difference domain is just the phase of the cosine wave divided by the frequency of the wave. The phase of a cosine wave is very trivial to obtain. It is just some simple middle school math. It can be obtained by the inverse cosine function arccosine. After the sampling position is determined, we can use the mathematical technique of interpolation to predict the signal value of the interference signal at any position we want. As a result, we can resample the data into a uniformly sampled one. This step is also trivial. If we use the simplest type of interpolation method linear interpolation, then even a primary schooler can figure out how to do it. The above is just the general principle of the data processing technique for nonuniform sampling Fourier transform spectrometers. The actual implementations are more complicated than that and there are many variants of it. For example, we need to take into account that real world interferograms are usually less ideal than an ideal cosine wave.

The phase of helium neon laser is not the only way to determine the position of sampling points. There are many more novel ways. For example, in this example of an ultraviolet Fourier transform spectrometer it uses a grating to determine the position [6]. And in this example of a static Fourier transform spectrometer the nonuniform sampling positions are calculated rather than measured [17]. All nonuniform sampling Fourier transform spectrometers need to determine the position of the sampling points through one way or another.

In this chapter, we will try to develop the according data processing technique and programs for this study. It will be similar in principle to the methods reported in the literature. But they are also not copies of each other and differ in many crucial aspects. The data processing technique developed in this chapter and the experience we gain in aligning the mirrors will allow us to build more advanced Fourier transform spectrometers in the later chapters.

4.2. Method

For an ideal monochromatic light source, the interference signal will be a cosine function and its phase will be proportional to the optical path difference. Hence, to determine the optical path difference at each sampling point will be equivalent to determining the phase of a monochromatic signal.

The simplest method would have been to do inverse cosine calculation on the sample in the case of ideal cosine wave. However, in practical situations such as in our experiment direct use of the inverse cosine function is not possible because the obtained interferogram is usually not ideal even though the helium neon laser is considered monochromatic. The amplitude of the interference signal will vary during the scan due to many reasons such as the divergence of the light beam as it propagates, slight misalignments of the movable mirror as it moves, intrinsic variations in output intensity of the laser in time, limited coherence length of the light source, and ambient pollution lights etc.

To address this issue, this study chose to develop a more complicated but also more versatile method based on the instantaneous phase of the time domain analytic signal of the helium neon laser interferogram. This method also has other benefits. The analytic signal is a complex valued signal containing only the positive frequency part of the spectrum of the real signal. The analytic signal will always contain the same information as the real signal because the spectrum of a real value signal is always symmetric with equal negative and positive parts according to the theory of Fourier transform. But calculation of the instantaneous phase of the analytic signal will not be affected by amplitude variation as opposed to the original real signal because it does not involve inverse cosine function. The time domain analytic signal can be obtained by first removing the negative part of the time domain spectrum of the interferogram and then perform an inverse Fourier transform on the resulting spectrum. Thus, in total two Fourier transform calculation needs to be performed. Now if we assume that the instantaneous phase of this analytic signal is the same as the phase of the original signal, then we have obtained the position of the sampling points.

The theoretical aspect of this method is provided below. First, we recognise that the mirror position is an irregular function of time due to the mirror moving speed being non-constant. If we assume that the interference signal of the helium neon laser is a simple cosine wave with varying amplitudes, then the signal can be written as:

$$f(t) = A(t)\cos\big(\omega x(t)\big) = A(t)(e^{i\omega x(t)} + e^{-i\omega x(t)})$$

where $f(t)$ represents the signal, $A(t)$ represents the signal amplitude, $x(t)$ represents optical path difference, ω represents the frequency of this monochromatic signal, t represents time.

The time domain analytic signal, z(t) of this real signal is then obtained by removing the negative frequency component from the original signal $f(t)$ and it can be assumed to be of the following form:

$$z(t) = A(t)e^{i\omega x(t)}$$

As a result, amplitude variations can now be easily separated from phase calculation. Thus, the relative optical path difference can be determined if the wavelength of the reference source is also known. There remains a minor problem however which is that whether the time domain analytic signal is exactly the same as the path domain analytic signal. Actually, they are not exactly the same mathematically speaking. But it is safe to assume that any difference between them, if exist, will be negligible because the mirror movement is largely linear.

After the determining sample point position of the nonuniformly sampled data, the next step would be to use this information to calculate the spectrum of the source. Methods exist to process nonuniformly sampled interferogram into spectrum. Generally, there are such ways. The most straight forward way would be to use interpolation to resample the original nonuniform data to obtain a new set of uniform data and then do Fourier transform. The other method would be to use the nonuniform Fourier transform equation. Actually, this is an area that has not been thoroughly investigated in the literature. We will explore this topic in more detail in subsequent chapters.

4.3. Results

Figure 14 shows an example of the calculated instantaneous phase profile and a zoom in segment of it of the helium neon laser interferogram shown in the previous chapter. It can be seen that the sampling positions are largely linear overall. However, from the zoom in segment it can be seen that there are large local variations in sampling speed.

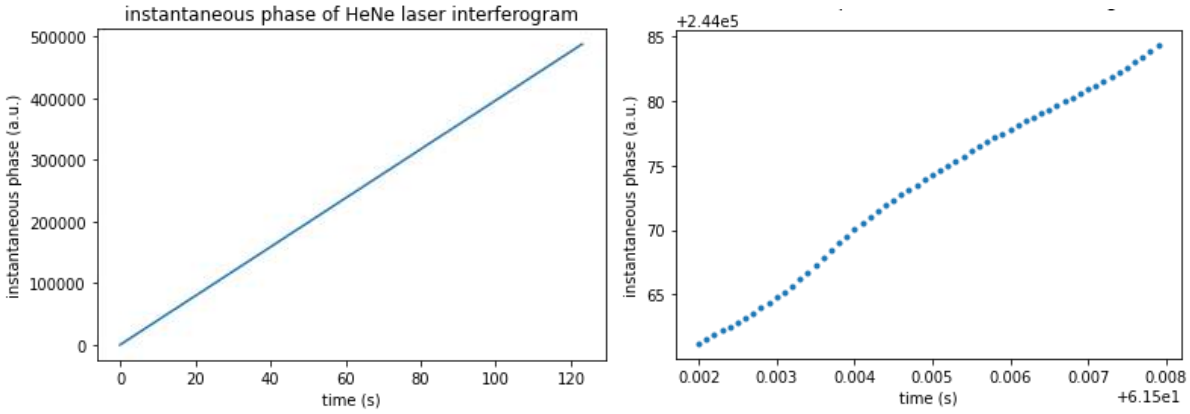

Figure 14 Calculated instantaneous phase of the example helium neon interferogram from the previous chapter (left) and a zoom in segment of it. (right)

With the sampling position determined, it is then trivial to obtain the instantaneous mirror movement speed profile. This can be done by calculating the derivative of the sampling position profile obtained just before. Figure 15 shows an example of the calculated mirror moving speed profile. It can be seen that the mirror moving speed varies by as much as 50 percent during the scan.

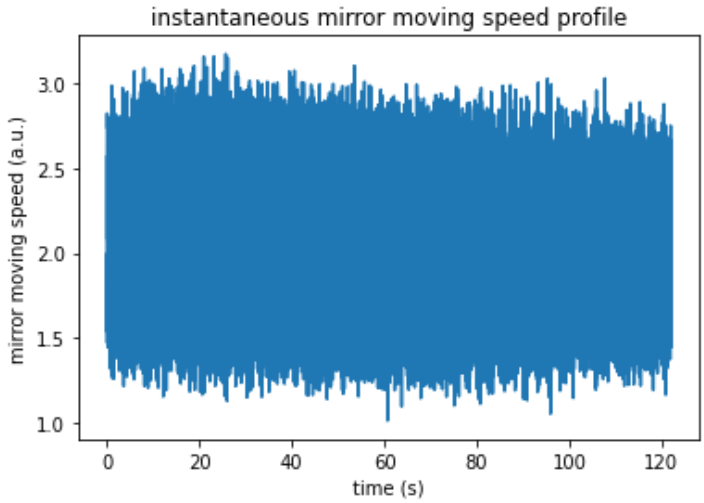

Figure 15 Calculated linear translation stage moving speed.

The sampling point position can then be used to obtain spectrum using the method outlined in the previous section. Although calculating spectrum is beyond the scope of this chapter, it is very worthwhile to calculate the spectrum of the helium neon laser itself with the sample point position information because it serves as a good indication on how accurate the determined sample positions are. Figure 16 shows the calculated corrected spectrum of the helium neon laser itself using the two example interferograms shown previously. It can be

seen that both corrected helium neon spectral profiles are nearly the same in shape and is mostly a single spike.

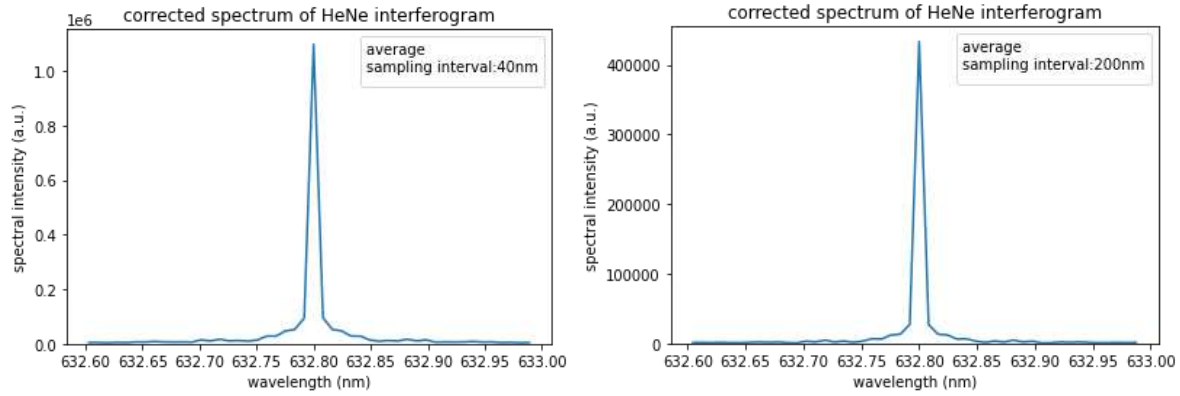

Figure 16 Calculated corrected spectrum profile of the first (left) and second (right) example of helium neon laser interferograms given in the previous chapter acquired under different sampling rates of 2 K/s and 10 K/s respectively.

4.4. Advantage of nonuniform sampling

At this point we have completed all steps to successfully implementing a nonuniform sampling Fourier transform spectrometer from building the hardware to writing the programming codes to transform the data into ultimate spectrum profiles.

It is time to stop and reflect on it a little bit. First is why did we build such a nonuniform sampling Fourier transform spectrometer in the first place? The reason is that our lab and equipment does not have the capacity to implement a uniform sampling Fourier transform spectrometer. But this also demonstrates the advantage of nonuniform sampling. It has much lower hardware requirements than nominal uniform sampling approach.

We would like show here that there is another advantage in that it has some electric noise mitigation properties compared to uniform sampling Fourier transform spectrometers. Both the photodetector and the data acquisition device will generate some electrical noises. These can be observed by blocking off the entrance of the photodetector reception area so that no light can enter it and then record some data. The resulting signal will then be purely of noises of electrical origin. Ideally these noises should be expected to be completely random. However, this is not the case with our devices. Our detector devices are probably not the best. The noises will not be completely random and will contain some specific frequencies. Figure 17 shows one example of such dark current noise spectrum from our photodetector devices.

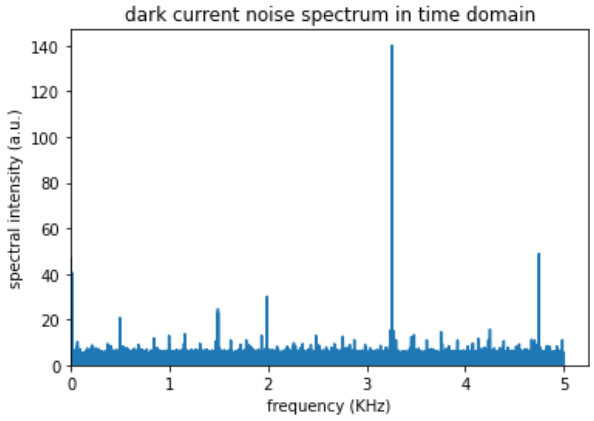

Figure 17 An example of the dark current noise spectrum in time domain.

In conventional uniform sampling schemes, such non-random electric noise can interfere with the spectrum results. For example, they may show up in the spectrum profile as false emission lines. But with nonuniform sampling, this problem will be mitigated because the interference signal exist in path domain while the electrical noise signal exist in time domain. So those non-random electric noise frquencies will not show up in the path domain spectrum profile. To demonstrate this property, we use the above dark current noise example and calculate its spectrum in path domain. To do this, we pretend that the spectrometer is still running while blocking off the entrance of photodectector and pretend that we know the sampling position. And then we use the sampling position profile obtained previously in this chapter to substitute it. Mathematically this is sound because they are two independent probality events. Figure 18 shows the result. It shows that all those spectral spikes have dissappear completely.

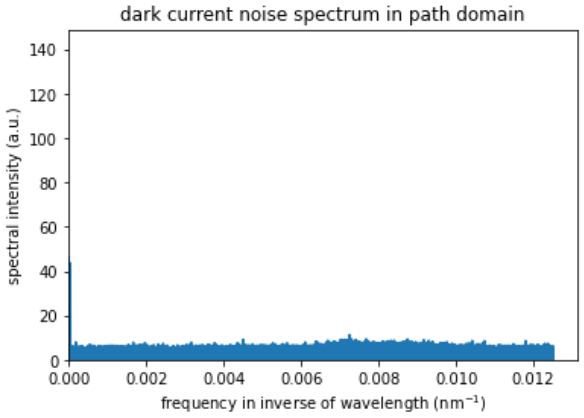

Figure 18 The spectrum of dark current noise in optical path domain in nonuniformly sampled interferogram.

4.5. Discussion

The corrected spectrum profile of the helium neon laser profile agrees with the presumption that the helium neon laser is a monochromatic source. And this result is repeatable with two different unrelated experiment results. This is an indication that our method of determining the sampling position is accurate enough. Although one can argue that this is not a good way to determine a laser spectrum because we are using the laser to determine the laser spectrum itself but that is not the point of this study.

4.6. Conclusion

We have developed the method to determine the sampling position of the nonuniform sampling Fourier transform spectrometer interferogram by using a monochromatic helium neon laser source. And we have used this information to calculate the correct spectrum profile of the helium neon laser itself. In the subsequent chapters we will build more advanced nonuniform sampling Fourier transform spectrometers to do some measurement.

Chapter 5. Using cube corner retroreflectors to build a high-resolution Fourier transform spectrometer

This chapter will try to build a Fourier Transform Spectrometer with as high as resolution possible with the available equipment and test it with some light sources.

5.1. Introduction

The resolution of a Fourier transform spectrometer is limited by its scanning length or the total change in optical path difference during a scan. Specifically, the resolution is proportional to the inverse of scanning length. And the resolution of Fourier transform spectrometer is often specified in inverse of scanning length. For example, a 1 cm^{-1} resolution means the scanning length is 1 cm. This study did a brief search of the market of Fourier transform spectrometers and found that Fourier transform spectrometers in the market typically advertise a modest resolution in the order of magnitude of 1 cm^{-1}. The spectrometer we just build in the previous chapters has a resolution comparable to the commercial ones. This may not be enough for research purpose. To know what scanning length of the Fourier transform spectrometer is adequate, we need to know what the state of art of scanning length of Fourier transform spectrometer is in literature.

In our not so comprehensive survey, we found that in 1978, a two-meter scanning length Fourier transform spectrometer was reported [31]. And as far back as 1987, a Far-infrared Fourier transform spectrometer with a scanning length of 4 meter has been reported [32]. And we have found a company called Bruker that is selling what it claims to be the world's highest resolution commercially available research grade Fourier transform infrared spectrometer the Bruker IFS 125HR as of the time of writing this thesis [33]. It claims to have a resolution of < 0.0009 cm^{-1} or a little more than 11 meters scanning length.

So, based on this survey, the benchmark for high resolution Fourier transform spectrometer seems to be 10 meter and it would be sensible to aim for this resolution when trying to construct a self-made Fourier transform spectrometer in the lab. It turns out that this research project does not have sufficient equipment to reach a scanning length of 10 meter. The longest linear translation stage available to this study is only about 30 centimetre long. But we managed find an innovative solution to create a Fourier transform spectrometer with a scanning length of about five meters by using retroreflectors.

Cube corner retroreflectors are in essence three plane mirrors carefully placed together perpendicularly to each other. Its function is that the reflected light will be parallel to the incoming light but travel in exactly the opposite direction no matter what the direction of incoming light is. There are generally two types of cube corner retroreflectors. The first type is made with three plane wave mirrors. The second type is made of cube corner shape prism. It is based on the phenomenon of total internal reflection. Rooftop mirrors and right-angle prisms can be considered as the two-dimension version of cube corner retroreflectors. Thus, they can be used as substitute for retroreflectors except that they will be much more difficult to align. But they also differ from cube corner retroreflectors. For one, rooftop mirrors will change the polarization direction of the light while cube corner retroreflectors would not. This property is often used to create Martin-Puplett type of Fourier transform spectrometers in conjunction with polarized beam splitters.

Cube corner retroreflector is a very useful optical component to Fourier transform spectrometers. The idea of using retroreflector in Michelson interferometer dates back to at least 1948 and can be even earlier [34]. Using retroreflector has many advantages. One of them is that it is much easier to align beams by using them instead of plane mirrors. Since high resolution Fourier transform spectrometer needs to move a long distance, this is a very welcoming advantage. In fact, one can consider the cube corner retroreflector to be mirror configurations that has been aligned by the manufacturer. It would be possible for one to create crude retroreflectors by arranging three pieces of mirror perpendicularly by themselves, but the effort it takes to align the mirrors will not be worth it. Another use by cube corner retroreflector is that it can be used to create Fourier transform spectrometers that use rotation rather than linear motion to generate change in optical path difference [35]. This may be useful for some situations. But we will not use this feature for this research because we do not have the equipment to generate rotational movement and that the scanning length generated by such rotation of retroreflector is also limited.

Finally, and most importantly, cube corner retroreflector is used to extend the scanning length of the Fourier transform spectrometer by folding the light beam several times. The principle of using cube corner retroreflectors to fold light beams is that the reflected light beam by retroreflector is parallel to but also some spatial distance away from the original beam. This is the feature that is most important to this chapter. There have been theoretical

proposals as well as experimental reports that uses retroreflectors to increase the effective scanning length of the spectrometer in the literature [36,37].

In this chapter, we will build a Fourier transform spectrometer with novel designs to achieve a scanning length of about five meters and use this spectrometer to measure the spectrum of some light sources.

5.2. Coming up with a solution

Although theoretically there are no technical limits to how far a mirror can be moved in a Fourier transform spectrometer and there should be no technical obstacles to build a linear translation stage of any length. It is not within this project's capacity to build a linear translation stage for Fourier transform spectrometer. The longest available linear translation stage is a commercial linear translation stage with 306 mm specified travel range. This is a far cry from the benchmark of 10-meter scanning length of the highest resolution Fourier transform spectrometers. Hence, in order to achieve more satisfactory scanning lengths, we need to find some ingenious tricks.

In the classic Fourier transform spectrometer design with one stationary mirror and one moving mirror, the total optical path difference of the spectrometer would be equal to twice that of the mirror's total travelled distance. Thus, the scanning length by using the 306 mm linear translation stage would have been about 0.6 meters. But if we move both mirrors of the two arms of the Michelson interferometer, the total optical path difference can be doubled. And only one linear translation stage is necessary because the two mirrors can be placed on the same linear translation stage. So now 1.2 meters scanning length can be achieved with the 306 mm linear translation stage. This is a very simple solution and certainly we are not the first one to have discovered it. But we do not encounter this very often because in many situations the scanning length is not a concern. For example, textbook examples usually do not consider these technical problems.

In addition, there are some cube corner retroreflectors available to this research that can be used to further extend the scanning length of the Fourier transform spectrometer. We first search the literature to look for possible solutions. We found some theoretical designs that can extend the scanning length by many times [36,37]. However, they usually require different retroreflectors of various sizes or many retroreflectors which are not possible for

this research. Thus, this chapter would use less ambitious but simpler solutions instead. It would use two cube corner retroreflectors to fold beams twice so that the eventual scanning length is sixteen times that of the travelling range of the linear translation stage.

It would be meaningless to achieve such long scanning length without being able to measure anything however. Previous chapters have only used helium neon laser as light source. Thus, this chapter would devise a simplest scheme to use this five metre nonuniform sampling Michelson interferometer to measure the spectrum of some light sources for demonstration purpose. It would use a second beam splitter to combine the test light beam and the reference helium neon laser beam into a single beam so that only a single photodetector is needed. We would then devise a way to separate the helium neon laser part of the interference signal from that of the test light source through software so that the reference helium neon interferogram can be used to calculate the sampling positions. The principle of this method is that in the time domain spectrum of the interferogram the reference helium neon laser part and the test light source part usually reside in different locations and can be separated if the frequency of the reference laser and the test light source are far away from each other. The drawback of this method is also obvious. It cannot be used to measure light sources whose frequency range is very close to that of the reference laser. After the sample position is determined the spectrum can then be calculated by either nonuniform Fourier transform method or resampling by interpolation method.

5.3. Design

Figure 19 shows the design of this unconventional variant of Michelson interferometer and Fourier transform spectrometer of this experiment to achieve a very long scanning length. The classical Michelson interferometer would have one stationary arm and another mobile arm with moving mirrors. However, in this experiment, we use two mobile arms moving in opposite directions to double the optical path difference. The interferometer is built on a 306mm linear translation stage and has an effective scanning length of about 5 meters. This translates to a resolution of 0.002 cm^{-1}. In order to achieve this scanning length, four retroreflectors are employed to fold the optical paths at each arm by 8 times and we place the moving mirror of both arms onto the linear translation stage in back-to-back fashion to further increase the optical path difference by 2 times and thus resulting in 16 times increase in optical path differences in total. A second beam splitter is used to add a reference helium

neon laser source to the test light source to assist in determining the sampling positions later. We would use this interferometer the record the interferogram of a 532 nm multimode solid state later and a 960 nm broad spectrum SLED infrared light source as well as the 632.8 nm Helium Neon laser reference source.

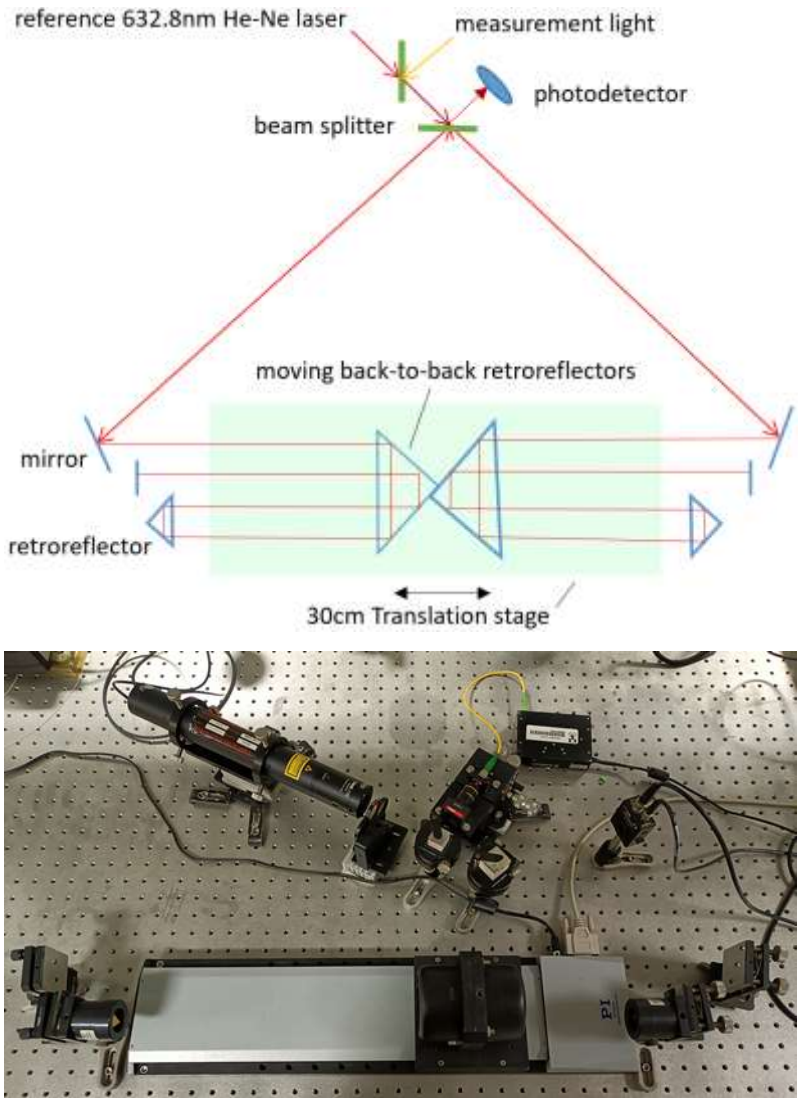

Figure 19 Schematic (top) and photgraph (bottom) of the interferometer used in this experiment

We identify all the relevant equipment available to this research. The equipment used are: A Physik Instrumente M-531.DDX linear translation stage with a moving range of 306 millimetre and is controlled by a Mercury C-860.10 DC-motor controller. A National Instrument NI-PCI-MIO-16E-4 data acquisition device with a maximum sampling rate of 1666666Hz. A 340 nm-1100 nm Thorlabs PDA100A-EC Switchable Gain Detector with several gain level setting ranging from 0 dB to 70 dB. Two Melles Griot surface coated cube corner retroreflectors with a diameter of 6.5 cm. Two smaller Newport surface coated cube corner retroreflectors with

a diameter of 2.5 cm. Several silver surface coated plane mirrors. There are also several light sources, among them are: one Thorlabs HRS015 frequency stabilized 632.8 nm helium neon laser, one 680 nm Superlum SLD-MS-261 SLED, one 960 nm Superlum SLD-MS-481-MP-SM SLED, one 532 nm CNI MGL-III-532-20mW solid state laser.

5.4. Data processing

The data processing method is similar to the one developed in the previous chapter. But an additional step is required which is to separate the reference helium neon laser signal from the test light signal. Afterwards the steps are the same. The principle is that in the time domain spectrum of the nonuniformly sampled interferogram the reference source and the test source can be separated in certain situations. No additional calculation step is actually required because the analytic signal of the reference source which is used to determine the sample position is also extracted through the time domain spectrum of the interferogram. In fact, this is the reason that in the previous chapter we developed the method to use analytic signal to determine sample point positions in the first place.

5.5. Results

Figure 20 shows an example of the raw interferogram of the helium neon laser and a zoom in segment of it as well as the positive part of the time domain Fourier transform of this interferogram and the cut out segment containing the helium neon laser part. It can be seen that this interferogram has highest amplitude around the middle where optical path difference is near zero and gradually taper off as it goes toward the other two sides. It can also be seen from the time domain spectrum that the spectrum profile of the helium neon

laser is broaden into a region with Gaussian-like shape by as much as ±30 % with respect to the position of the central peak frequency.

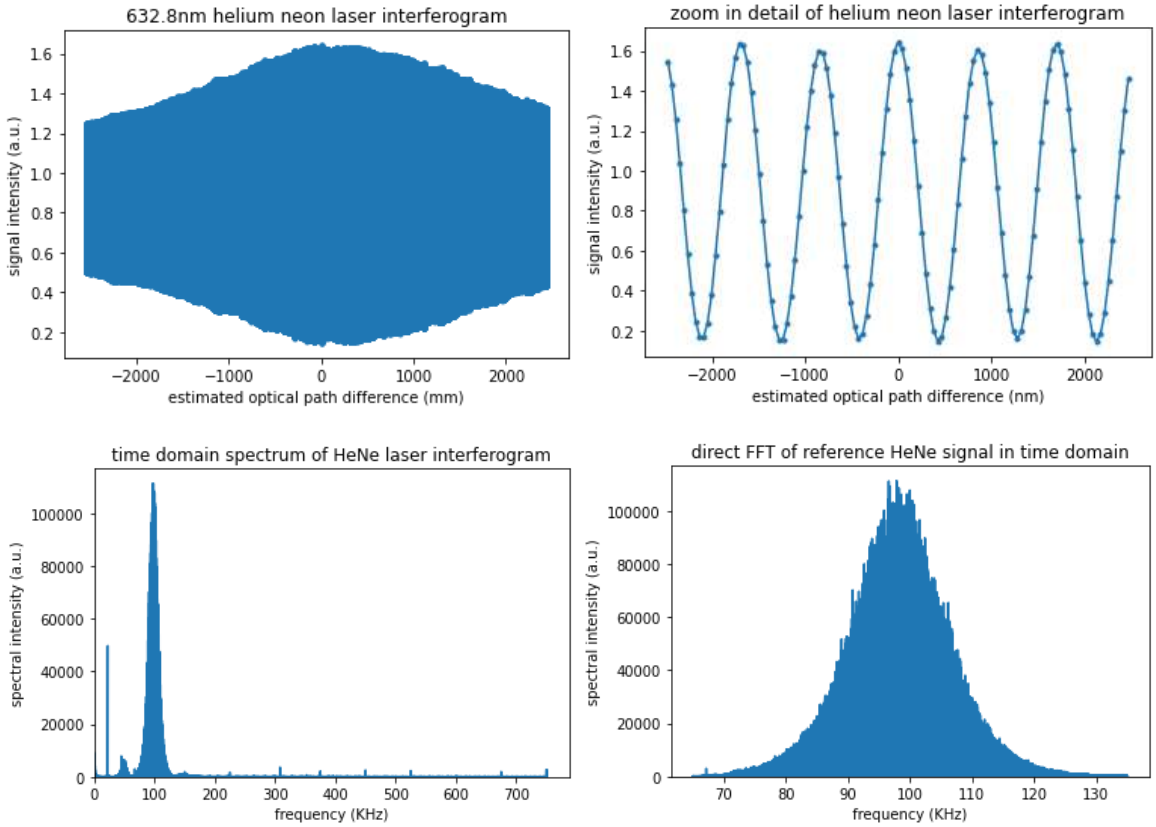

Figure 20 An example of the raw interferogram (top left) of the helium neon laser, a zoom-in detailed segment of it (top right), the positive part of the corresponding time domain Fourier transform spectrum (bottom left) and the nonzero segment of this spectrum containing helium neon laser (bottom left) where it can be seen that the frequencies vary by as much as about ±30 % compared to the middle peak frequency located near 100 KHz.

Next, the sample point position is calculated using the same method as in the previous chapter. Figure 21 shows the calculated position profile of the sample points. As outlined in the previous chapter, the position is directly proportional to the instantaneous phase of the real interferogram obtained from the complex analytic signal. To examine the variability in sampling, a sampling "speed" in optical path difference domain is obtained by differentiation of this sampling position profile. As can be seen from Figure 21 the sampling position shows a mainly linear behaviour, however the graph of sampling speed indicates large speed variations as the highest and lowest speed is roughly ±30 % of the median speed.

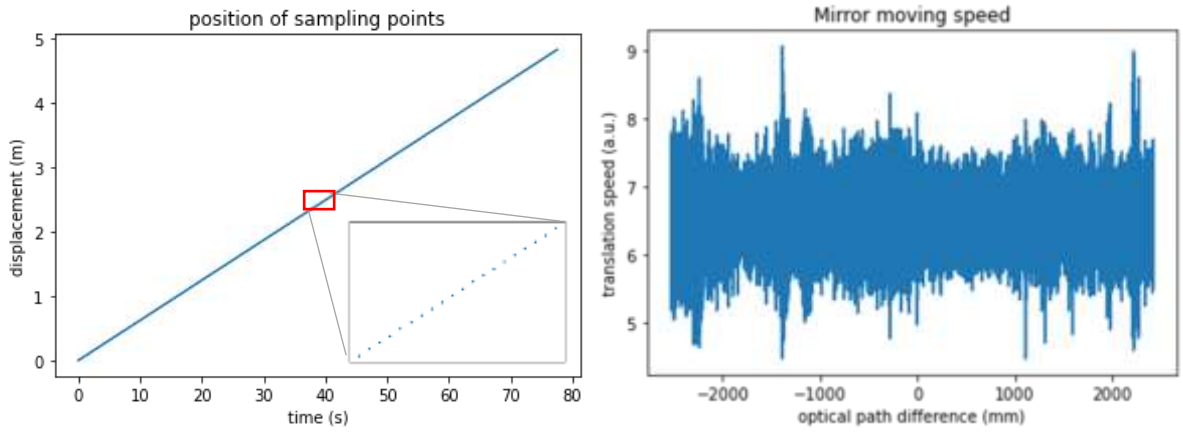

Figure 21 An example of the sampling point position profile (left) and the calculated linear translation stage speed profile (right) where the median speed is about 6.5 a.u. while the highest and lowest speed is about ±30 % of that. The linear translation stage is set to move at about 4 mm/s in this example and the sampling rate is 1500 KHz.

Next, we start to measure the spectrum of a 532 nm multimode solid-state laser and a 960 nm super luminescent diode (SLED) continuous broadband light source for demonstration purpose. First, an example of the interferogram of the 532 nm laser and 960 nm SLED is provided below (Figure 22) to demonstrate the signal characteristics of these test light sources. It can be seen as expected that the coherence length of the laser is very long while the coherence length of the SLED is very short. These interferograms are obtained with the reference helium neon laser turned off and the optical path difference is estimated from average mirror moving speed. The optical path difference is estimated to give the reader a better sense of the scanning length and the general characteristics of the light sources. For the SLED source, we will not use the full scanning length of this spectrometer because its coherence length is very short.

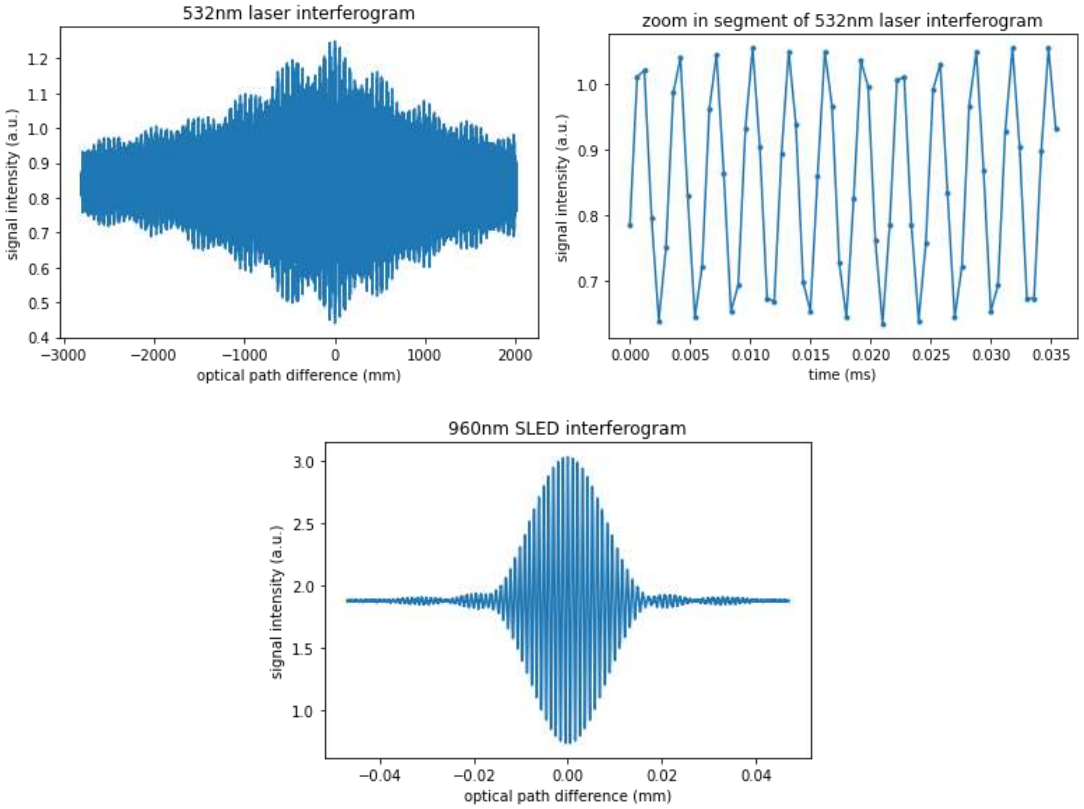

Figure 22 An example of the interferogram of the 532 nm laser (left) and the 960 nm SLED (right). The optical path differences are estimated from average mirror moving speed.

In addition, it can be seen that the aforementioned 960 nm SLED interferogram has a bell shape profile. We also plot the bell shape envelop of the 960 nm SLED interferogram to better showcase the very short coherence length of the 960 nm SLED light source.

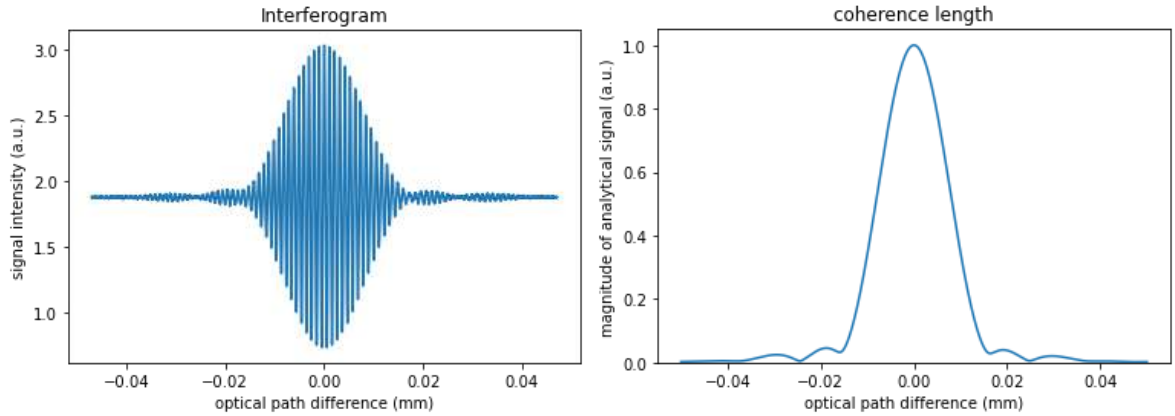

Figure 23 The bell shape 960 nm SLED interferogram (left) and the amplitude envelop of it (right).

Finally, we plot the time domain spectrum of the interferogram to show how interference signal from the reference helium neon can be separated from the test light signal, which are the 532 nm laser and 960 nm SLED respectively (Figure 24).

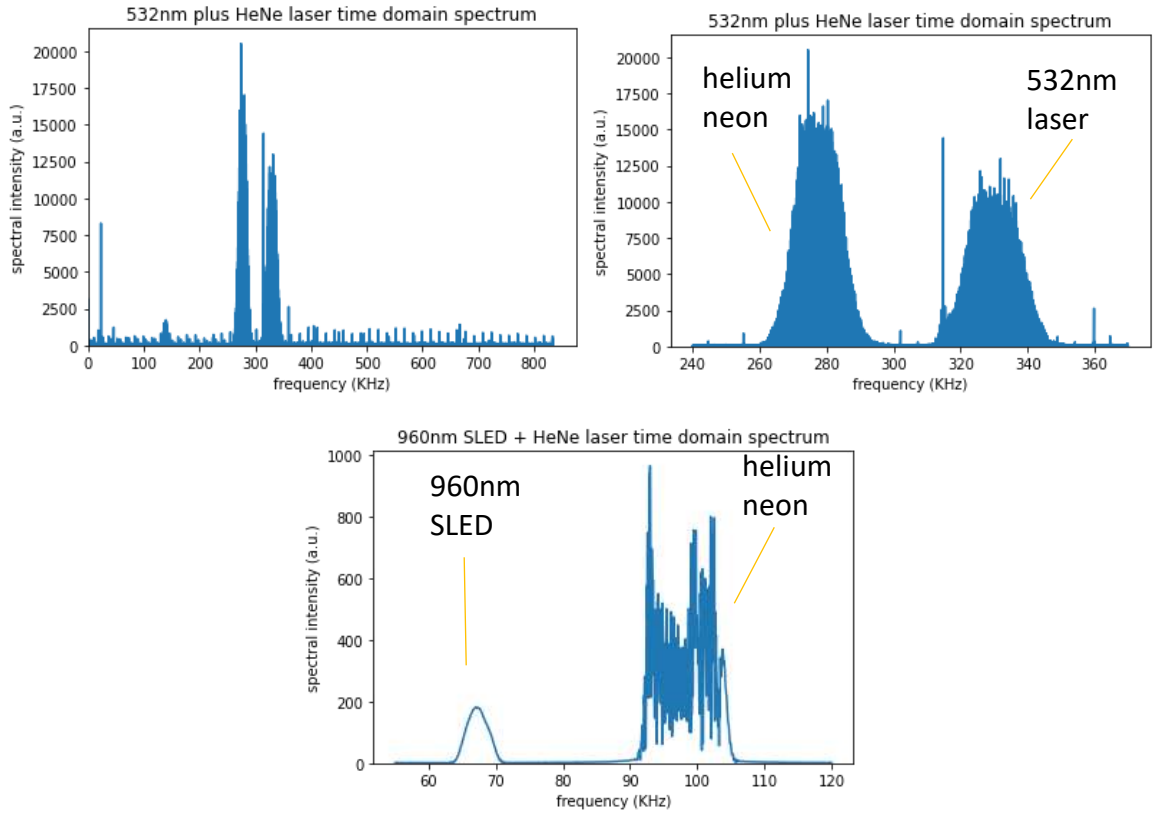

Figure 24 The time domain spectrum of the 532 nm laser interferogram (top left), the nonzero section of it (top right) and that of the 960 nm SLED (bottom.

Finally, with the sample point position determined, we can calculate the spectrum of the two test light sources. We will leave the detail discussion of this calculation to the next chapter and show only the spectral results. In addition, the spectrum of the 960 nm SLED is calculated 5 times to demonstrate repeatability by setting the linear translation stage to move at different speeds respectively. It can also be seen from the 532 nm laser spectral profile that it can comfortably resolve lines much smaller than 0.005 nm.

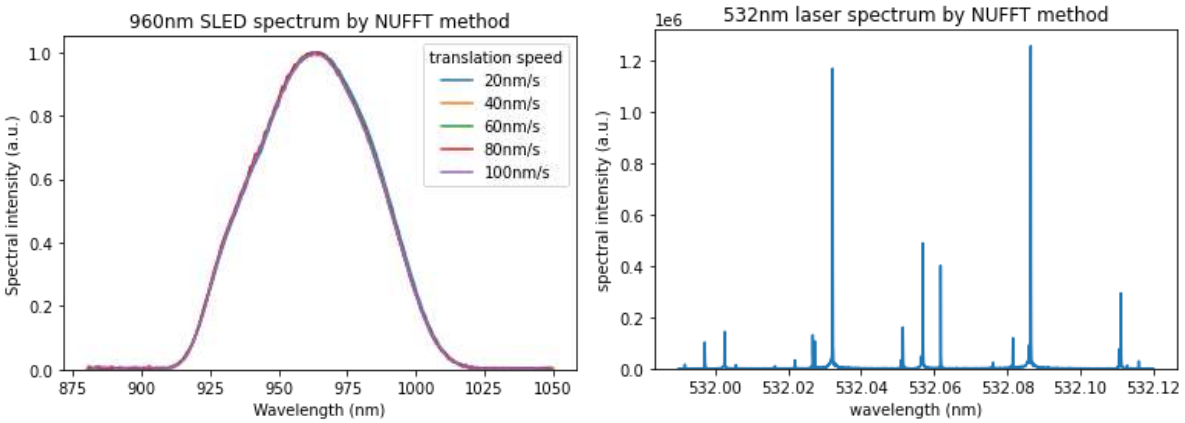

Figure 25 The spectrum of the 960 nm SLED (left) and that of the 532 nm laser (right).

In addition, the spectrum of a 680 nm SLED is also measured to demonstrate how close in frequency can the test light source and reference source be seperated (Figure 26). It shows that this 680 nm SLED which is only about 50 nm away from the reference 632.8 nm frequency is already at the limit of seperation.

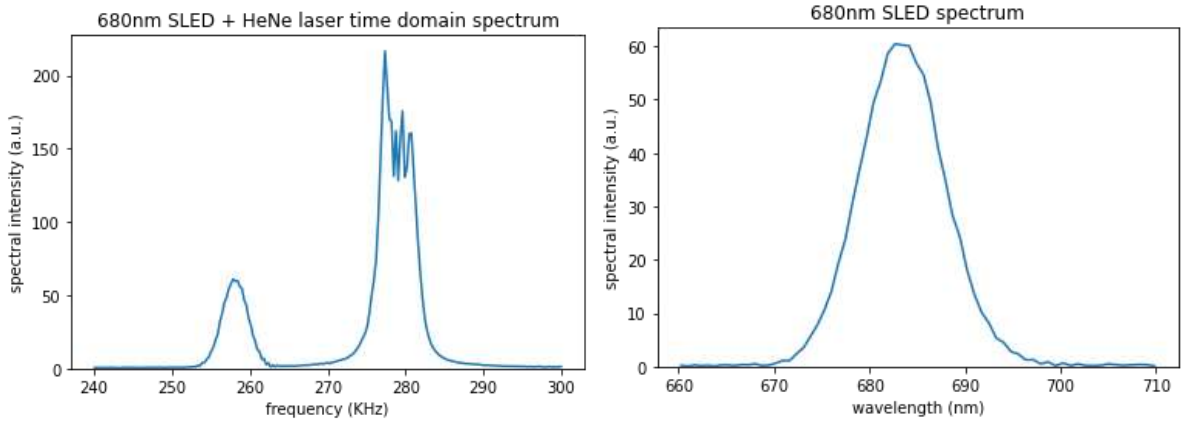

Figure 26 The time domain spectrum of a 680 nm SLED (left) and the corrected path domain spectrum of it (right).

5.6. Discussion

The speed profile and the time domain spectrum shown in the previous section show that the 306 mm linear translation stage used in this chapter is more stable than the 25 mm one used in previous chapters. This is because this linear translation stage is controlled by a PID controller. It will actively adjust the translation speed based on the real time position. This is a very useful feature because it allows us to separate test light and reference light in time domain spectrum more easily. It can be seen that as close to 632.8 nm as 680 nm frequency can be separated from the reference helium neon laser signal although only barely. This is also helped by the fact that the linear translation stage moving speed will vary less within a

shorter segment than a longer segment. This is easily understandable because the moving component contains momentum. Even if the friction force has changes abruptly, it still takes time to change the moving speed. Thus, we can expect that the translation stability will be affected by the weight of the moving component. But it is beyond the scope of this chapter to study the property of the linear translation stage.

Although the 680 nm SLED spectrum can still be measured, the quality and accuracy of the profile is affected due to its proximity to the helium neon laser frequency. It can be seen from the spectrum profile that its spectral peak is not exactly 680 nm. This is not an indication of inaccuracy but just that the label value of this light source has been rounded up to better looking numbers for convenience's sake.

Apodization and zero padding are commonly used pre-processing steps to process the acquired interferogram before doing Fourier transform in Fourier transform spectroscopy. However, this study does not need these additional processing steps because the purpose of the experiments of this study are for demonstration purpose only and it is more desirable to use pristine interferograms to avoid unintended distortion of the conclusions. Nevertheless, we will give a short discussion below in this section on these two topics in case that they are useful for potential future studies and to make this study more complete.

Apodization is a concept and a process describing a modification of the interferogram envelope in order to produce "nice-looking" spectral lines relatively free from noise. In plain language this means to multiply the acquired interferogram with a bell shape function. The reason for this is that an ideal cosine wave is infinitely long but the sample data is of finite length. This would be equivalent to multiplying the infinitely long signal with a rectangular function. Now there is a property in Fourier transform called convolution theorem which states that the Fourier transform of the product of two functions will equal to the convolution of the separate Fourier transform functions of these two functions. The Fourier transform of the rectangular function, which is integrable, is the sinc function. We give the derivation of the formula of it in the following equation:

$$I(v) = \int_{-\frac{l}{2}}^{\frac{l}{2}} e^{-2i\pi vx} dx = \frac{\sin \pi lv}{\pi v} = l \operatorname{sinc} \pi lv$$

As a result, the resulting spectrum profile of this cosine wave signal would also become a sinc function instead of its theoretical profile which is delta function. The problem is that the sinc function is ugly in that at its base it has a lot of oscillations or ringing. These oscillations can be mistaken to be false spectral lines in some situations. The solution would be to change the window function from the rectangular function to a bell shape function to smoothen these oscillations. For example, the Fourier transform of a Gaussian function which is bell shape is also a Gaussian function. Hence, the problem is solved. This feature can be useful in some situations. For example, in commercial Fourier transform spectrometers it is certainly very important to remove the various instrumental artifacts from the output spectrum results to avoid adding confusion and annoyance to those non-expert end users. Not all situations require apodization. For example, with broadband light sources the interference signal is already bell shape thus is not necessary to anodize. This property is called self-apodization. It should be stressed that apodization cannot magically improve the resolution of the result but will on the contrary cause some information loss. It merely improves the aesthetic appeal of the spectral profile and makes it more readable for human eyes especially for the non-expert users. Excessive apodization will only cause unnecessary information loss. Thus, it has been strongly advised that apodization be avoided at all costs [16]. P. Fellgett once said that: "the orthogonal properties of the sine function are easily destroyed by apodization; that is why I believe that apodization should be done only by experts"[16]. Therefore this study did not use apodization.

Zero padding is another commonly encountered processing step. It means to append more zero values to the sample data to make the sample size larger artificially. One of the reasons is to prevent information loss. The reason is that the spectral profile is usually symmetric with equal positive and negative parts. As a result, one half of the spectral profile is duplicate information and is discarded. So, the number of data points in the spectrum result is reduced by half compared to the original sample sizes. This may cause information loss in some situations. The solution is to zero pad the sample to increase its size first. This can be useful for analysing spectral features that has approached the instrument resolution limits. Another reason is to increase the aesthetic appeal of the spectrum. Spectrometers with low resolutions will have very sparse spectral points. This would make an originally smooth spectrum profile appears to be rugged. The most straight forward solution would be to

increase spectral point density by interpolation. But zero padding the sample can also produce the same effect. Because the resolution of Fourier transform spectrometer is determined by scanning lengths. Thus, it can be used as an interpolation method. It should be stressed that zero padding cannot magically improve the resolution of Fourier transform spectrometry. It merely serves to prevent potential information losses. Excessive zero padding would be useless at best if not harmful. It will unnecessarily increase data processing time. In fact, all Fourier transform spectrometers have unknowingly used zero padding to some extent. This is because fast Fourier transform algorithms usually requires the data size to be the power of 2. So, the FFT software libraries will always zero pad the sample to the required size without the users' explicit consent.

They are probably standard practice in commercial Fourier spectrometer. But since the experiments in this study are used for the purposes of demonstrating and studying the properties of data processing techniques themselves, it is better to only use pristine interferograms in this study to avoid unnecessary distortions which may cause wrong conclusions.

5.7. Conclusion

This chapter has built a high-resolution Fourier transform spectrometer with a scanning length that is just half that of the highest resolution Fourier transform spectrometer reported in literature and has used this spectrometer to measure the spectrum profiles of several test light sources. The measurement demonstrates that this spectrometer functions as intended. It can resolve the fine discrete spectral lines of a multimode laser and can consistently reproduce the spectrum profile of a broadband super luminescent light emitting diode source.

Chapter 6. Application of the non-uniform Fourier transform to non-uniformly sampled Fourier transform spectrometers

This chapter will present a systematic and thorough study of the properties of the new NUFFT based data processing technique for Fourier transform spectrometry and compare it with the traditional interpolation based method. It found that the NUFFT method has significant advantage in areas like under-sampling and computing efficiency etc over the traditional interpolation method among many discoveries. It also describes a novel variant of nonuniform Fourier transform that shows improvement over the standard nonuniform Fourier transform for use in Fourier transform spectrometers.

6.1. Introduction

The Michelson interferometer and its many variants are the foundation of many optical and non-optical spectrometry designs. One particular type is the Fourier transform spectrometer [16]. It uses a moving mirror in one of the arms of Michelson interferometer to generate interference signals and uses a single pixel photodetector to record the interferogram. It is one of the most common types of optical spectrometers and has seen applications up to the ultraviolet range at 40nm wavelength [5]. Although its principle is relatively simple, it has many advantages. It can allow relatively large percentage of light to reach the photodetector, records all frequency component simultaneously, has intrinsic wavelength calibration and is able to achieve high wavelength resolutions with relative ease. It is especially advantageous in infrared region where it is the most preferred technique of choices.

One of the challenges in Fourier transform spectroscopy is the difficulty in obtaining evenly spaced samples in optical path difference space due to the difficulty to precisely maintain constant mirror moving speed. One of the simplest solutions is to sample non-uniformly instead and then use interpolation to resample the data uniformly such as the example here [6]. This method has the advantage of minimising hardware requirements and can be readily realized with off-the-shelf optical components and thus is suitable for many situations. However, in such cases of non-uniform sampling Fourier transform interferometers there also exists another overlooked method to process the data into spectrum which is to use the non-uniform fast Fourier transform (NUFFT).

The NUFFT is a concept that has been discussed in many areas in recent decades [38]. It has many applications in a diverse range of fields ranging from magnetic resonance imaging(MRI) [39], ultrasound imaging [40] and radar imaging [41], to numerical solutions of differential and integral equations [42], finite-impulse-response (FIR) filter design [43], electron microscope image alignment [44], to mention a few. It has been used and proven superior in various interferometric applications such as spectral domain optical coherence tomography (SD-OCT)[45], holography diffraction calculation [46], wavelength-tuning interferometry (WTI)[47], and static single-mirror Fourier transform spectrometer (sSMFTS) [17], etc. However, while the NUFFT has been seen extensively in more complicated interferometric systems, to our best knowledge its application in optical spectrometry systems has been very rare and has not been experimentally reported in the simplest type of Michelson interferometer-based optical spectrometers, the single dimensional Fourier transform spectrometer with moving mirror. There has been one theoretical study on the comparison of NUFFT with the interpolation method [48] which shows numerically that NUFFT method is superior to the interpolation method in simulation in emission/absorption spectrum line amplitude, width, position etc. However, this behaviour has yet to be studied experimentally. Studying the application of NUFFT to this simplest spectrometry case of non-uniform sampling may not only help improve the technology of Fourier transform spectroscopy but can also have implications for other applications that employs interferometers. Although nonuniform Fourier transform is not a very new concept, its fast computation algorithm and software library are relatively new developments. Thus, its potential in many fields has yet to be fully explored. Therefore, this paper will report an experimental study of the application of the NUFFT to the Michelson interferometer type Fourier transform spectrometer and outline the various related advantages and disadvantages. Not all variants of Fourier transform spectrometer use moving mirrors to generate optical path difference changes, but as long as the interferogram is nonuniformly sampled, the result of this study will still be relevant.

This chapter will use the 5 meter long, ultra-high-resolution nonuniform sampling Fourier transform spectrometer from the previous chapter to systematically study the performance and differences of NUFFT method over resampling by interpolation FFT method. The visible and IR ranges are investigated by using the interferograms of a 532 nm solid-state multimode laser, a 960 nm broad spectrum SLED as well as a 632.8 nm Helium Neon laser reference

source. Using this long scanning length interferometer will allow the NUFFT performance at very high spectral resolutions to be evaluated.

6.2. Calculation

This chapter will only be a theoretical/numerical study. It will use the experiment data obtained in the previous chapter to do calculations. It will assume that the nonuniformly sampled interferogram has been obtained and the sample point position of it has also been obtained. It is not in this chapter's concern to know how the sample point positions of the nonuniformly sampled data is obtained. It should be noted that all data processing methods for nonuniformly sampled signal require knowledge of the positions of the sampling points. It is a simple mathematical fact that it will be mathematically impossible to obtain the spectrum of an unknown signal without knowledge of the sampling position. In the experiments of this study the sampling positions are obtained from the analytic signal of a reference laser. But that is certainly not the only way.

In this chapter the NUFFT calculation will be performed using the FINUFFT [49,50] python package while the interpolation and FFT calculations are based on the SciPy [51] python package using its interpolation module and FFT module. Theoretically, the FFT speed is proportional to $O(N \log N)$ where N is the number of sample or spectral points and NUFFT speed is also similarly proportional to $O(N \log N + M)$ where N is the number of spectral points and M is the number of sample points [49,50].

For the resampling by interpolation FFT method, it has been reported that cubic spline interpolation gives better results than linear interpolation for nonuniform sampling Fourier transform spectrometer application [48]. We also find that it gives better results among the available interpolation methods in the software library used in this study, so we will follow this approach throughout.

6.3. Results

This section will show the detailed calculation results using the interferograms obtained in the previous chapter for the purpose of studying the property of the NUFFT method and comparison with the traditional interpolation method.

6.3.1 Spectral profile comparison

First, we compare the spectrum profile of the 960 nm SLED and 512 nm laser calculated from both methods. It should first be noted here that there is one technical difference between NUFFT and interpolation method regarding the handling of 0Hz or DC component in obtained interferogram. Raw unfiltered interference signals will always contain a large DC component due to the nature of interference. For the regular or interpolation based FFT method this component will not affect other parts of the spectrum and can simply be ignored. However, for the NUFFT this 0Hz component can in theory generate noise in the rest of spectrum and so removing this component first before NUFFT calculation can in some situations significantly improve the spectral result. We use an interferogram of the 960 nm SLED (Figure 27) to demonstrate this phenomenon which demonstrated that the large impact on spectrum quality this effect can have. In general, this impact is less pronounced when the sampling rate is higher or when the spectral amplitude is relatively high such as in the case of a laser source.

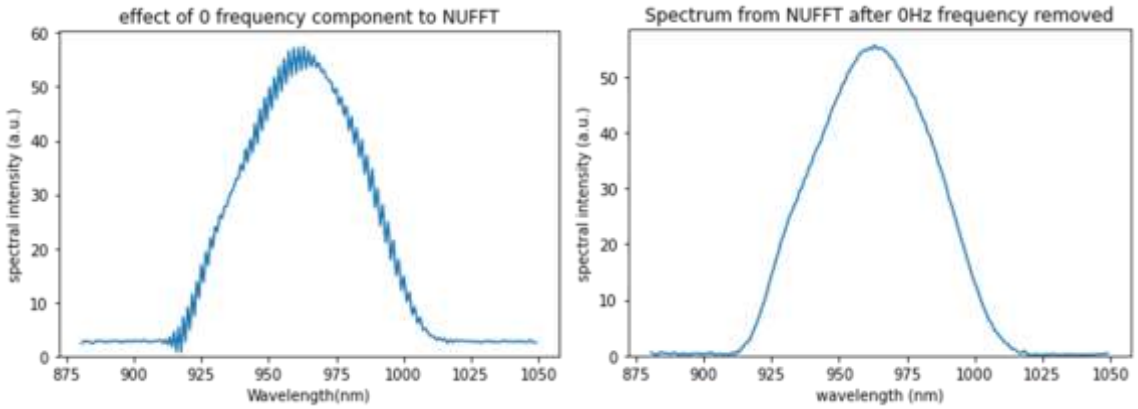

Figure 27 Spectral noise in NUFFT spectrum due to presence of 0Hz component. The sampling interval is about 105nm.

While this problem may seem trivial as the 0Hz component can be easily removed by simply subtracting the mean value of the interferogram, this issue is important in a practical sense as this source of error can be very tricky to identify without knowing it in advance. The reason for this behaviour is that the 0Hz component amplitude is much larger than the amplitude of the actual interference wave components.

6.3.1.1 spectral profile:

Next, we show examples of the calculated spectra of the 960 nm SLED and 532 nm laser sources (Figure 28 and Figure 29 respectively). In both SLED and laser cases, the two methods produce almost identical spectral profiles in terms of overall profile shape. In these examples,

the NUFFT spectrum amplitude is about 5% higher than that of interpolation method for 960nm SLED and about 0.5% higher for the 532nm laser case. The dependence of these percentage on source type / spectral method will be further investigated in the later section.

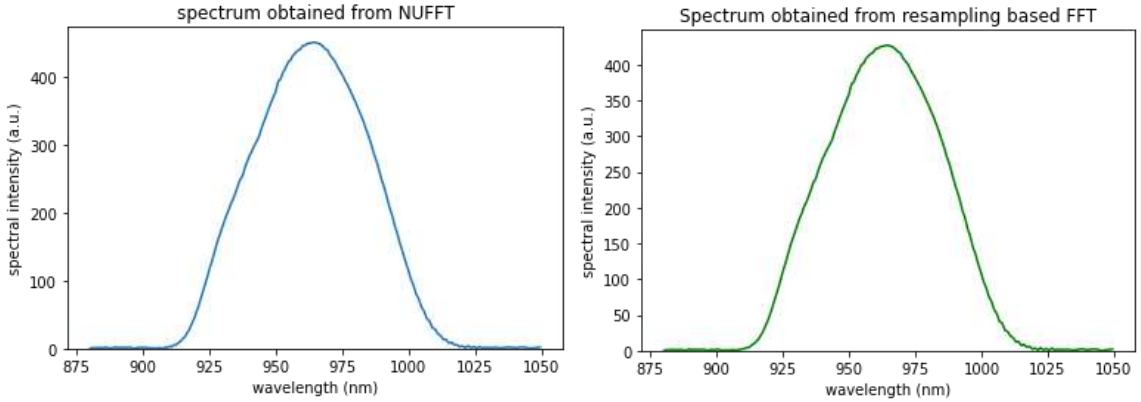

Figure 28 Comparison of the NUFFT (left) and interpolation FFT method (right) obtained spectrum of the 960nm SLED source. The linear translation stage average moving speed is 2mm/s while sampling rate is 1500KHz.

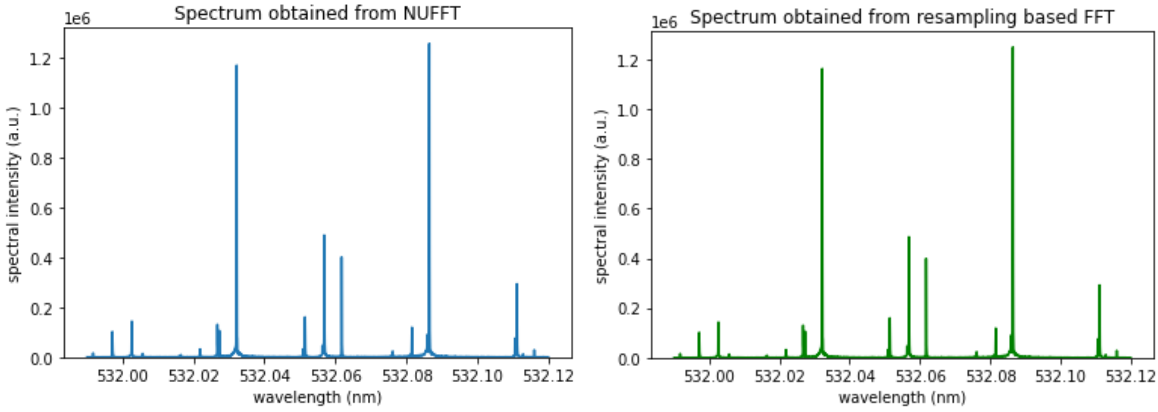

Figure 29 Comparison of the NUFFT (left) and interpolation FFT method (right) obtained spectrum of the 532nm multimode laser. The linear translation stage average moving speed is 11mm/s while sampling rate is 1666666Hz.

6.3.1.2 Spectral noise:

To compare the spectral noise levels for both conventional and NUFFT methods, Figure 30 contains the 532 nm laser with reference He-Ne spectra on a log scale. Again, here it can be seen that their spectral noise profiles are very similar when the sampling rate is around 1 sample per 100 nm. The mean to peak ratio of the log value of the spectrum is 0.162 for NUFFT and 0.156 for interpolation cases. The standard deviation to mean ratio of the log spectrum is 0.33 for NUFFT and 0.36 for interpolation method in the example shown.

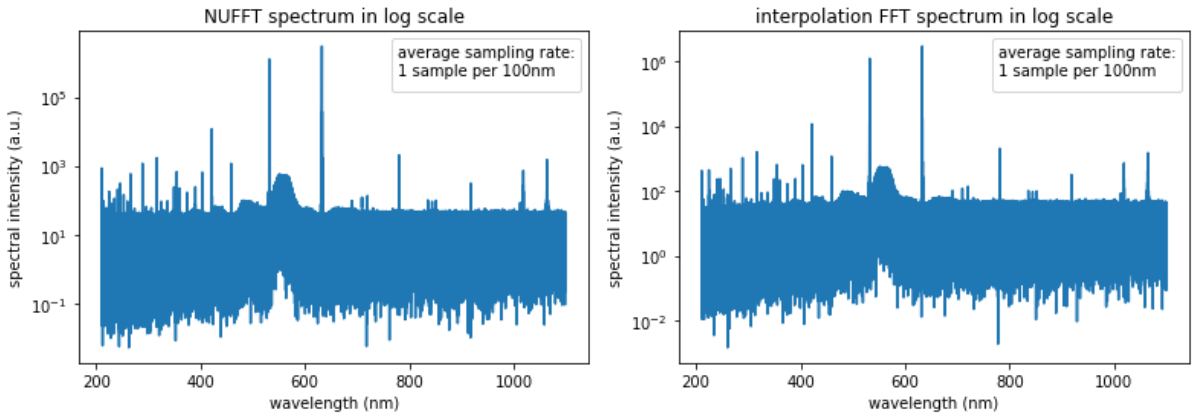

Figure 30 The log scale spectrum of 532nm laser for NUFFT (left) and interpolation (right) methods. The method for interpolation is Cubic Spline.

6.3.1.3 Spectral amplitude

In section 6.3.1 it was mentioned that the spectral amplitude produced by the two methods can be significantly different. To investigate whether the amplitude difference depends on source type / spectral method, we looked at the spectral amplitude differences in more detail by investigating whether the difference is related to the sampling rate. We found that this is the case with the 532nm laser. For the 532nm laser, the NUFFT amplitude is about 0.5% higher than interpolation method when the sampling rate is about 1 per 105nm. This percentage does not change from run to run. When the sampling rate is reduced by half by omitting 1 point for every 2 sample points to about 1 per 210nm (corresponding Nyquist rate for 532nm is 1 per 266nm), the spectral amplitude of the NUFFT method is 20% higher (Figure 31) than the Interpolation method. Furthermore, the obtained NUFFT spectral amplitude is proportional to the sampling rate and thus the 20% difference is due to the interpolation method not scaling linearly with sampling rate.

Interestingly, this behaviour is not observed in the 960nm SLED case. We found that while the NUFFT amplitude is still proportional to the sampling rate, the amplitude difference with interpolation methods is inconsistent for different sets of acquired samples. Sometimes the NUFFT amplitude is higher than interpolation method while sometimes it is lower with no apparent trend. And for the same scan, reducing the sampling rate by omitting points will not change this amplitude difference. But although the amplitude difference varies with different samples, we found that the difference is always the same shape as the spectrum shape regardless of the sign. To illustrate this, we subtract one example of the NUFFT spectrum of the 960nm SLED source with the interpolation FFT spectrum (Figure 32). Thus, this

proportionality ensures that the obtained spectral profiles from NUFFT and interpolation will be very similar even though the amplitudes differ slightly. The difference between cubic spline interpolation and linear interpolation is also shown for comparison showing much less difference and so the method of interpolation is not a factor.

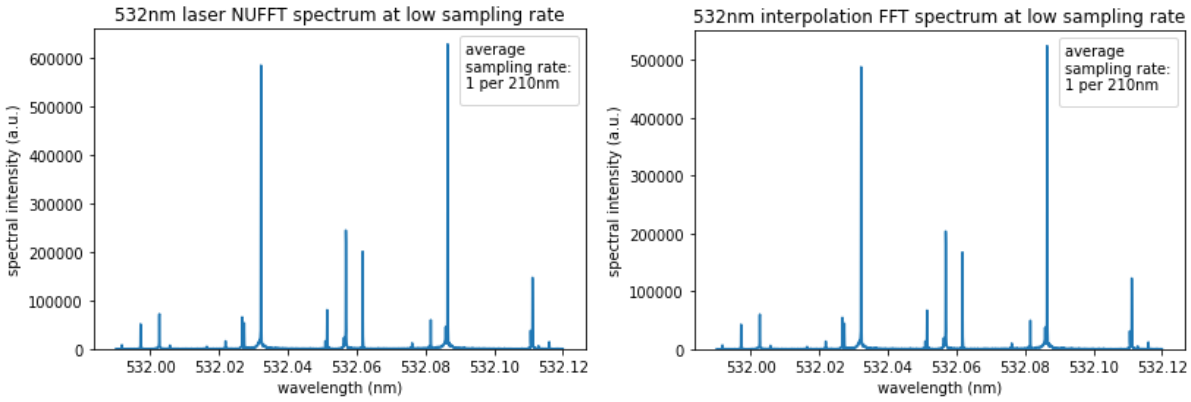

Figure 31 The spectral amplitude difference of NUFFT (left) and interpolation FFT (right) for the 532nm laser

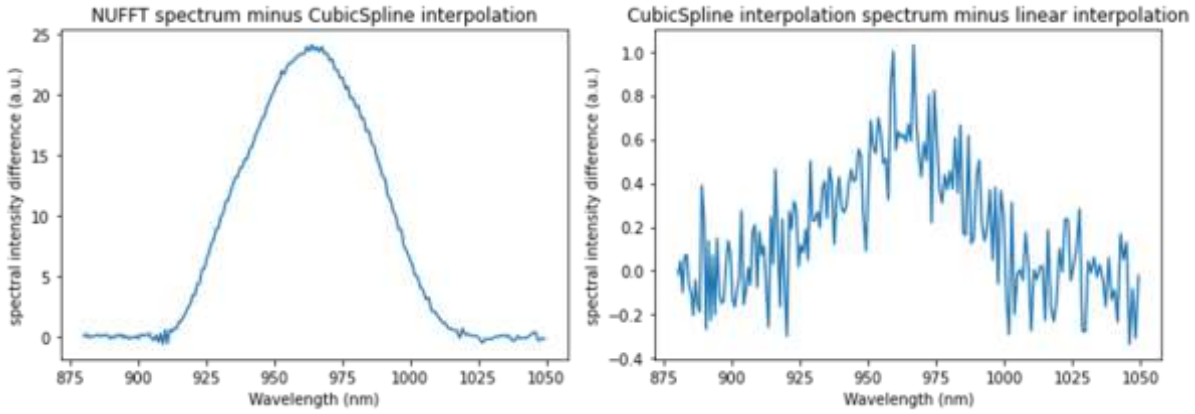

Figure 32 The magnitude difference between the NUFFT spectrum and interpolation spectrum (left). The difference between the Cubic Spline interpolation and linear interpolation (right). The average sampling interval is about 20nm.

Thus, we have shown that, when normalised to number of samples, in general the NUFFT amplitude is less affected by sampling rate and is larger in the 532nm laser case. The difference in behaviour of the spectral amplitude between the laser and the SLED may be due to the fact that laser spectrum is discrete while the SLED spectrum is broad and continuous.

6.3.2 Under-sampling and aliasing behaviour

The periodic nature of the regular discrete Fourier transform equation means that the calculated spectrum has a maximum limit in frequency and any frequency higher than the limit will fold back into the spectrum thereby distorting the calculated spectrum, as can be seen from the equation. This problem is called aliasing.

$$f(n) = \sum_k F(k) e^{i2\pi \frac{nk}{N}} = \sum_k F(k) e^{i2\pi \frac{n(k+N)}{N}}$$

where k+N will be the false frequency appearing in the spectrum because k+N and so on is fundamentally undiscernible from k in the equation. Figure 33 gives an intuitive illustration of this aliasing phenomenon.

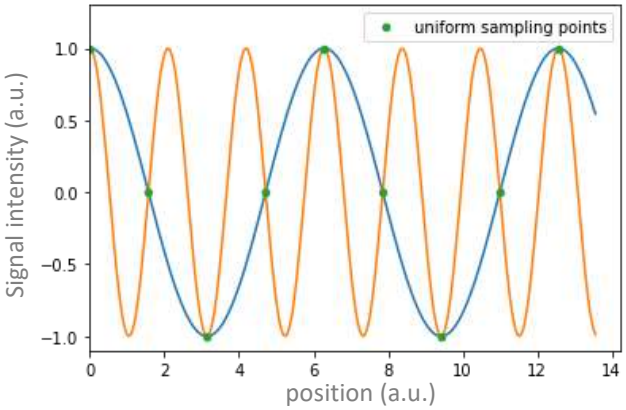

Figure 33 An illustration of aliasing in a uniformly sampled situation. Two signals with different frequencies give same signal values at the uniform sampling points.

By contrast, the NUFFT is inherently non-periodic since usually the sample positions are randomly distributed and so should have no maximum frequency limits and be immune to aliasing if the sample position distribution is random enough.

To illustrate this, we used a 532 nm laser interferogram and reduced the sampling rate by dropping two out of three sampling points (sampling rate reduces to 1 point per 316 nm from 1 point per 105 nm). For the interpolation FFT spectrum the 532 nm signal is folded into the spectrum and appears as a false 775 nm signal while in the NUFFT case there is only an elevated noise level around the expected aliasing region due to the quasi-periodic nature of the sampling (see Figure 34). In addition, the NUFFT also has no maximum frequency limit and can still calculate the 532 nm spectrum in the under-sampled case (see Figure 35 for both original and under-sampled cases).

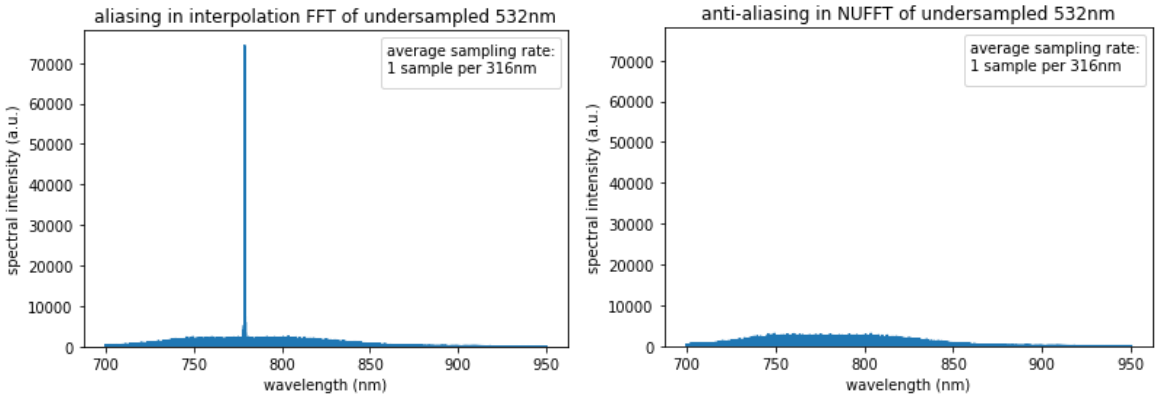

Figure 34 Illustration of aliasing in interpolation FFT (left) and compared to NUFFT (right)

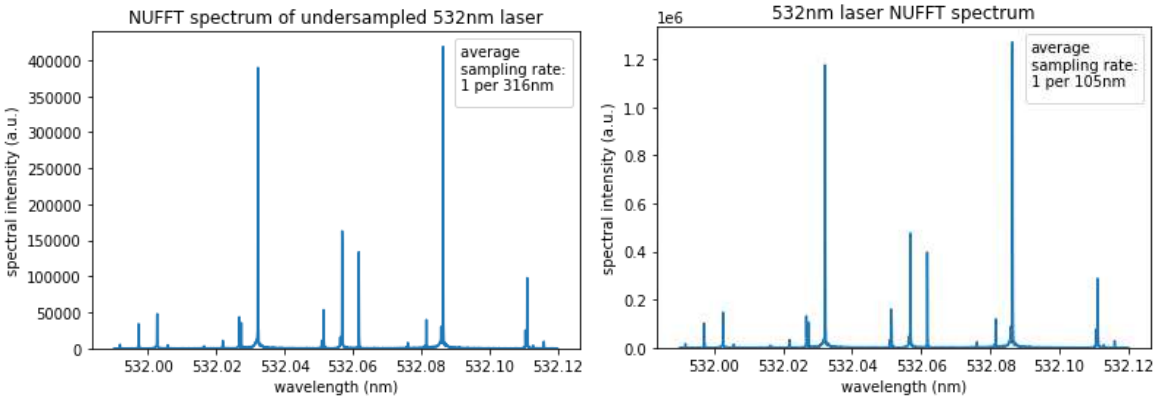

Figure 35 Under-sampled 532nm laser spectrum (left) compared to the normally sampled one (right).

To illustrate the effect of severe under sampling in NUFFT, we under sampled the 532 nm laser by omitting 9 out of every 10 sample points from the master interferogram and calculate the spectrum by NUFFT. We also plot the spectrum in log scale to compare the noise levels (see Figure 36). It shows that the severely under-sampled interferogram can reproduce the laser spectrum as well as the original one, however its noise level is significantly higher. It's worth mentioning here that the spectral resolution is unchanged because the frequency resolution of Fourier transform spectrometers depends on the total scan length rather than the number of sampling points.

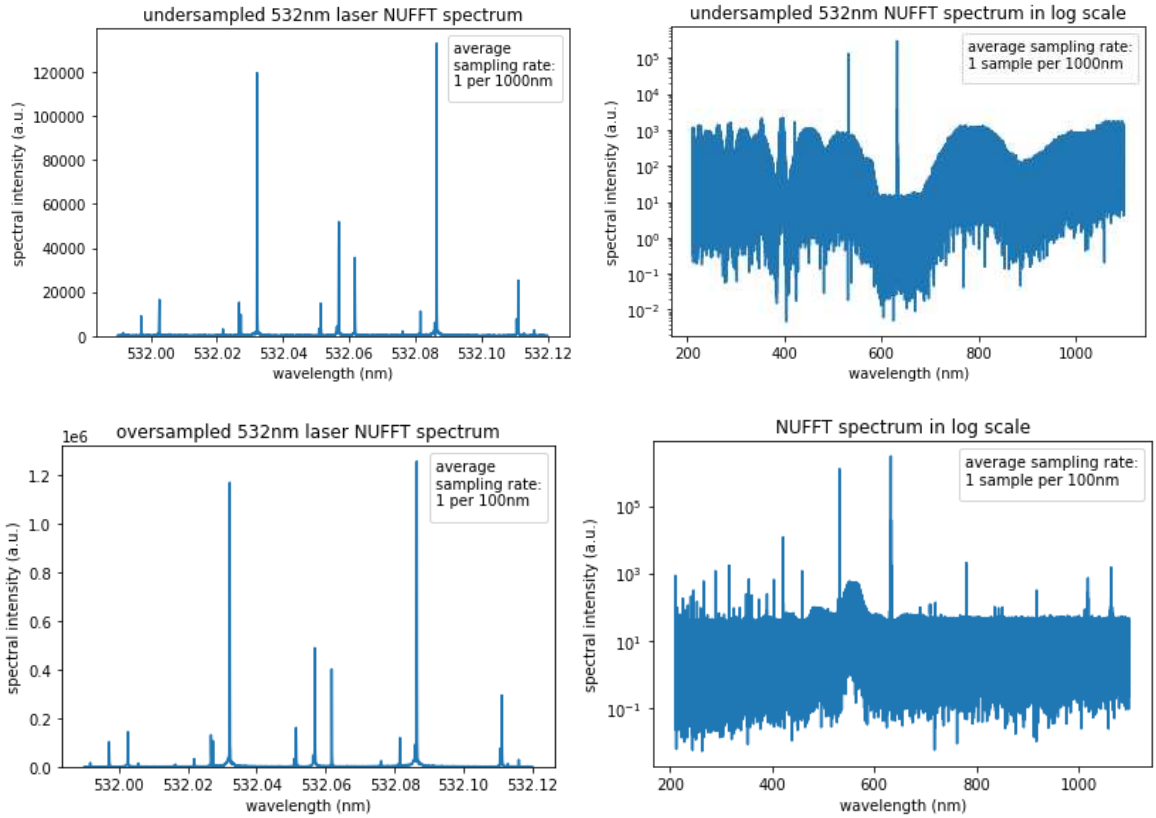

Figure 36 An under-sampled 532nm laser spectrum plotted on linear (top left) and log scales (top right) and the corresponding oversampled cases (bottom).

6.3.3 Non-random electrical noise

The photodetector and the data acquisition device will contribute some electrical noise to the measured interferogram. This noise can be directly observed by measuring the signal in the absence of any light. An example of the spectrum of one such scan is shown on Figure 37 and shows the presence of some particular frequencies. In the conventional uniformly sampled interferogram cases these frequencies can contribute to the overall signal and reduce the accuracy of the final spectrum.

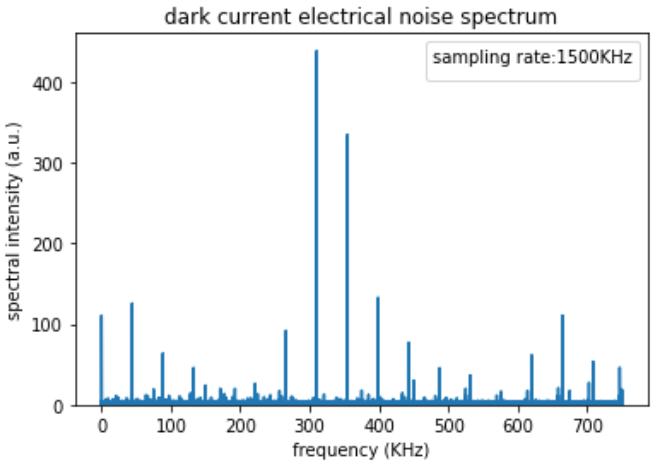

Figure 37 An example of dark current noise spectrum. Sampling rate is set at 1500KHz.

However, non-uniform sampling is inherently advantageous over uniform sampling in mitigating this kind of non-random electric noise because the electric noise exists in the time domain while the interferometric signal exists in the optical path difference domain. This property of nonuniform sampling spectrometer was tested with both NUFFT and interpolation method by running the experiment with the reference helium neon laser on and other sources off (Figure 38). The intensity of helium neon laser is reduced to make the electrical noise more prominent. It can be seen from the figure that in the time domain spectrum of the HeNe interferogram there is one broad HeNe peak plus some sharp spikes due to electrical noise. However, in the optical path domain spectra calculated by either NUFFT or interpolation FFT method, the HeNe peak sharpens while the electrical noise spikes disappear (plotted on log scale to view noise level). Both the NUFFT method and interpolation FFT method performs similarly in reducing these electrical noise periodic components because of the non-uniform sampling.

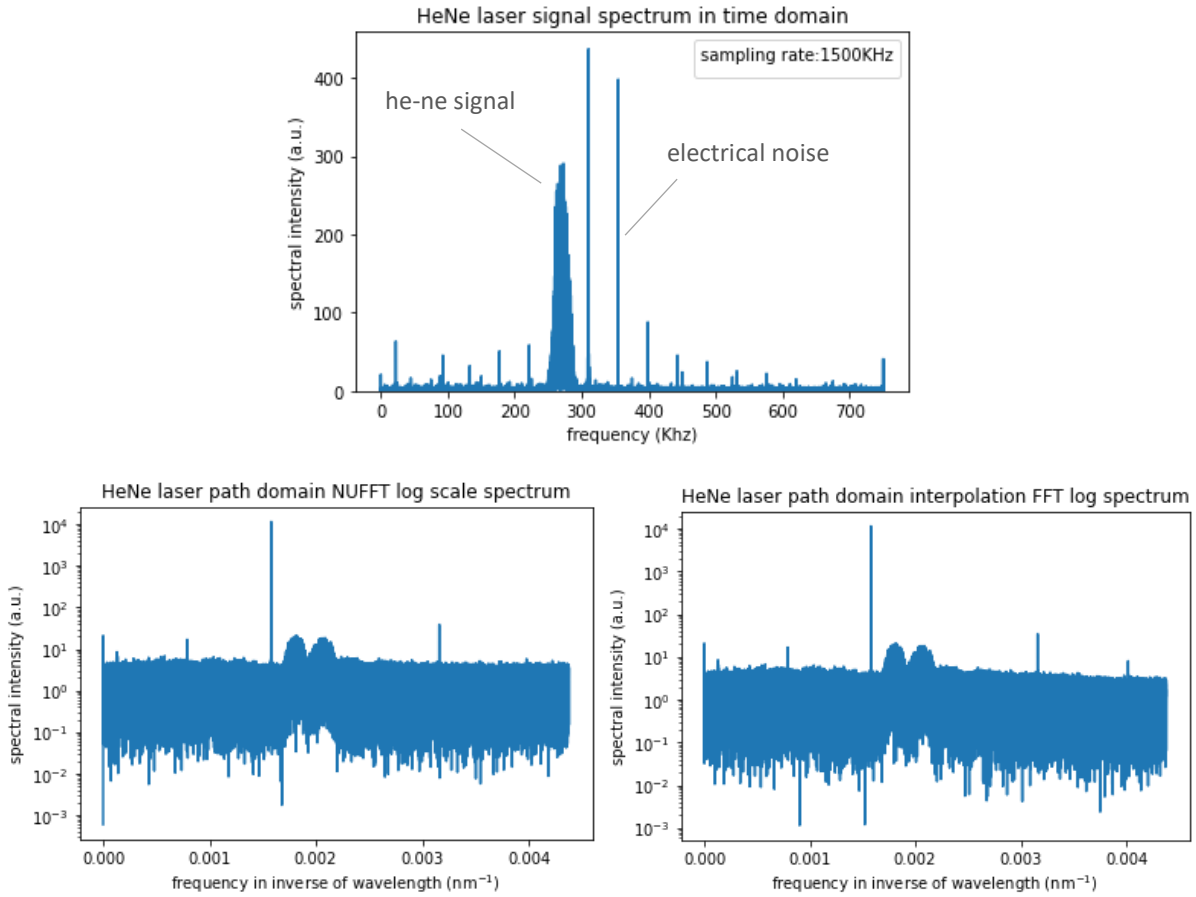

Figure 38 Time domain spectrum (top) of a Helium neon laser interferogram and optical path difference domain spectrum from NUFFT method (bottom left) and interpolation FFT method (bottom right).

6.3.4 Computation performance comparison in practice

It is usually impractical to develop NUFFT or FFT software codes because those are relatively complex algorithms that would take a huge amount of time to create. Thus, the availability of corresponding software packages is very important in a practical sense. In this section we compare the software availability and computing performance of both methods in our implementation.

The availability of software for NUFFT is a relatively weak point compared to the interpolation method. Both FFT and interpolation are very mature mathematical techniques that have standard packages in many programming languages. By contrast NUFFT is a newer and less developed technique and for many software programs there are no standard software libraries for it. As a result, many existing NUFFT implementations are only made for specific applications. This makes those libraries lack usability for users from other fields. In fact, many of the third party NUFFT packages we attempted to try for this experiment seem to be poorly

maintained and lack adequate supporting documents while the FINUFFT package used by this study comes into existence only in 2017.

Theoretically both NUFFT and FFT speed scale up similarly with the logarithm of the number of spectral points [49,50]. So there should not be no fundamental speed advantage or disadvantage by either NUFFT or interpolation methods. To investigate this issue, we carried out a rough comparison of the actual performance of our implementation of NUFFT method (FINUFFT Python package [49,50]) with our interpolation FFT method (Python SciPy interpolate and FFT packages [51]) from both a computation time and memory consumption perspective.

For CPU computing time the NUFFT method is generally as fast (and sometimes faster) than the cubic spline interpolation /FFT method. The difference depends on sample size because the speed does not scale linearly with the number of sample points. For example, for a data size of 40 million sampling points, the NUFFT is is tested to be about 32 seconds while the interpolation method is around 48 seconds. However, for other sample sizes the difference can be much less. In addition, the NUFFT method consumes less memory than the interpolation / FFT method i.e. the linear interpolation / FFT method requires 50 % more memory than the NUFFT and the cubic interpolation / FFT method requires 3 times as much memory.

Also, it is important to note another very significant practical advantage of the FINUFFT package in that it allows users to select only a subset of spectral points to calculate which can significantly reduce computing time while standard FFT packages always compute the whole spectrum.

Thus, overall NUFFT is more efficient in our Python implementation, although the time / resource saving may be small compared to other processing procedures such as graph plotting etc. While it is entirely possible that this advantage of NUFFT is only due to better optimization by the FINUFFT package, this at least demonstrates that NUFFT has practical advantages.

6.4. Discussion

We have used experiments to compare the results of both NUFFT and interpolation FFT methods in spectral shape, spectral amplitude, spectral noise levels, aliasing and under

sampling behaviour and computer performance. Next, in this section we would use simulation and theoretical derivation to better understand the findings from the experiment results. We simulate a signal from an ideal monochromatic source to compare the difference between both methods in spectral amplitude and noises. We also tested a non-standard form of nonuniform Fourier transform equation devised by us and shows better noise level than the standard nonuniform Fourier transform.

6.4.1 Spectral noise

Usually an experiment contains many kinds of noises. However, we are only interested in the noise differences between the two methods. Thus, we use simulation to better compare the spectral noises generated by the two methods. According to the equation of either nonuniform Fourier transform and uniform transform, a signal of a single frequency can introduce values to other parts of the calculated spectrum. This could be considered a type of spectral noise/error. In addition, for the interpolation FFT method the interpolation could also introduce some errors to the interpolated interferogram which would result in additional noises.

We construct the interferogram of an ideal non-uniformly sampled monochromatic 632.8 nm source (essentially a cosine wave) using the sampling position information from one of the experimental measurements. We then calculate the spectrum from this simulated interferogram using both NUFFT and interpolation methods and plot the result on a log scale. Figure 39 shows the result of cubic spline interpolation, linear interpolation, NUFFT and an under-sampled NUFFT result. The average sampling rate was set to about twice the Nyquist rate so that the signal's characteristic spectral peak appears in the centre of the calculated spectrum. It shows that the noise level of NUFFT is comparable to interpolation, but their noise shape is significantly different, with the NUFFT shape being much more irregular. We also test the under-sampling feature of NUFFT and show that under-sampling will result in significantly higher noise levels. In addition, the figure also indicates the value of the peak of the spectrum. We have chosen the amplitude of the simulated signal such that the theoretical spectral amplitude should equal 1. It can be seen that linear interpolation has a much lower spectral peak value than other methods while the NUFFT value agrees perfectly with the predicted one. We will discuss the theoretical spectral amplitude further in the next section.

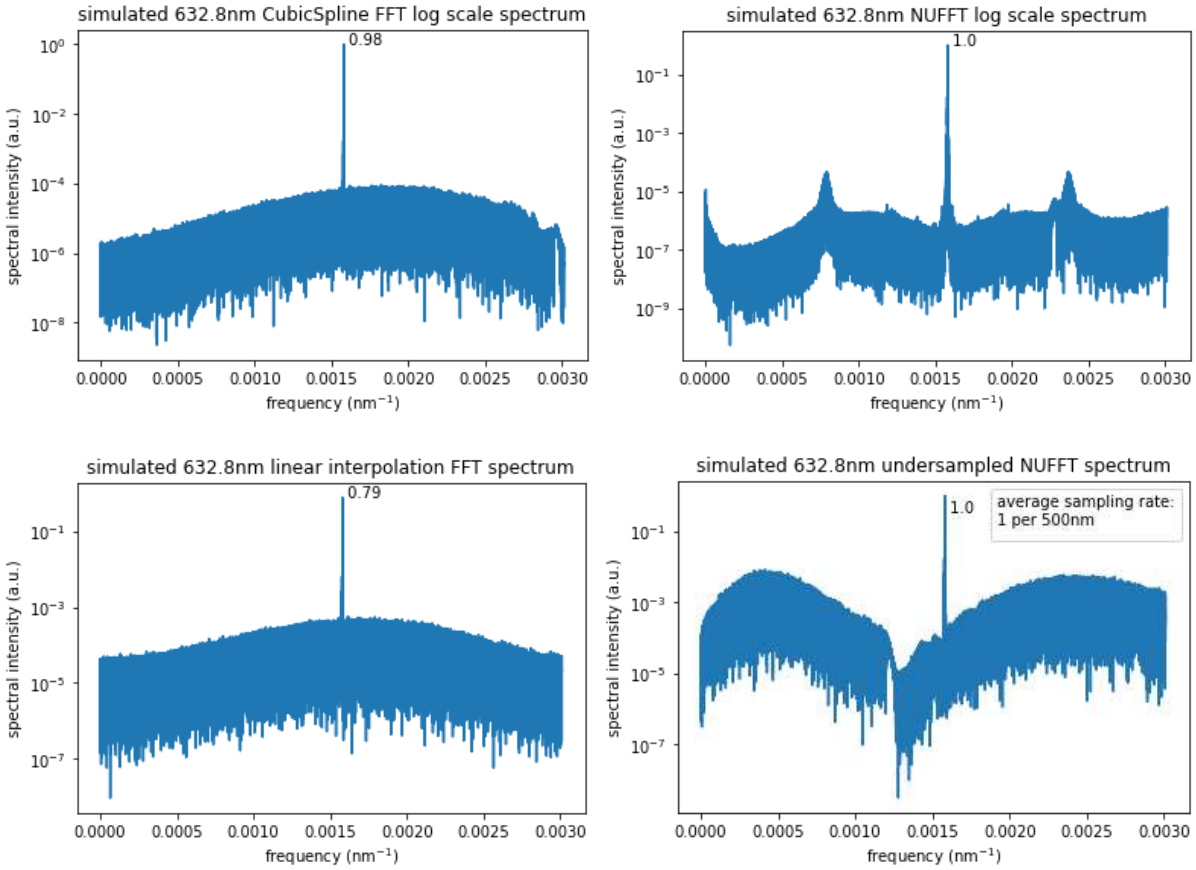

Figure 39 Comparison of simulated spectral noise by cubic spline interpolation (top left), NUFFT (top right), linear interpolation (bottom left), and under-sampled NUFFT (bottom right). The average sampling rate is about 1 per 170nm except the last graph which is under sampled at around 1 per 500nm.

6.4.2 Spectral amplitude

In section 6.4.1.3 it was demonstrated that the NUFFT spectral amplitude is proportional to the average sampling rate but the interpolation FFT spectral amplitude is not linearly related to sampling rate and is also dependent on the type of optical source.

To better understand this phenomenon, we first try to determine the theoretical spectral amplitudes for both non-uniform and uniform discrete Fourier transform equation. According to the equation of both non-uniform and uniform discrete Fourier transform, the calculated spectral amplitude for an ideal monochromatic signal without normalization is equal to the signal amplitude times the number of sample points if the signal frequency happens to fall on one of the spectral points calculated i.e.

$$F(v_k) = \sum_{n=1}^{N} (Ae^{i2\pi v x_n}) e^{-i2\pi v_k x_n} = NA \quad for\ v_k = v$$

where $Ae^{i2\pi vx}$ is the monochromatic source and A, v are the signal amplitude and frequency respectively. When spectral noise is considered, the above equation may not be true. However, the level of noise in the experiment is not sufficient to account for the differences between NUFFT and interpolation methods.

Combined with the fact that the NUFFT spectral amplitude is proportional to sampling rate in the experimental result. We can postulate that the amplitude difference between the two methods is due to the interpolated signal being not the same as the actual signal. Suppose that on the contrary interpolation can perfectly reproduce the actual signal value, then we should expect no amplitude difference in the calculated results. For the 532nm laser source the experiment result shows that the interpolated signal amplitude decreases with decrease of sampling rate. For the 960 nm SLED source the result shows that the interpolated signal amplitude can be larger or smaller than the actual amplitude with no apparent trend. We postulate that this is due to that the interferogram of a broadband source is very sharp, its amplitude is strongest when the optical path difference equals 0 and quickly loses strength as the optical path difference increases. Thus, the position of interpolation points and sample points may cause the amplitude of the interpolated interferogram to be either overestimated or underestimated.

6.4.3 A non-standard variant of NUFFT

As far as we know, there are no fundamental reasons why the equation for the non-uniform Fourier transform has to be the way as it is defined and perhaps there can be other definitions that would be more suitable for Fourier transform spectrometry applications. To explore this point, we devised and tested a nonstandard variant of the non-uniform Fourier transform equation by giving each sample points a weight based on the local sampling interval to see if it can give better spectral results. The definition is given below:

$$F(v_n) \equiv \sum_{k=1}^{N} f(x_k) \frac{(x_{k+1} - x_{k-1})}{2} e^{-i2\pi v_n x_k}$$

The reasoning behind this modification is that the summation formula of this nonstandard variant of nonuniform Fourier transform will converge to the formula of the continuous Fourier transform when the average sampling rate is sufficiently high:

$$\sum_{k=1}^{N} f(x_k)\frac{(x_{k+1}-x_{k-1})}{2}e^{-i2\pi v_n x_k} \xrightarrow{\Delta x\to 0} \int_{x_0}^{x_N} f(x)e^{-i2\pi v_n x}dx$$

A positive aspect of this modification is that almost no speed penalty will be incurred by its inclusion and the existing NUFFT package can still be utilised. To clearly illustrate the effect of this modification, a similarly constructed interferogram is utilised again here (shown on Figure 40 where the average sampling rate was set at about 1 per 125 nm and the frequency is shown in inverse of wavelength). The corresponding maximum frequency limit (Nyquist frequency) in the uniformly sampling discrete Fourier transform would have been 250 nm or 0.004 nm^{-1}. But as outlined in section 6.3.2 the NUFFT has no maximum frequency limit. It can be seen from Figure 40 that this nonstandard variant of NUFFT has a significantly lower spectral noise level for frequencies lower than the Nyquist frequency (<0.004 nm^{-1}). However, it shows no improvement in the under sampled region (>0.004 nm^{-1}). This demonstrates again that even though there are no theoretical maximum frequency limits to the NUFFT there are still behavioural differences between under sampled and sufficiently sampled region. Testing with the experimental data shows that the difference with the standard NUFFT is minimal with very marginal improvements.

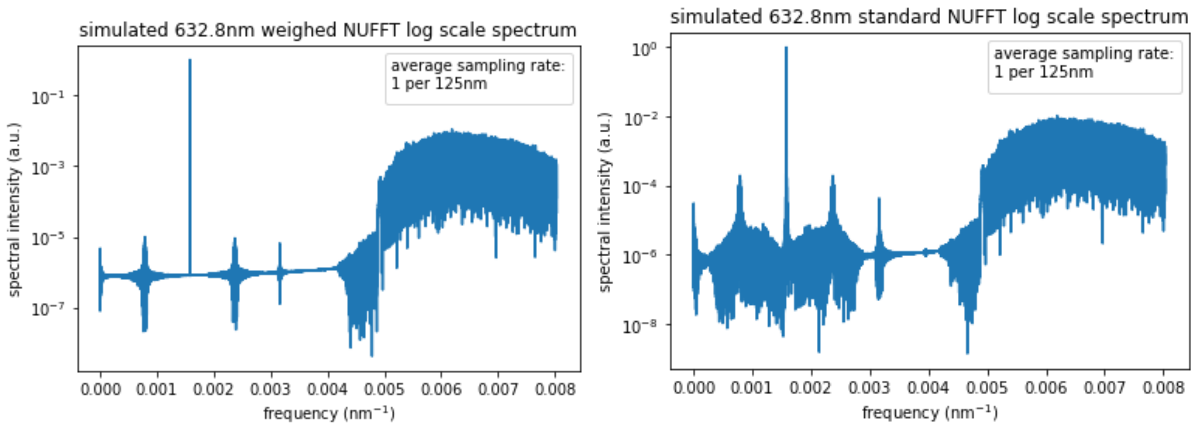

Figure 40 Comparison of spectrum of an ideal 632.8 nm cosine wave signal by weighted NUFFT (left) to that of standard NUFFT (right).

6.4.4 Computation

It may seem surprising that nonuniform Fourier transform has not been tried in Fourier transform spectrometry even though it has been well known in many other fields. One of the reasons is the general lack of suitable software and libraries. The software library used in this study, FINUFFT, only comes into existence in 2017. And in fact, it is the only actually usable

NUFFT library out of all the alternative libraries this study has found and attempted to try. All the other alternative libraries we found are practically unusable due to lack of sufficient documentations. Those libraries are often created for specific applications and is therefore difficult for users from other fields. Meanwhile, the traditional interpolation method has worked well enough in most cases that there is little incentive for researchers to explore alternative techniques. Another reason is that most Fourier transform spectrometers are commercial ones nowadays and relatively few researchers build Fourier transform spectrometers themselves. This prevents most researchers from innovating on the data processing methods for Fourier transform spectrometers.

6.5. Conclusion

A detailed experimental study has been carried out to show that the NUFFT method is as good (and sometime better) than the resampling by interpolation / FFT method for a non-uniformly sampled Fourier transform spectrometer in terms of spectral shape and spectral noise levels. The NUFFT method is also better in reproducing spectral amplitudes and has advantages in under-sampled situations where aliasing may be an issue. It was also shown that non-uniform sampling has fundamental benefits over uniform sampling due to its non-periodic nature with under sampling, anti-aliasing and electric noise mitigation properties. The NUFFT method also consumes less computer memory and can be faster than interpolation FFT in certain cases. A nonstandard form of NUFFT was also investigated and showed marginal improvement over the original standard form of non-uniform Fourier transform. As a result, it can be concluded that NUFFT is an equal or superior alternative to traditional interpolation / FFT method for a non-uniformly sampled Fourier transform spectrometer.

Chapter 7. Properties of Equipment and Software Libraries

7.1. Introduction

Analysing experiment result is much more than applying textbook theories. That is because textbook theories are usually highly simplified idealised cases. For example, textbooks will simply say that a monochromatic source will produce a simple cosine wave signal in Michelson interferometer while our experimental results with the single mode helium neon laser is much more complicated than that. Actual experiment results are heavily influenced by the idiosyncratic properties of the instrument which are often idealised and ignored by textbooks. Thus, it is very important to know the properties of the various hardware properties and software libraries in order to better understand and quantitatively analyse the experiment results.

The equipment and software used in this experiment are: a Physik Instrumente M-531.DDX linear translation stage with a moving range of 306 millimetre and is controlled by a Mercury C-860.10 DC-motor controller and a 25 millimetre PMC linear translation stage, a National Instrument NI-PCI-MIO-16E-4 data acquisition device with a maximum sampling rate of 1666666Hz and a National Instrument USB-6341 X series Multifunction I/O data acquisition device with a maximum sampling rate of 500 KHz. A 340 nm-1100 nm Thorlabs PDA100A-EC Switchable Gain Detector with several gain level setting ranging from 0 dB to 70 dB, a pair of Melles Griot surface coated cube corner retroreflectors with a diameter of 6.5 cm and a pair of Newport surface coated cube corner retroreflectors with a diameter of 2.5 cm, a BS013 50:50 400 - 700 nm non-polarizing beam splitter cube, several silver surface coated plane mirrors. Several light sources are used: a Thorlabs HRS015 frequency stabilized 632.8 nm helium neon laser, a Melles Griot 05-LHR-991 632.8 nm helium neon laser, a 960 nm Superlum SLD-MS-261 SLED, a 680nm Superlum SLD-MS-261 SLED, a 960nm Superlum SLD-MS-481-MP-SM SLED, a 532 nm CNI MGL-III-532-20mW solid state laser. Notable software used are: National Instrument LabVIEW 2011, Python 3.10, FINUFFT 2.1.0 python package, SciPy and NumPy python package.

This chapter will discuss the properties of all the instrument components and software libraries used for this research. These equipment are about two decades old with all of their

documents missing. They have long past their service life and some of their manufacturers have since went defunct. We can only find back some specification documents of them.

7.2. Equipment

7.2.1. Optical elements

Several optical components including plane mirrors, cube corner retroreflectors, and beam splitters are used. The regular mirrors ubiquitous in our daily life are back coated. As a result, light will reflect twice from both the surface and the backside. This is not desirable for experiments. Hence, the plane mirrors and the cube corner retroreflectors used in this research are surface coated. But the drawback is that the surface can be easily damaged. The plane mirrors used in the experiment have been very old. There are many surface damages to them.

All cube corner retroreflectors used are made from three separate plane mirrors pieced together. The main property of retroreflector is their accuracy in how parallel the reflected beam is relative to the incoming beam. We are not able to find the specification documents of our retroreflectors. The parallelism of the Newport retroreflector is specified to be 1 second.

The primary beam splitter used in this experiment is a Thorlabs BS013 400 - 700 nm 50:50 non-polarizing 25.4 mm cube beam splitter. Figure 41 shows its transmission and reflectance graph for both polarization directions, respectively.

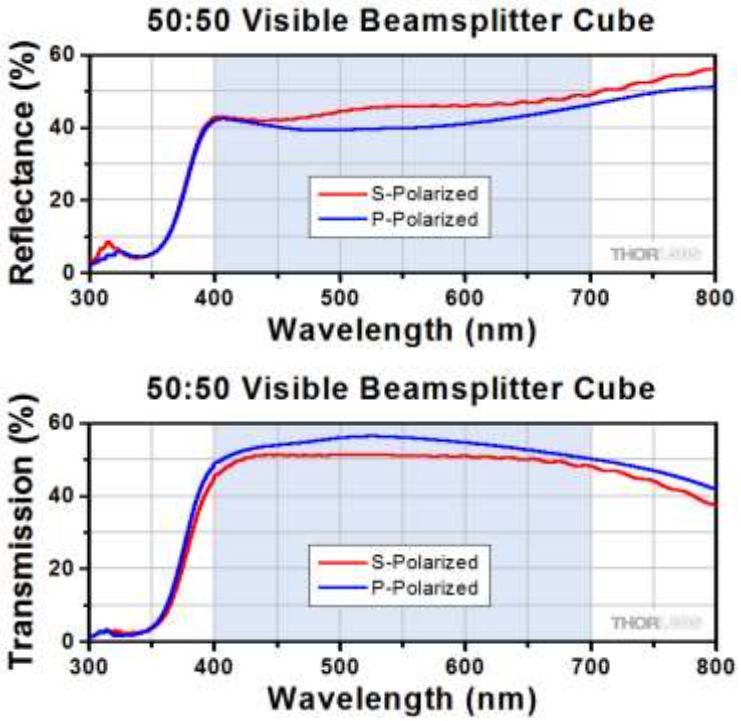

Figure 41 transmission and reflectance curves for the beamsplitter Thorlabs BS013. Source: [52]

7.2.2. Light sources

Two helium neon laser sources have been used. The first one, a Melles Griot 05-LHR-991 632.8 nm helium neon laser, is a 20 years old product. Its manufacturer has gone defunct. We are not able to find back its specification document. The second one is a Thorlabs HRS015 stabilized 632.8 nm 1.2 mW polarized helium neon laser. Since the stabilized HeNe laser features a single mode output, the coherence length is increased to hundreds of meters. Figure 42 shows the spec sheet as well as the design schematics of this laser.

Item #	HRS015
Wavelength	632.991 nm
Long Term Beam Drift	<0.05 mrad
Series Resistors in Housing	94 KΩ
Operating Current	5.0 mA
Shock	15 g for 11 msec
Weight	600 g
CDRH/CE Classification	IIIa/3R (HRR005 is IIa/2)
Un-stabilized Power	1.2 mW min, 2.7 mW max
Stabilized Power	>1.2 mW
Polarization	Linear > 1000:1
Mode Structure	TEM00 > 99%
Beam Diameter	0.7 mm
Beam Divergence	1.25 mrad
Beam Drift	<0.2 mrad
Long-Term Beam Drift	<0.05 mrad
Noise (30 Hz – 10 MHz)	<0.3% rms max.
Starting Voltage	10 kV (DC)
Operating Voltage (DC)	1500 V
Length (L)	13.65" (346.7 mm)
Diameter	Ø1.77" (Ø45 ± 0.5 mm)
Operating Temperature[2]	15 – 30 °C
Time to Lock[3]	< 25 minutes, Typical
Power Input	100 - 240 VAC, 50 - 60 Hz
Power Consumption	<40 VA
Lifetime (Typ.)[4]	25,000 h
Frequency Stabilized Mode	
1 min	±1 MHz
1 hour	±2 MHz
8 hours	±2 MHz
Intensity Stabilized Mode	
1 min	±0.1 %
1 hour	±0.2 %
8 hours	±0.3 %

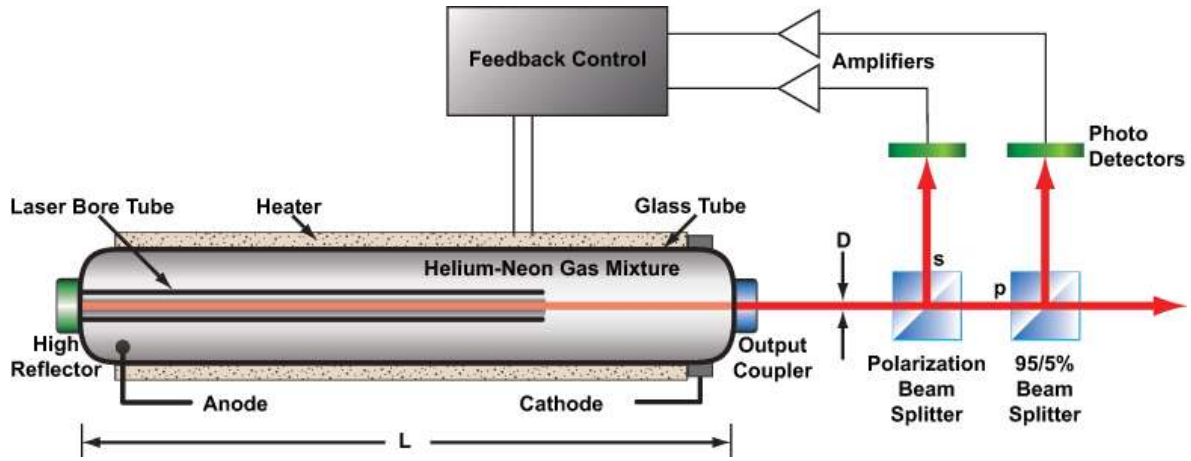

Figure 42 Spec sheet (top) and design drawing (bottom) of Thorlabs HRS015 laser. Source: [53]

This Thorlabs stabilized HeNe laser offer the ability to change between two modes of operation: frequency and intensity stabilization. Figure 42 shows the mode stabilization mechanism principle of this laser. According to the documentation [53]: "*The frequency stabilization mode will balance the intensity of two modes under the gain curve in order to keep the frequency of the laser stable. The tube length is specifically chosen to only allow two cavity modes at the output. The polarization states of the modes are orthogonal (i.e. one will be s-polarized and the other will be p-polarized). Using a polarizing beamsplitter, one of the*

modes is directed to a photodetector, while the remaining mode passes through a second beamsplitter where 5% of the output is reflected to a second photodetector, as shown in the schematic above. An error signal generated by the two photodetectors is used to control a heater wrapped around the glass tube. The heater causes the tube to expand and contract as necessary to stabilize the frequency. The frequency stabilization mode also delivers some intensity stability. The intensity stabilization mode will stabilize the intensity of the output beam. This mode operates on the same principle as frequency stabilization; however, only one of the photodectectors is used to generate the feedback error signal to control the heater. The intensity stabilization mode also delivers some frequency stability. It should be noted that back reflections into the laser aperture will impair the ability of the control loop to stabilize the frequency or intensity of this laser. Furthermore, large amounts of back reflections can potentially disturb the population inversion of the laser, rendering it unable to lase properly."

A 532 nm CNI MGL-III-532-20mW solid state laser is also used. Figure 43 shows the spec sheet of it.

Wavelength (nm)	532±1	
Operating mode	CW	
Output power (mW)	>1, 5, 10, 20, … ,200	>200, …, 300
Power stability (rms, over 4 hours)	<1%, <2%, <3%	<2%, <3%
Transverse mode	TEM_{00}	
M^2 factor	<1.2(<1.1 optional)	
Beam diameter at the aperture $1/e^2$ (mm)	~1.2	
Beam divergence, full angle (mrad)	<1.2	
Polarization ratio	>100:1, Horizontal±5 degree (Vertical Optional)	
Warm-up time (minutes)	<10	
Beam height from base plate (mm)	24. 8	
Pointing stability after warm-up (mrad)	<0.05	
Operating temperature (℃)	10~35	
Power supply (90-264VAC or 5VDC)	PSU-III-LED/PSU-III-FDA/PSU-III-OEM-97	
Modulation option	TTL on/off, 1Hz-1KHz, 1KHz-10KHz, 10KHz-30KHz; and Analog modulation option	
Expected lifetime (hours)	10000	
Warranty	1 year	

Figure 43 spec sheet of CNI MGL-III-532-20mW laser. Source: [54]

Two Superlum superluminescent diode is used, a 680 nm Superlum SLD-MS-261 SLED and a 960 nm Superlum SLD-MS-481-MP-SM SLED. According to the manufacturer, [55] ''*SLD-MS-series Miniature Broadband Light Source Modules are miniature broadband SM fiber light source modules at different wavelengths in 670 – 880 nm spectral range for applications requiring a reliable, powerful, stable and low noise SLD light source with a broad and flat*

spectrum and a short coherence length. The SLD module inside a light source is powered by a high-precision current and temperature controller.'' We could not exactly find their specification documents but found documents for similar models to them. Figure 44 shows specs table for models of their series and an example spectral profile of a specific 670 nm model.

– bell-shaped spectrum, – multi-humped spectrum.

Model number	Center wavelength (nm)	Spectral width, FWHM (nm)		Output power, SM (mW)		Optical spectrum and coherence function
		Min.	Typ.	Min.	Typ.	
SLD-MS-261-MP-SM-670	670 ± 10	6	7	2.0	-	HTML | PDF (43 KB)
SLD-MS-381-MP-SM-795	795 ± 5	15	20	2.0	-	HTML | PDF (43 KB)
SLD-MS-381-MP-SM-830	830 ± 10	15	20	2.0	-	HTML | PDF (40 KB)
SLD-MS-351-MP-SM-830	830 ± 10	70	75	2.0	2.5	HTML | PDF (47 KB)
SLD-MS-341-MP-SM-840	840 ± 10	45	47	2.0	-	HTML | PDF (46 KB)
SLD-MS-371-MP-SM-840	840 ± 10	45	50	2.0	2.5	HTML | PDF (46 KB)
SLD-MS-381-MP-SM-850	850 ± 10	15	20	2.0	-	HTML | PDF (43 KB)
SLD-MS-351-MP-SM-850	850 ± 10	57	60	2.0	-	HTML | PDF (45 KB)
SLD-MS-341-MP-SM-880	880 ± 10	45	47	2.0	-	HTML | PDF (47 KB)

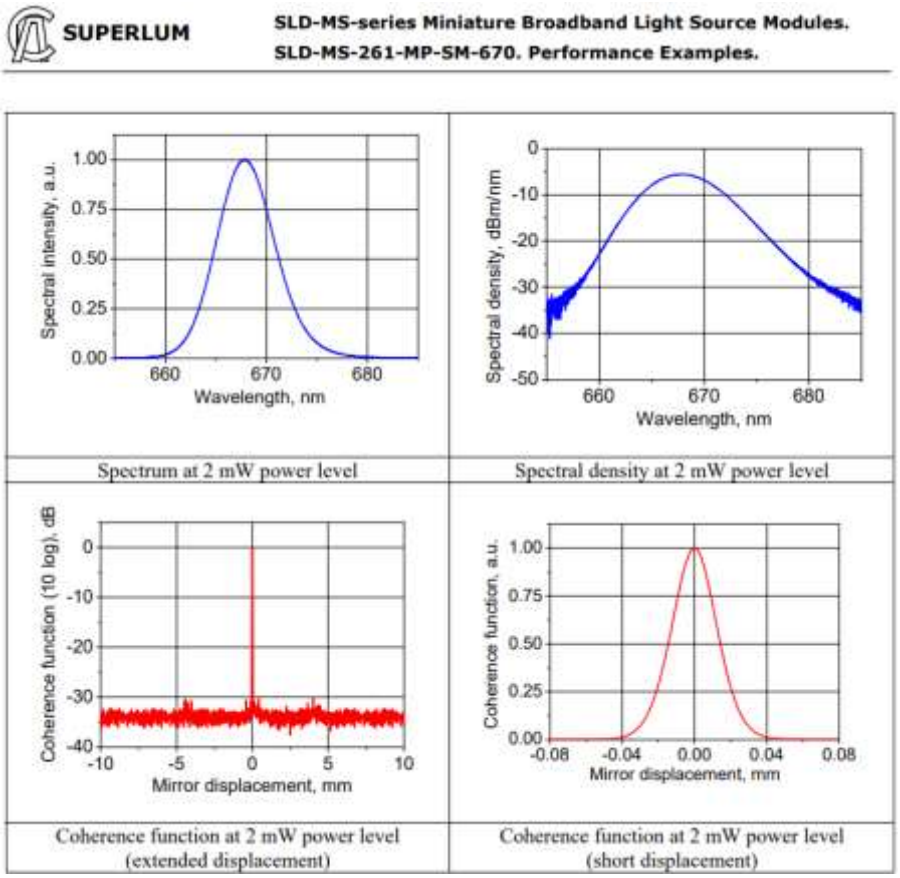

Figure 44 Spec sheet(top) and example spectral profile of the Superlum SLD products. Source: [55]

7.2.3. Photodetectors

The photodetector used is a Thorlabs PDA100A-EC Switchable Gain Detector with frequency range of 340 nm-1100 nm and adjustable output gain level ranging from 0 dB to 70 dB. The property of photodetector is especially important because it directly affects the resulting spectrum profile. This photodetector is consisted of two parts, one photodiode and an amplifier. The first property of this photodetector is the responsivity of the photodiode. It is defined as a ratio of generated photocurrent (I_{PD}) to the incident light power (P) at a given wavelength:

$$R(\lambda) = \frac{I_{PD}}{P}$$

The responsivity is a function of the wavelength of the light and is highly nonlinear. Figure shows the responsivity curve of this photodetector. The second property is the bandwidth and response of the photodetector circuit. The function of a photodetector is to convert variation in light intensity into variation in electric voltage. But this conversion is also not linear. It is a function of the frequency of variation in light intensity. It is related to the photodiode junction capacitance and terminal resistance. The bandwidth is defined as the width when the gain has fallen to 50 percent. The specification manual does not give the response curve of this photodetector. But it provides the table of bandwidth under different gain level settings. Figure 45 shows the design principle of this photodetector, responsivity curve, the table of gain level and bandwidth as well as other properties at different gain settings.

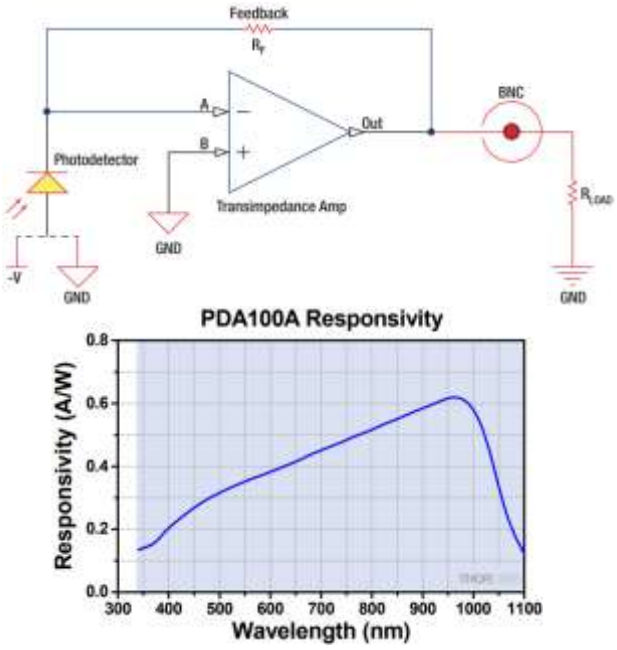

Performance Specifications[2]			
0 dB Setting		**40 dB Setting**	
Gain (Hi-Z)	1.51×10^3 V/A ±2%	Gain (Hi-Z)	1.51×10^5 V/A ±2%
Gain (50 Ω)	0.75×10^3 V/A ±2%	Gain (50 Ω)	0.75×10^5 V/A ±2%
Bandwidth[3]	2.4 MHz	Bandwidth[4]	225 kHz
Noise (RMS)	254 µV	Noise (RMS)	799 µV
NEP (@ λ_p)	2.7×10^{-11} W/√Hz	NEP (@ λ_p)	3.55×10^{-13} W/√Hz
Offset	±5 mV (10 mV max)	Offset	±8 mV (15 mV max)
10 dB Setting		**50 dB Setting**	
Gain (Hi-Z)	4.75×10^3 V/A ±2%	Gain (Hi-Z)	4.75×10^5 V/A ±2%
Gain (50 Ω)	2.38×10^3 V/A ±2%	Gain (50 Ω)	2.38×10^5 V/A ±2%
Bandwidth[4]	1.6 MHz	Bandwidth[4]	78 kHz
Noise (RMS)	261 µV	Noise (RMS)	998 µV
NEP (@ λ_p)	1.1×10^{-11} W/√Hz	NEP (@ λ_p)	2.42×10^{-12} W/√Hz
Offset	±6 mV (12 mV max)	Offset	±8 mV (15 mV max)
20 dB Setting		**60 dB Setting**	
Gain (Hi-Z)	1.5×10^4 V/A ±2%	Gain (Hi-Z)	1.5×10^6 V/A ±5%
Gain (50 Ω)	0.75×10^4 V/A ±2%	Gain (50 Ω)	0.75×10^6 V/A ±5%
Bandwidth[4]	860 kHz	Bandwidth[4]	20 kHz
Noise (RMS)	349 µV	Noise (RMS)	1163 µV
NEP (@ λ_p)	8.91×10^{-12} W/√Hz	NEP (@ λ_p)	1.22×10^{-12} W/√Hz
Offset	±6 mV (15 mV max)	Offset	±8 mV (15 mV max)
30 dB Setting		**70 dB Setting**	
Gain (Hi-Z)	4.75×10^4 V/A ±2%	Gain (Hi-Z)	4.75×10^6 V/A ±5%
Gain (50 Ω)	2.38×10^4 V/A ±2%	Gain (50 Ω)	2.38×10^6 V/A ±5%
Bandwidth[4]	480 kHz	Bandwidth[4]	5.9 kHz
Noise (RMS)	561 µV	Noise (RMS)	1490 µV
NEP (@ λ_p)	4.65×10^{-12} W/√Hz	NEP (@ λ_p)	9.73×10^{-13} W/√Hz
Offset	±8 mV (15 mV max)	Offset	±30 mV (Max)

Figure 45 Schematics (left top), responsivity curve (left bottom) and bandwidth spec (right) of the Thorlabs PDA100A-EC photodetector. Source: [56]

7.2.4. Data acquisition devices

There are two data acquisition devices, one is a National Instrument PCI-MIO-16E-4 Multifunction I/O Device. It is a 20-year-old product. The other is a USB-6341 X series Multifunction I/O Device. We give the relevant specification of them we found from the internet here to give the reader a better idea of the characteristics of the experiment results in this thesis such as the noise levels. These are not high-tech products nowadays. They are of similar technology to the computer GPUs but for different purpose. However modern GPUs have much higher performance than them. The accuracy of the device is very important. Figure 46 shows the accuracy specification table of the PCI-MIO-16E-4 product provided in the specification document and Figure 47 shows that for the USB-6341 device.

Accuracy Information

Nominal Range (V)	Absolute Accuracy							Relative Accuracy Resolution (mV)	
	% of Reading		Offset (mV)	Noise + Quantization (mV)		Temp Drift (%/°C)	Absolute Accuracy at Full Scale (mV)		
	24 Hours	1 Year		Single Pt.	Averaged			Single Pt.	Averaged
±10	0.0672	0.0714	7.38	4.64	0.846	0.0010	15.373	6.27	1.11
±5	0.0272	0.0314	3.70	2.32	0.423	0.0005	5.697	3.14	0.557
±2.5	0.0672	0.0714	1.86	1.16	0.211	0.0010	3.859	1.57	0.278
±1	0.0672	0.0714	0.757	0.464	0.085	0.0010	1.556	0.627	0.111
±0.5	0.0672	0.0714	0.389	0.269	0.042	0.0010	0.789	.0339	0.056
±0.25	0.0672	0.0714	0.205	0.134	0.021	0.0010	0.405	0.169	0.028
±0.1	0.0672	0.0714	0.095	0.076	0.010	0.0010	0.176	0.088	0.013
±0.05	0.0672	0.0714	0.058	0.056	0.006	0.0010	0.100	0.064	0.008
0 to 10	0.0272	0.0314	3.70	2.32	0.423	0.0005	7.269	3.14	0.557
0 to 5	0.0672	0.0714	1.86	1.16	0.211	0.0010	5.645	1.57	0.278
0 to 2	0.0672	0.0714	0.757	0.464	0.085	0.0010	2.271	0.627	0.111
0 to 1	0.0672	0.0714	0.389	0.269	0.042	0.0010	1.146	0.339	0.056
0 to 0.5	0.0672	0.0714	0.205	0.134	0.021	0.0010	0.583	0.169	0.028
0 to 0.2	0.0672	0.0714	0.095	0.076	0.010	0.0010	0.247	0.088	0.013
0 to 0.1	0.0672	0.0714	0.058	0.056	0.006	0.0010	0.135	0.064	0.008

Note: Accuracies are valid for measurements following an internal E Series calibration. Averaged numbers assume dithering and averaging of 100 single-channel readings. Measurement accuracies are listed for operational temperatures within ±1 °C of internal calibration temperature and ±10 °C of external or factory-calibration temperature. NI recommends a one-year calibration interval. The Absolute Accuracy at Full Scale calculations were performed for a maximum range input voltage (for example, 10 V for the ±10 V range) after one year, assuming 100 points of averaged data. Go to ni.com/info and enter info code rdepec for example calculations.

Figure 46 Accuracy spec table of the PCI-MIO-16E-4 data acquisition device. Source: [57]

Nominal Range Positive Full Scale (V)	Nominal Range Negative Full Scale (V)	Residual Gain Error (ppm of Reading)	Residual Offset Error (ppm of Range)	Offset Tempco (ppm of Range/°C)	Random Noise, σ (μVrms)	Absolute Accuracy at Full Scale (μV)
10	-10	65	13	23	270	2,190
5	-5	72	13	23	135	1,130
1	-1	78	17	26	28	240
0.2	-0.2	105	27	39	9	60

Table 1. AI Absolute Accuracy

Figure 47 Accuracy spec table of the USB-6341 data acquisition device. Source: [58]

The absolute accuracy is a property defined by National Instrument to quantify the overall maximum error of measurement. According to the document: [57,58] *"It only applies to a calibrated DAQ device. There are four components of an absolute accuracy specification: % of Reading is a percent of the actual input voltage. Offset is a constant offset applied to all measurements. Noise + Quantization is based on noise and depends on the number of points averaged for each measurement. Drift is based on variations in your ambient temperature. Based on these components, the formula for calculating absolute accuracy is: Absolute Accuracy = ±[(Input Voltage * % of Reading) + (Offset + Noise + Quantization + Drift)]. Drift is already accounted for unless your ambient temperature is outside +15 to +35 °C. For instance, if your ambient temperature is at 45 °C, you must account for 10 °C of drift. This is calculated by: Drift = Temperature Difference * % Drift per °C * Input Voltage. Absolute Accuracy at Full Scale is a calculation of absolute accuracy for a specific voltage range using the maximum*

voltage within that range, the one year after calibration Accuracy Drift Reading and the Noise + Quantization averaged value."

In our experiments and tests we did not find any significant difference between the two PCI-MIO-16E-4 and USB-6341 data acquisition devices. Since these devices are long out of service life and there is no guarantee that they are still functioning properly, out of precaution we would often use both devices to double check each other to make sure that we are not getting erroneous results.

7.2.5. Linear translation stages

A 25mm linear translation stage and a 306mm linear translation stage were used in this experiment. The linear translation stage determines how nonuniformly the interference signal is sampled. Both stages work by rotating a ball screw linear actuator which turns rotational movement into linear movement. We cannot find the document for the 25 mm linear translation stage. The 306 mm Physik Instrumente M-531.DDX linear translation stage is more advanced than the 25mm linear translation stage. It is controlled by a Proportional-Integral-Derivative (PID) controller Mercury C-860.10 which means it will have a more linear movement profile. According to the document, [59] '*M-5x1 series linear stages are low-profile, high-accuracy linear translation devices for industrial use and laboratory applications with integrated linear scale encoder providing 0.1 µm minimum incremental motion and 1 µm full-travel accuracy. High-precision linear guiding rails with recirculating ball bearings guarantee 1 µm / 100 mm straightness and flatness*'. Figure 48 shows the picture and the mechanical specifications of this stage.

General Mechanical Data	
Straightness / Flatness:	1 µm per 100 mm
Origin Repeatability:	1 µm
Max. Load capacity:	100 kg
Max. push/pull force:	80/80 N
Max. lateral force:	200 N
Ballscrew pitch:	2 mm
Material:	Aluminum

Figure 48 Mechanical spec table of the Physik Instrumente M-531.DDX linear translation stage. Source: [59]

We would give the general principle of the PID controller here. A PID controller is a feedback control loop mechanism that uses the real-time error value from the system sensor to

compute the real-time correction value used to adjust the system in real time. The equation to calculate the control value from error is:

$$u(t) = K_{\mathrm{p}} e(t) + K_{\mathrm{i}} \int_0^t e(\tau)\,\mathrm{d}\tau + K_{\mathrm{d}} \frac{\mathrm{d}e(t)}{\mathrm{d}t}$$

Where e(t) is the error provided by the system. This equation has three parameters which is where the PID controller gets its name from.

7.2.6. Python libraries

Several python functions were used in this study from the third-party python libraries SciPy 1.9.3 and FINUFFT 2.1.0. We would list those functions below.

scipy.interpolate.CubicSpline(x, y, axis=0, bc_type='not-a-knot', extrapolate=None)

Cubic spline data interpolator.

scipy.interpolate.interp1d(x, y, kind='linear', axis=-1, copy=True, bounds_error=None, fill_value=nan, assume_sorted=False)

Interpolate a 1-D function.

scipy.fft.fft(x, n=None, axis=-1, norm=None, overwrite_x=False, workers=None, *, plan=None)

Compute the 1-D discrete Fourier Transform.

scipy.fft.ifft(x, n=None, axis=-1, norm=None, overwrite_x=False, workers=None, *, plan=None)

Compute the 1-D inverse discrete Fourier Transform.

scipy.fft.rfft(x, n=None, axis=-1, norm=None, overwrite_x=False, workers=None, *, plan=None)

Compute the 1-D discrete Fourier Transform for real input.

finufft.nufft1d1(x, c, n_modes=None, out=None, eps=1e-06, isign=1, **kwargs)

1D type-1 (nonuniform to uniform) complex NUFFT.

finufft.nufft1d3(x, c, s, out=None, eps=1e-06, isign=1, **kwargs)

1D type-3 (nonuniform to nonuniform) complex NUFFT.

7.3. Discussion

So far, we have built Fourier transform spectrometers and used them to measure spectrum profile of some light sources. But the calculated the spectrum profile may not be the true emission profile of the light source. This depends on equipment properties like the mirror reflectance curve, photodiode responsivity and circuit bandwidth. It is possible to reconstruct the true spectral profile of the light sources if these properties are known. But this is beyond the scope of this study.

The linear translation stage is also important in that it determines how nonuniform the signal is sampled. For the 306 mm linear translation stage, its controller has parameters that can be tuned by the customers. Determining the optimal values for the parameters of this controller is a very complex engineering topic and time-consuming process. There are many studies on how to tune the PID parameters [60]. The parameters of the PID controller can be tuned manually or automatically using various methods such as Ziegler-Nichols, Cohen-Coon, or model-based optimization techniques [60]. It is beyond the scope of this study to tune the parameters of the controller of the linear translation stage. We would leave the device parameters to their default values for this study.

Knowing the specific software library functions used for computations as well as the version number is very important. Because the actual algorithm used by those functions for complicated calculations such as the Fourier transform and interpolation are likely more complicated than the idealised theoretical equations and they may take more approximations during calculation than would appear from theories. For example, fast Fourier transform algorithm usually require the number of samples to be the power of two, so the fast Fourier transform software functions will often zero pad the sample without explicit knowledge of the user. This can be a source of discrepancy with theoretical results. In addition, complex software codes will inevitably potentially contain some bugs which can potentially cause errors in the computation results. Thus, it is important to record the relevant software function and version number used for each calculation.

7.4. Conclusion

This chapter lists the important relevant properties of the equipment and software libraries used in this study and discusses their implications to the experimental results. This chapter's study could be useful for the Fourier transform spectrometer manufacturers and for future studies of this project.

Conclusion and Future Work

This thesis has studied the application of a new nonuniform fast Fourier transform based data processing method to nonuniform sampling Fourier transform spectrometer and systematically compare the advantages and disadvantages of this nonuniform Fourier transform method over the traditional interpolation method. It made some significant discoveries.

The significances include: Overall It is found that the nonuniform Fourier transform method is an equally good and sometimes better data processing method than the traditional interpolation method for nonuniform sampling Fourier transform spectrometer and that the nonuniform Fourier transform method has some significant advantages over the traditional interpolation method due to the non-periodic nature of nonuniform Fourier transform equation. It can allow under sampling while this is not possible with the interpolation method and also will not suffer from aliasing problem. Its spectral amplitude is independent of relative sampling rate while the interpolation method's spectral amplitude is dependent on the percentage between the light frequency and average sampling rate and is also affected by the type of light sources. It also found that nonuniform Fourier transform method is comparable to the interpolation method in spectral profile shape and the level of spectral noises. In addition, a novel variant of nonuniform Fourier transform equation was devised and tested by this study and found to have significant advantage in spectral noise level than the standard nonuniform Fourier transform equation. An unusual high resolution Michelson interferometer with novel design was also devised and implemented to support this experimental study.

The above result is included in chapter 5 and 6 and has been published to the journal Optics Communications. Besides the aforementioned main results of this thesis, this thesis also contains some unpublishable yet noteworthy results. Chapter 3 and 4 developed a rather unusual method to determine sampling position in nonuniform sampling Fourier transform spectrometers and although many similar techniques have been developed before in literature it is not a copy from literature but independent development by this study so some details of it can be innovative and worthwhile to other researchers. Chapter 7 analyses the influences of the various properties of experiment equipment and their implications which would be useful for future studies.

This study is not without shortcomings. There are a number of areas where this work can be improved. For example, this study has only used a single linear translation stage to study the properties of the nonuniform Fourier transform method. It would be very worthwhile to also try different linear translation stages with different movement characteristics to see if there will be any differences. And this study has only tested two light sources. Fourier transform spectrometry has a wide range of applications. It is also worthy to apply this method to more application scenarios. For example, non-uniform Fourier transform has been applied to Fourier domain optical coherence tomography systems. It would be worthy to investigate whether the findings from this study would also be relevant to optical coherence tomography applications. Optical Fourier transform spectrometer is often used to detect the Raman emission spectrum, fluorescence emission spectrum and infrared absorption spectrum of sample materials. It would be worthwhile to experimentally investigate how nonuniform Fourier transform performs under these scenarios. Fourier transform spectrometer is also used extensively in astronomy often in the form of imaging Fourier transform spectroscope. Some of these Fourier transform spectroscope systems use nonuniform sampling scheme. Therefore, it is also another possibility to explore applying nonuniform Fourier transform to these systems. Imaging Fourier transform spectrometer tends to have large data sizes because each pixel of the camera sensor corresponds to a Fourier transform spectrometer. Hence the under-sampling feature of nonuniform Fourier transform discovered in this study may be particularly useful in this case to potentially help reduce data sizes. Nonuniform Fourier transform is also not limited to optical systems. It has a wide variety of applications. It is also a possibility to apply the findings from this study to other non-optical signal processing applications. These are examples that could be explored for future studies.

Reference

1. National Institute of Standards and Technology (NIST), Commerce Department. Introduction to Fourier Transform Spectroscopy. Commerce Department, 1 Jan 1986, https://www.govinfo.gov/app/details/GOVPUB-C13-b09ab4872dc98367d7643d422ef6047a
2. Loewenstein, Ernest V. "The history and current status of Fourier transform spectroscopy." Applied optics 5.5 (1966): 845-854.
3. Griffiths, Peter R. "Fourier transform infrared spectrometry." Science 222.4621 (1983): 297-302.
4. Yang, Zongyin, et al. "Miniaturization of optical spectrometers." Science 371.6528 (2021): eabe0722.
5. De Oliveira, Nelson, et al. "High-resolution broad-bandwidth Fourier-transform absorption spectroscopy in the VUV range down to 40 nm." Nature photonics 5.3 (2011): 149-153. https://doi.org/10.1038/nphoton.2010.314.
6. Meng, Yijian, et al. "Interferometric time delay correction for Fourier transform spectroscopy in the extreme ultraviolet." Journal of Modern Optics 63.17 (2016): 1661-1667. DOI:10.1080/09500340.2016.1165872
7. Drissen, Laurent, et al. 'Imaging Fourier Transform Spectroscopy for Astronomy'. Fourier Transforms - New Analytical Approaches and FTIR Strategies, InTech, Apr. 2011. Crossref, doi:10.5772/15485.
8. Beer, Reinhard. Remote sensing by Fourier transform spectrometry. Vol. 170. John Wiley & Sons, 1992.
9. Suto, Hiroshi, et al. "Thermal and near-infrared sensor for carbon observation Fourier transform spectrometer-2 (TANSO-FTS-2) on the Greenhouse gases Observing SATellite-2 (GOSAT-2) during its first year in orbit." Atmospheric Measurement Techniques 14.3 (2021): 2013-2039.
10. Gross, Kevin C., Kenneth C. Bradley, and Glen P. Perram. "Remote identification and quantification of industrial smokestack effluents via imaging Fourier-transform spectroscopy." Environmental science & technology 44.24 (2010): 9390-9397.

11. Swinyard, B. M., et al. "Calibration of the Herschel SPIRE Fourier transform spectrometer." Monthly Notices of the Royal Astronomical Society 440.4 (2014): 3658-3674. https://doi.org/10.1093/mnras/stu409
12. Martin, T., L. Drissen, and Simon Prunet. "Data reduction and calibration accuracy of the imaging Fourier transform spectrometer SITELLE." Monthly Notices of the Royal Astronomical Society 505.4 (2021): 5514-5529. https://doi.org/10.1093/mnras/stab1656
13. Wang, Rong, and Yong Wang. "Fourier transform infrared spectroscopy in oral cancer diagnosis." International journal of molecular sciences 22.3 (2021): 1206. https://doi.org/10.3390/ijms22031206
14. Chen, Yanyan, et al. "Applications of micro-fourier transform infrared spectroscopy (FTIR) in the geological sciences—a review." International journal of molecular sciences 16.12 (2015): 30223-30250. https://doi.org/10.3390/ijms161226227
15. Wolfram, Fourier Transform Spectrometer, https://scienceworld.wolfram.com/physics/FourierTransformSpectrometer.html. Accessed 20 Feb. 2023.
16. Davis, Sumner P., Mark C. Abrams, and James W. Brault. Fourier transform spectrometry. Elsevier, 2001.
17. Schardt, Michael, et al. "Static Fourier transform infrared spectrometer." Optics Express 24.7 (2016): 7767-7776.
18. Li, Jie, et al. "Spectral resolution enhanced static Fourier transform spectrometer based on a birefringent retarder array." Optics express 27.11 (2019): 15505-15517.
19. Tingkui Mu, Chunmin Zhang, and Baochang Zhao. "Analysis of a moderate resolution Fourier transform imaging spectrometer." Optics communications 282.9 (2009): 1699-1705.
20. Davis, M. A., and A. D. Kersey. "Application of a fiber Fourier transform spectrometer to the detection of wavelength-encoded signals from Bragg grating sensors." Journal of Lightwave Technology 13.7 (1995): 1289-1295. doi: 10.1109/50.400685.
21. Hecht, Eugene. "Optics 2nd edition." Wokingham, England: Addison-Wesley 1987.
22. Pedrotti, F. L., and L. S. Pedrotti, Introduction to Optics, 2nd ed. Englewood Cliffs, N.J., USA: Prentice Hall, 1993.
23. Department of Physics. Michelson Interferometer, Columbia University, https://musr.ca/~jess/lab/8/node4.html. Accessed 20 Feb. 2023.

24. Malacara-Hernandez, Daniel, and Daniel Malacara-Doblado. "Optical testing and interferometry." Progress in Optics. Vol. 62. Elsevier, 2017. 73-156.
25. Reliable Instruments House. Mach-Zehnder Interferometer OE-7014. http://www.reliable-instruments.com/product/mach-zehnder-interferometer-oe-7014 Accessed 20 Feb. 2023.
26. Zhang Boyang, et al. "Sagnac interferometer based digital shearography for simultaneous dual sensitivity measurement." Optics and Lasers in Engineering 152 (2022): 106984.
27. Austerlitz, H. Data Acquisition Techniques Using PCs: Analog Signal Transducers. 2nd ed. Academic Press. 2003.
28. Brault, James W. "New approach to high-precision Fourier transform spectrometer design." Applied Optics 35.16 (1996): 2891-2896.
29. Kauppinen, J., T. Kärkkäinen, and E. Kyrö. "Correcting errors in the optical path difference in Fourier spectroscopy: a new accurate method." Applied Optics 17.10 (1978): 1587-1594.
30. Ahro, Mikko, Jyrki Kauppinen, and Ilkka Salomaa. "Detection and correction of instrumental line-shape distortions in Fourier spectroscopy." Applied Optics 39.33 (2000): 6230-6237.
31. Balashov, A. A., et al. "High resolution Fourier transform spectrometer (0.005 cm− 1) for the 0.6–100-μm spectral range." Applied Optics 17.11 (1978): 1716-1722.
32. Carli, Bruno, et al. "Far-infrared high-resolution Fourier transform spectrometer." Applied optics 26.18 (1987): 3818-3822.
33. Bruker. IFS 125HR. 2023. https://www.bruker.com/en/products-and-solutions/infrared-and-raman/ft-ir-research-spectrometers/ifs-125hr-high-resolution-ft-ir-spectrometer.html. Accessed 20 Feb. 2023.
34. Peck, Edson R. "A new principle in interferometer design." JOSA 38.1 (1948): 66-66.
35. Haschberger, Peter, and Volker Tank. "Optimization of a Michelson interferometer with a rotating retroreflector in optical design, spectral resolution, and optical throughput." JOSA A 10.11 (1993): 2338-2345.
36. Vitushkin, Artyom L., and Leonid F. Vitushkin. "Design of a multipass optical cell based on the use of shifted corner cubes and right-angle prisms." Applied optics 37.1 (1998): 162-165.
37. Wei, Ruyi, et al. "Designs of multipass optical configurations based on the use of a cube corner retroreflector in the interferometer." Applied Optics 50.12 (2011): 1673-1681.

38. Marvasti, Farokh, ed. Nonuniform sampling: theory and practice. Springer Science & Business Media, 2012.
39. Bondesson, David, et al. "Nonuniform Fourier-decomposition MRI for ventilation-and perfusion-weighted imaging of the lung." Magnetic Resonance in Medicine 82.4 (2019): 1312-1321. https://doi.org/10.1002/mrm.27803
40. Kruizinga, Pieter, et al. "Plane-wave ultrasound beamforming using a nonuniform fast Fourier transform." IEEE transactions on ultrasonics, ferroelectrics, and frequency control 59.12 (2012): 2684-2691.
41. Salehi-Barzegar, Alireza, et al. "A fast diffraction tomography algorithm for 3-D through-the-wall radar imaging using nonuniform fast Fourier transform." IEEE Geoscience and Remote Sensing Letters 19 (2020): 1-5. doi: 10.1109/LGRS.2020.3021793.
42. Liu, Qing Huo, et al. "Applications of nonuniform fast transform algorithms in numerical solutions of differential and integral equations." IEEE Transactions on geoscience and remote sensing 38.4 (2000): 1551-1560. doi: 10.1109/36.851955.
43. Bagchi, Sonali, and Sanjit K. Mitra. "The nonuniform discrete Fourier transform and its applications in filter design. I. 1-D." IEEE Transactions on Circuits and Systems II: Analog and Digital Signal Processing 43.6 (1996): 422-433. doi: 10.1109/82.502315.
44. Yang, Zhengfan, and Pawel A. Penczek. "Cryo-EM image alignment based on nonuniform fast Fourier transform." Ultramicroscopy 108.9 (2008): 959-969. https://doi.org/10.1016/j.ultramic.2008.03.006
45. Chan, Kenny KH, and Shuo Tang. "High-speed spectral domain optical coherence tomography using non-uniform fast Fourier transform." Biomedical optics express 1.5 (2010): 1309-1319.
46. Shimobaba, Tomoyoshi, et al. "Nonuniform sampled scalar diffraction calculation using nonuniform fast Fourier transform." Optics letters 38.23 (2013): 5130-5133.
47. Guo, Renhui, et al. "Optical homogeneity measurement of parallel plates by wavelength-tuning interferometry using nonuniform fast Fourier transform." Optics Express 27.9 (2019): 13072-13082.
48. Naylor, David A., et al. "Data processing pipeline for a time-sampled imaging Fourier transform spectrometer." Imaging Spectrometry X. Vol. 5546. SPIE, 2004. https://doi.org/10.1117/12.560096.

49. Barnett, Alexander H., Jeremy Magland, and Ludvig af Klinteberg. "A parallel nonuniform fast Fourier transform library based on an “Exponential of semicircle" kernel." SIAM Journal on Scientific Computing 41.5 (2019): C479-C504.
50. Barnett, Alex H. "Aliasing error of the exp(β1− z2) kernel in the nonuniform fast Fourier transform." Applied and Computational Harmonic Analysis 51 (2021): 1-16.
51. Virtanen, Pauli, et al. "SciPy 1.0: fundamental algorithms for scientific computing in Python." Nature methods 17.3 (2020): 261-272.
52. Thorlabs. Non-Polarizing Cube Beamsplitters (400 - 700 nm). https://www.thorlabs.de/newgrouppage9.cfm?objectgroup_id=754. Accessed 20 Feb. 2023.
53. Thorlabs. HRS015 Stabilized Red HeNe Laser Manual. https://www.thorlabs.com/drawings/3395b7d09f8a91d8-6859BCA5-0CCF-0052-BDBA6861CF79F647/HRS015-Manual.pdf. Accessed 20 Feb. 2023.
54. Changchun New Industries Optoelectronics Technology. MGL-III-532. http://www.cnilaser.com/MGL-III-532.htm. Accessed 20 Feb. 2023.
55. Superlum. SLD-MS-series Miniature Broadband Light Source Modules. https://www.superlumdiodes.com/sld-ms-series.htm. Accessed 20 Feb. 2023.
56. Thorlabs. PDA100A(-EC) Si Switchable Gain Detector User Guide. https://www.thorlabs.de/thorProduct.cfm?partNumber=PDA100A. Accessed 20 Feb. 2023.
57. National Instruments. PCI-MIO-16E-4 Family Specifications. https://www.ni.com/docs/en-US/bundle/370722c/page/download.html. Accessed 20 Feb. 2023.
58. National Instruments. USB-6341 Specifications. 20 Feb. 2023. https://www.ni.com/docs/en-US/bundle/usb-6341-specs/page/specs.html. Accessed 20 Feb. 2023.
59. Physik Instrumente. M-5x1 Series Linear Positioning Stages User Manual. 2004.
60. Kushwah, Manoj, and Ashis Patra. "Tuning PID controller for speed control of DC motor using soft computing techniques-A review." Advance in Electronic and Electric Engineering 4.2 (2014): 141-148.

Publications

The corresponding published paper from this study:

Optics Communications, April 2023, Muqian Wen, John Houlihan. “Application of the Non-Uniform Fourier Transform to Non-Uniformly Sampled Fourier Transform Spectrometers”. https://doi.org/10.1016/j.optcom.2023.129491